Microstructure and mechanical properties of fibrin gels.

Davies, Thomas Marc

Microstructure and Mechanical Properties of Fibrin Gels

Swansea University
Prifysgol Abertawe

THOMAS MARC DAVIES

B.Eng (Hons.) (Swansea University)

Thesis submitted to Swansea University
in partial fulfilment of the requirements for the
Degree of Doctor of Philosophy

Department of Multidisciplinary Nanotechnology
School of Engineering
Swansea University
September 2009

ProQuest LLC.
789 East Eisenhower Parkway
P.O. Box 1346
Ann Arbor, MI 48106 – 1346

Declaration

This work has not previously been accepted in substance for any degree and is not being currently submitted in candidature for a degree at any University.

Signed.....(candidate)

Date.....29/09/09.....

Statement 1

This thesis is the result of my own investigation, except where otherwise stated. Other sources are acknowledged, giving explicit references. A bibliography is appended.

Signed.....(candidate)

Date.....29/09/09.....

Statement 2

I hereby consent for my thesis, if accepted, to be available for photocopying and for inter-library loan, and for the title and summary to be available to outside organisations.

Signed.....(candidate)

Date.....29/09/09.....

Certificate of Originality

This thesis is submitted to the University of Wales, Swansea, under the supervision of Prof. P.R. Williams in the department of Multidisciplinary Nanotechnology Centre, in Swansea University, in candidature for the degree of Doctor of Philosophy. The material in this thesis is the original work of the author except where acknowledgement to other authors is expressed.

Signed .....

Date 29/09/09

Thomas Marc Davies

(Candidate)

Signed .....

Date.....

Prof. P.R Williams

(Supervisor)

Abstract

This thesis reports an extensive study of the structural and rheological characteristics of the three-dimensional fibrin clot network. The importance of blood clotting in the area of NanoHealth is testified to by the fact that complications due to thrombosis accounts for about 10 per cent of all deaths in hospitals in the UK. It is therefore imperative to understand the clotting process of blood as fully as possible. The techniques implemented include confocal laser scanning microscopy, and rheological methods such as Fourier transform mechanical spectroscopy. Both techniques provide a foundation for performing a fractal analysis as a quantitative basis for defining, where appropriate, morphological/micro structural differentiation in clotting. Fractal analysis provides the framework for structural complexity and allows us to develop relationships between the structural features of blood clots and their rheological properties. The experimental methods involve following the mechanical properties of a gelling system up to and beyond the gel point. The mechanical (viscoelastic) properties of fibrin are significant and unique among polymers. Hence, they are essential to the physiology of blood clotting and vital for the understanding and therefore prevention and treatment of thrombosis. An unsatisfactory aspect of work in this area is that the microstructures of such clots are usually reported in only adjectival terms (e.g., "dense" or "tight") - usually on the basis of a visual inspection of fragments of desiccated clots in SEM micrographs. This work includes an extensive approach using confocal microscopy to visualise fibrin clot networks, with several forms of fractal analysis investigated for quantifying structural complexity.

The present study is the first to report a modification of the fractal characteristics of incipient clots in fibrin-thrombin gels due to the availability of thrombin. This work confirms the hypothesis that the self-similar (fractal) stress relaxation behaviour recorded at the Gel Point of samples of coagulating blood (Evans *et al.*, 2008) is associated with the micro structural characteristics of the incipient blood clot's fibrin network. It also supports the hypothesis that in various pathologies prothrombotic conditions can modify the underlying microstructure of a blood clot. The provision of a new technique capable of detecting the formation of altered clot microstructures at their incipient state could have significant clinical diagnostic potential e.g. in thromboembolic disease screening applications.

Contents

Acknowledgements

I would like to take this opportunity to acknowledge the people who have helped to make this work possible. First, I would like to express my sincere gratitude to my thesis advisor Professor Rhodri Williams, head of Complex Fluid Processing, Swansea University, for his consistent and thoughtful advice, continuous encouragement and support during the course of this work.

I thank Dr Karl Hawkins and Dr Martyn Brown, Multidisciplinary Nanotechnology Centre, Swansea University for their thoughtful advice and help in my study. I also thank Mrs Sally James, Institute of Life Science, School of Medicine Swansea for her help in completing the Confocal Microscopy images on the structures of fibrin-thrombin systems.

I am grateful to my fellow graduate students for assisting me with my research and offering advice and discussion. Specifically I would like to thank Mathew Lawrence, Daniel Curtis and Oliver Puckering.

Finally, I would like to express my heartfelt gratitude to my parents, Keith and Christine and my fiancée, Hayley for their continuous support and encouragement, which enabled me to overcome difficulties and hardship encountered in the course of this study.

List of Figures

List of Tables

Nomenclature

Greek Letters

α	Stress Relaxation Exponent	
β	Auxiliary Stress Relaxation Exponent	
ε	Molar extinction coefficient	m^2/mol
γ	Shear Strain	
$\dot{\gamma}$	Strain Rate	s^{-1}
$\dot{\gamma}_T$	Total Rate of Strain	s^{-1}
γ_0	Maximum Strain Amplitude	
γ^*	Complex Shear Strain	
δ	Phase Angle	rad or °
μ	Combined Mean	
η	Shear Viscosity	Pa s
η_0	Zero Shear Viscosity	Pa s
η^*	Complex Viscosity	Pa s
η'	Dynamic Viscosity	Pa s
η''	Imaginary Part of the Complex Viscosity	Pa s
θ	Angle of shear	rad
λ	Wavelength	m
λ_N	Characteristic Wavelength	m
λ_τ	Characteristic Wavelength from τ_L	m
λ_{FFT}	Characteristic Wavelength from FFT	m
λ_s	Shear Wavelength	m
ν	Wave velocity	$m\ s^{-1}$
ν_s	Shear Wave Phase Velocity	$m\ s^{-1}$
ρ	Density	$Kg\ m^{-3}$
σ	Shear Stress	Pa
$\sigma(t)$	Time-Dependent Shear Stress	Pa
σ_0	Maximum Stress Amplitude	Pa
σ^*	Complex Shear Stress	Pa
$\dot{\sigma}$	Rate of Stress	$Pa\ s^{-1}$
σ_T	Total Stress	Pa

σ^2	Combined Variance	
$\sigma_B^{2\|}(T)$	Variance of the pixels in the background	
$\sigma_O^2(T)$	Variance of the pixels in the foreground	
τ_{mat}	Characteristic Material Time	s
τ_{exp}	Experimental Time	s
τ	Relaxation Time	s
τ_p	polydispersity Index	
τ_J	Retardation Time	s
ω	Angular Frequency	rad s^{-1}
ω_0	Resonant Frequency	rad s^{-1}

Roman Letters

A	Area	$m\ s^{-2}$
d	Distance	m
d	Euclidean Dimension	
d_f	Fractal Dimension	
D_b	Box Dimension	
D_i	Information Dimension	
f	Functionality	
f	Frequency	Hz
f_0	Resonant Frequency	Hz
F	Force	N
FPA	Fibrinopeptide A	
FBA	Fibrinopeptide B	
G	Shear Modulus	Pa
G (t)	Shear Stress Relaxation Modulus	Pa
G*	Complex Shear Modulus	Pa
G′	Shear Storage Modulus	Pa
G″	Shear Loss Modulus	Pa
G_e	Equilibrium Shear Modulus	Pa
I (d)	Information Entropy	
l	Length	m
L	Length	m
M	Mass	Kg
m	Mass	Kg
M_w	Molecular Weight	$Kg\ mol^{-1}$
N_D	Deborah Number	
N_M	Power Law Cluster Number Distribution	
p	Probablity	
p_r	Percolation Probability	
p_c	Critical Extent of Reaction or Percolation Threshold	
r	Stoichiometric Ratio	
R	Radius	m

R_z	Cluster Radius	m
S	Critical Gel Strength	Pa s^{α}
t	Time	s
t_c	Critical Reaction Time	s
TF	Tissue Factor	
tPA	Tissue Type Plasminogen Activator	
v	Velocity	m s^{-1}
V	Volume	m^3

Introduction

Fibrin-thrombin gels form the principal micro structural component of a blood clot and are of wide scientific and biomedical interest. Blood coagulation involves the action of (the enzyme) thrombin on the soluble protein fibrinogen to form a branching 3-dimensional network of insoluble fibrin monomer strands (Blomback and Bark 2004; Weisel 2004). In various disease states, such as atherothrombotic vascular disease, prothrombotic processes reportedly lead to an increased density of fibrin strands in blood clots, thereby creating a more "compact" network structure (Isogai et al. 1973). In studies of whole mature blood clots it has been observed that such "tight" (or "compact") clot structures are associated with several pathological states (Scott et al. 2004). Thus the ability to characterise the microstructure of clots formed under pathological conditions has potential relevance to the diagnosis of various diseases.

Chapter 1 introduces the extensive area of blood coagulation, the pivotal role played by fibrinogen and thrombin, and the central importance of blood clotting to our well-being and life.

Rheology is introduced in Chapter 2, and includes the relationship between rheological behaviour and the structure of gelling systems. Rheology is defined in this Chapter with respect to linear viscoelastic theory in terms of the basic concepts of stress, strain and dynamic viscoelastic properties. The second part of this Chapter gives an account of various rheological aspects of gelation in terms of the Winter-Chambon Gel Equation. A brief review of gel point determination is made and the rheological properties of the critical gel are described, together with descriptions of pre- and post-gel viscoelastic behaviour. The significance of the stress relaxation exponent in the Gel Equation is discussed and its influence on the evolution of rheological properties explained.

Chapter 3 employs the theory and rheological techniques discussed in Chapter 2. The Chapter discusses the significance of viscoelasticity in fibrin clots, and the rheological characterisation of fibrinogen-thrombin gel formation. The results of simulated sequential frequency sweep data, which have been reconstructed from time resolved viscoelastic data obtained by Fourier Transform Mechanical

Spectroscopy for fibrin-thrombin gel formation are revealed. Furthermore, using appropriate rheometry, we report values of α for fibrin-thrombin gels formed by the addition of thrombin to a physiologically relevant level of human fibrinogen, and relate these values to the microstructure of the fibrin gel network in terms of a fractal dimension.

Following the rheological characterisation of fibrin-thrombin gels using fractal analysis, Chapter 4 proceeds with an in depth look into the nature of fractals, self-similarity and fractal geometry. The second part of Chapter 4 discusses fractal models for gelling systems such as Diffusion Limited Cluster Aggregation (DLCA). Chapter 4 concludes discussing a dynamic approach using confocal microscopy to visualise fibrin clot networks and several forms of fractal analysis are investigated for quantifying structural complexity.

Laser Scanning Confocal Microscopy (LSCM) is introduced in Chapter 5, with discussion around confocal scanning implementations, advantages and disadvantages of confocal microscopy, and molecular fluorescence. Following the introduction, optical based characterisation of the fractal structure of fibrin clot networks is considered.

The final Chapter reveals the structural characterisation of maturing clot growth in fibrin-thrombin gels. Using LSCM techniques the structural evolution is monitored and quantified using fractal analysis. Using microscopy techniques, representations of extensive fibrin-thrombin networks are characterised as set point-masses spatially arranged, in a 3-dimensional volume, exhibiting diverse fractal dimensions. At the end of every chapter, a conclusion is drawn to summarize the important points in the chapter. At the end of this thesis, we present a general conclusion and suggest future directions of our work.

The significance of this work is essential to the physiology of blood clotting and vital for the understanding and therefore prevention and treatment of thrombosis. In Western Society, Thromboembolic disease and associated blood coagulation abnormalities cause significant morbidity and mortality, with stroke being the third leading cause of death in the UK. In stroke, the processes of endothelial and vascular

damage, activation of the coagulation cascade and decreased fibrinolysis result in abnormal clots, often with excessively cross-linked fibrin networks.

The aims and objectives for this piece of work are summarised as follows,

- Studies of the structural and rheological characteristics of fibrin clots.
- Develop an appropriate quantitative basis for defining what is meant by clot 'quality'/'structure' (good, bad, dense, tight, and loose).
- Seek to develop quantitative relationships between the structural features of clots and their rheological (viscoelastic) properties.
- Exploit fractal analysis, where appropriate, to quantify morphological/micro structural differentiation in clotting.
- Study will involve different fibrinogens/pathologies/clot structures.

Chapter 1

Fibrinogen and Fibrin

1.1 Blood Coagulation

Blood clotting is of central importance to our well-being and life and has thus been studied for many decades. When blood vessels are cut or damaged, the loss of blood from the system must be stopped before shock and possible death occur. This is accomplished by solidification of the blood, a process called coagulation or clotting. Coagulation involves the formation of a blood clot (thrombus) that prevents further blood loss from damaged tissues, blood vessels or organs. This is a complicated process with a cellular system comprised of cells called platelets that circulate in the blood and serve to form a platelet plug over damaged vessels. The formation of the primary platelet plug is temporally and spatially coordinated with the activation of the blood coagulation system leading to the generation of thrombin and the formation of the fibrin network.

These two systems work in tandem to form a clot; irregularity in either system can yield disorders that cause either too much or too little clotting. Ultimately a blood clot consists of a plug of platelets enmeshed in a 3D network of insoluble fibrin molecules (see Fig 1.1).

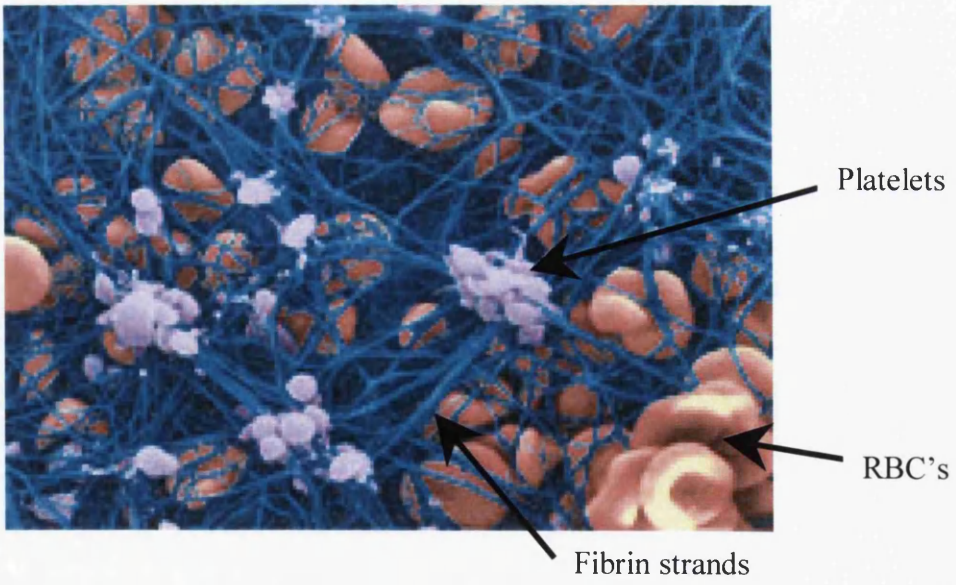

Figure 1.1. SEM image of Blood Clot (John Weisel)

Blood coagulation and platelet-mediated primary haemostasis have evolved as important defence mechanisms against bleeding. The coagulation system is triggered in response to rupture of endothelium, which allows exposure of blood to the extravascular tissue. The responses of the coagulation system are coordinated with the formation of the platelet plug that initially occludes the vascular lesion. Anticoagulant mechanisms ensure careful control of coagulation and, under normal conditions; they prevail over the procoagulant forces.

Disturbances of the natural balance between the procoagulant and anticoagulant systems due to genetic or acquired factors may result in bleeding or thrombotic diseases.

1.1.1 The Coagulation Cascade

The coagulation cascade of secondary hemostasis has two pathways, the Contact Activation pathway (formerly known as the Intrinsic Pathway) and the Tissue Factor pathway (formerly known as the Extrinsic pathway) that lead to fibrin formation. It was previously thought that the coagulation cascade consisted of two pathways of equal importance related to a common pathway. It is now known that the primary pathway for the initiation of blood coagulation is the Tissue Factor pathway. The pathways are a series of reactions, in which a zymogen (inactive enzyme precursor) of a serine protease and its glycoprotein co-factor are activated to become active components that then catalyze the next reaction in the cascade, ultimately resulting in cross-linked fibrin.

Thrombin is the key effector enzyme of the coagulation system, having many biologically important functions such as the activation of platelets, conversion of fibrinogen to a fibrin network, and feedback amplification of coagulation. The precise and balanced generation of thrombin at sites of vascular injury is the result of an ordered series of reactions collectively referred to as blood coagulation (figure 1.2).

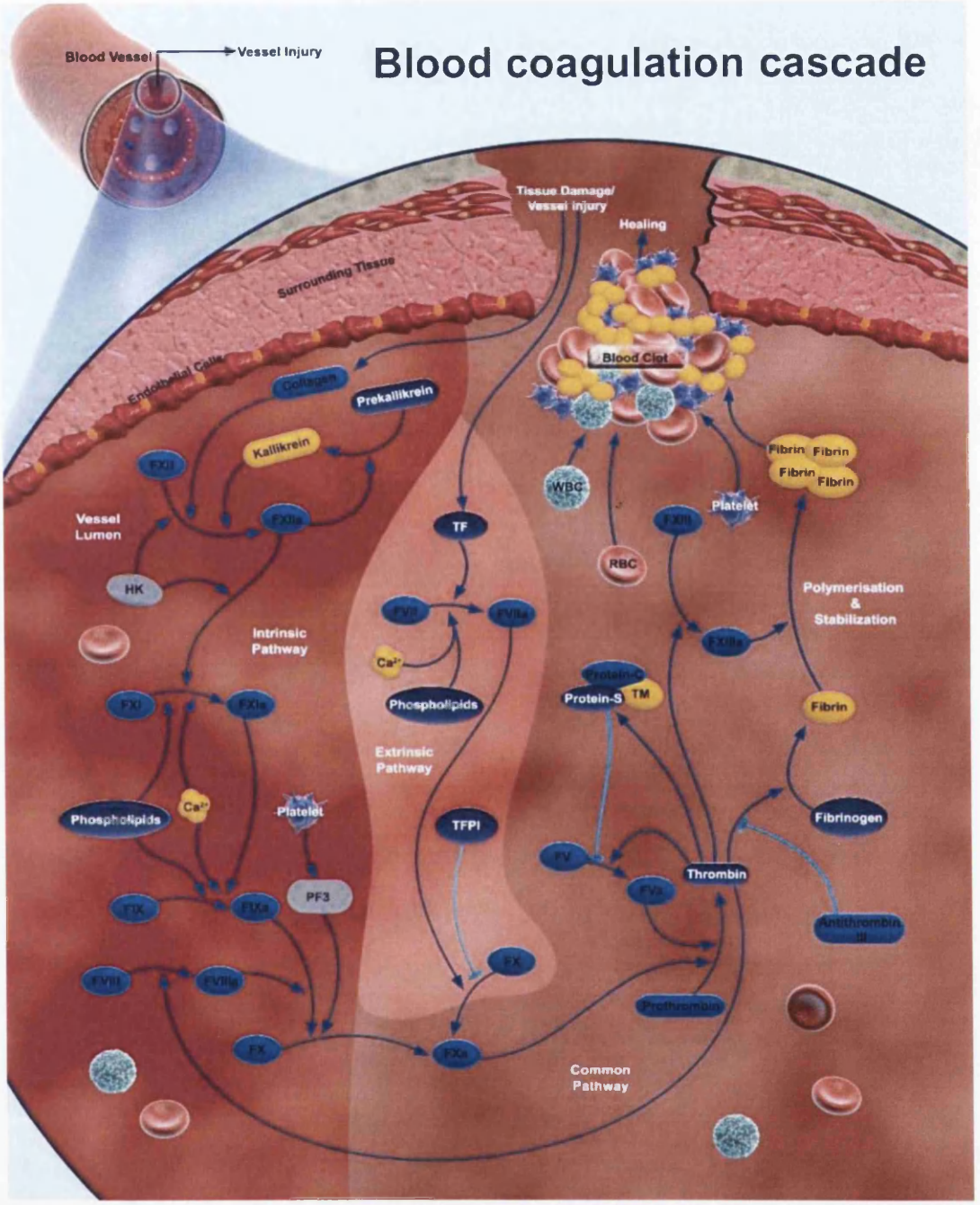

Figure 1.2. Schematic presentation of the coagulation cascade.

1.1.2 Activation and Propagation of the Coagulation Pathway

The system is triggered on the surface of extravascular cells by the exposure of tissue factor to blood (figure 1.3). Tissue factor is a membrane protein abundantly present in cells surrounding the vascular bed. A fraction of FVII in blood is activated (FVIIa) and binding of FVIIa to TF initiates coagulation. Circulating factor IX (FIX) and factor X (FX) are converted by the FVIIa-Tfcomplex to active enzymes FIXa and FXa, which feedback amplify the system by activating FVII that is bound to TF. FIXa and FXa may remain associated with the TF-bearing cell or diffuse into fluid phase and bind to the membrane of activated platelets (Hoffman, 2003). Activation of platelets is associated with the exposure of negatively charged phospholipids, which have high potential to bind coagulation factors and assemble enzyme-cofactor complexes that are crucially important for efficient propagation of the system.

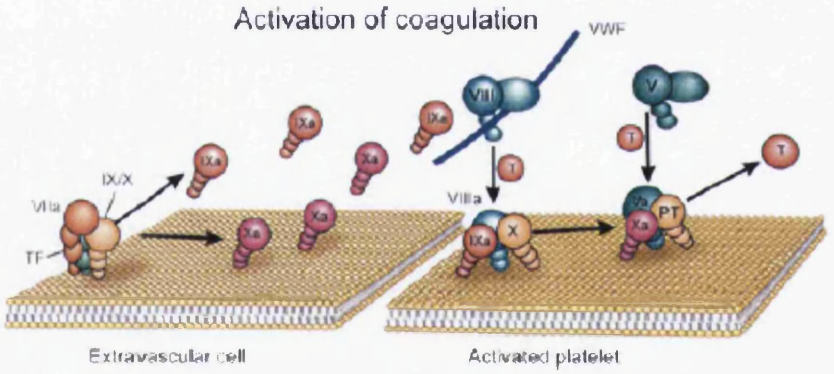

Figure 1.3. Schematic model illustrating some of the phospholipid-bound reactions that are involved in the activation and regulation of coagulation.

Prothrombin is activated to thrombin by the prothrombinase complex, which consists of the phospholipid-bound complex between the enzyme, factor Xa, and its cofactor, activated factor V (Va). The substances that activate factor V are factor Xa (on the phospholipid surface) and thrombin (both in solution and on the surface). Thrombin feedback amplifies the system by activating not only factor V, but also factors VIII and XI. Factor VIII circulates bound to von Willebrand factor, which is an adhesive protein important for the generation of the initial platelet plug (Sadler,

1998). After activation, factor VIIIa dissociates from von Willebrand factor and forms a complex on the platelet surface with factor IXa; this complex (denoted the tenase complex), then activates factor X. Activation of factor XI by thrombin is another amplification loop, resulting in the generation of additional factor IXa, which in turn activates factor X (Gailani and Broze, 1991).

Maximum thrombin generation occurs after the formation of the fibrin clot. Thrombin is important for additional fibrin generation as well as for activation of factor XIII and the thrombin-activatable fibrinolysis inhibitor. Activated factor XIII (XIIIa) is a transglutaminase that stabilises the clot by covalent crosslinking of fibrin (Davie, 1995). Thrombin-activatable fibrinolysis inhibitor is a carboxypeptidase that releases carboxyterminal lysines from fibrin. Because these lysines are important for the binding of fibrinolytic enzymes to fibrin, activation of the inhibitor prevents further fibrinolytic attack (Nesheim *et al.*, 1997).

The initiation of coagulation via the exposure of tissue factor (tissue-factor pathway) as described above, the extrinsic pathway, is the mechanism by which coagulation is initiated in vivo in response to trauma. An alternative pathway by which the coagulation system can be initiated involves factor XII, high molecular weight kininogen, prekallikrein and FXI and results in the generation of FXIa, which in turn can activate FIX. These reactions are collectively called the 'intrinsic' pathway and their physiological importance is not fully understood. Thus, inherited deficiencies of proteins of this system are not associated with bleeding problems, except for deficiency of factor XI, which leads to a moderately severe bleeding disorder (Mannucci *et al.*, 2004).

Both the extrinsic and intrinsic pathways serve the common purpose of proteolytic cleavage of fX into the active Xa. It is generally thought that the extrinsic pathway, as it more rapidly initiates coagulation, is the predominant mechanism of Xa and downstream factor IIa and Ia generation. However, it is well appreciated that clinical deficiencies in components of the intrinsic pathway, particularly fIX (haemophilia B – Christmas disease) and fVIII (haemophilia A), result in deleterious impairments in coagulation and haemostasis.

Various coagulation proteins circulate in blood at very different concentrations related to their specific roles in the blood coagulation system (Mann and Lorand,

1993). Fibrinogen is the predominant clotting factor (10 μmol L^{-1}), having a concentration that is approximately 50 000-fold higher than that of FVIII (0.2 nmol L^{-1}). The high level of fibrinogen is required for the formation of the fibrin clot, whereas the low concentration of FVIII is more than sufficient to support FIXa in the activation of FX. There are also variations in the concentrations of the vitamin-K-dependent proteins, with factor VII (10 nmol L^{-1}) the least abundant, factors IX and X present in intermediate concentrations (100 nmol L^{-1}), and prothrombin circulates at the highest concentration (2 μmol L^{-1}). Thus, early components of the pathway circulate at lower concentrations than the factors that act at later stages, which is consistent with the principal organisation of the system with multiple reactions and amplification potential.

1.2 Fibrin Gels – the Principle Architecture of a Blood Clot

1.2.1 Introduction

Fibrinogen is defined as that soluble protein in blood and tissue extract, which, in presence of thrombin, is transformed into the insoluble fibrin network structure. Fibrinogen, forming in clotted blood the white cap, Crusta Phlogistica, was not known as a protein until the middle of last century, and remarkably, was at that time the first plasma protein to be purified in almost homogenous form. Denis de Commercy's and Olof Hammarsten's work showed that fibrinogen was a unique protein compound in plasma. Olof Hammarsten saw the similarity between casein's activation by rennin and fibrinogen's activation by thrombin. He considered that activation was accompanied by limited proteolysis of the molecule. However, this idea was refuted and the predominant view until about 1950 was that thrombin acted as a 'denaturase' in inducing clotting of the fibrinogen. In the early 1950's, Bailey and Bettelheim and independently Lorand and Middlebrook showed that thrombin initiates the clotting of fibrinogen by proteolysis, thus splitting off fibrinopeptides from the fibrinogen molecule (Bailey *et al.*, 1951, 1955).

During this time, Ferry's group had pioneered stages of the polymerisation process that follow the action of thrombin. They demonstrated that, on addition of thrombin to fibrinogen, initial polymers or protofibers were formed and after reaching certain lengths gel formation took place due to interaction between the polymers, in three dimensions (Ferry *et al.*, 1951). In initial polymerisation the activated fibrinogen molecules align non-covalently to each other in a half staggered fashion and thus build up two identical polymer strands (Ferry *et al.*, 1952). Early investigations of fibrin clot structures using transmission electron microscopy first revealed these aspects of fibre morphology and clot structure. Ferry and Morrison had already in 1947 published their pioneering work on optical properties of hydrated fibrin gels, as ranging between the extremes transparent and opaque. In transparent gels they deduced the polymer strands being thin and the meshwork fine, whereas in the opaque or turbid gels thick polymer strands are encompassing wide liquid spaces. Thrombin was an important modulator of the process, thus, increasing concentrations led to more transparent gels as clotting time decreased.

More than a hundred years have passed since Denis De Commercy and Olof Hammersten carried out their pioneering studies on isolation of fibrinogen from plasma and its conversion into fibrin. Presently, we have gained an extensive knowledge of the properties of fibrinogen and fibrin, and we are also getting insight into the processes that govern clot formation and clot dissolution in the blood vessels. The formation of fibrin blood clots from fibrinogen has been extensively studied by biochemical and biophysical methods, with important contributions coming from electron microscopy and light scattering techniques (Doolittle 1984; Blomback 1996; Ferri *et al.*, 2002). These studies have revealed that fibrin gels are three-dimensional networks made of entangled fibres whose physical properties (average size, spatial distribution, extent of branching, flexibility) determine the properties of the entire network, such as its morphology, porosity, and elasticity. By varying the physical-chemical conditions of the gelling solution, such as the pH, the presence of ions of different type and concentration, and the activating enzyme, one can obtain gels with very different characteristics (Ferri *et al.*, 2002).

Clots formed under various ionic conditions revealed dramatic differences in structure. A wide variety of studies by transmission electron microscopy have

provided extensive information about the structure of supramolecular assemblies at different stages of polymerization. Some of these studies have established the significance of the two pairs of fibrinopeptides and their relationship to the lateral aggregation of fibrin fibre assemblies in clot formation (Weisel, 1986) as well as the role of fibre twisting (Weisel *et al.*, 1987). The formation of small fibrin aggregates and protofibrils has also been studied using transmission electron microscopy (Medved *et al.*, 1990). Several factors appear to play important roles in determining the final fibre diameter and clot structure, and all are greatly affected by the kinetics of each individual step (Medved *et al.*, 1990; Mosesson *et al.*, 1987; Langer *et al.*, 1988).

Blood clots, which mainly consist of a meshwork of fibrin fibres attached to platelets, ultimately have the task of creating a blockage that stems the flow of blood. Since this is essentially a mechanical task, there has been much interest in determining the mechanical properties of such systems. In the past, the bulk mechanical properties of whole clots were investigated extensively (Ferry *et al.*, 1951; Roberts *et al.*, 1973; Gerth *et al.*, 1974; Mockros *et al.*, 1974; Glover *et al.*, 1975; Shen *et al.*, 1975; Nelb *et al.*, 1976, 1981; Janmey *et al.*, 1983; Shen and Lorand, 1983; Ryan *et al.*, 1999a,b).

However, we still do not know the answers to some of the most fundamental questions in this field. On a basic science side, we do not even know the origin of the viscoelastic properties of fibrin. On a clinical side, almost nothing is known about the mechanical properties of in vivo clots or thrombi, albeit these properties are critical for the physiological function of fibrin and for the treatment of pathological conditions, such as bleeding and thrombotic disorders, including angioplasty and thrombolytic therapy.

The mechanical properties of fibrin are essential for its functions. In haemostasis, the clot must form a plug to stop bleeding and this structure must be strong enough to withstand the pressure of arterial blood flow. The importance of the mechanical properties of fibrin are discussed in greater detail later in the chapter.

It is our proposal to study the microstructure and mechanical properties of fibrin gels in association with blood clotting using a series of different techniques,

and exploiting fractal analysis where appropriate, to quantify morphological/micro structural differentiation in clotting.

1.2.2 The Fibrinogen molecule

Fibrinogen is a large glycoprotein, consisting of two identical halves, each comprised of three peptide chains, designated Aα, Bβ, and γ, with molecular masses of 66,500, 52,000, and 46,500 Da, respectively. The posttranslational addition of asparagines-linked carbohydrate to the Bβ and γ chains brings the total molecular mass to about 340,000 Da.

The entire amino acid sequence of all polypeptide chains of human fibrinogen has been determined by the methods of protein chemistry and later deduced from the nucleotide sequences of the cDNA coding (Doolittle, 1984; Henschen and McDonagh, 1986). There are 610, 461, and 411 amino acids in each of the common forms of the human Aα, Bβ, and γ chains, respectively. The amino acid sequences of the three chains are homologous, but important differences exist, giving rise to specific functions for certain molecular domain. A total of 29 disulfide bonds hold the six chains together (Henschen and McDonagh, 1986) creating the dimeric structure of the molecule. Three interchain disulphide bonds link the two halves of the molecule together, one between the two Aα chains and two between the two γ chains. The A and B fibrinopeptides are also located at the N-terminal ends of the α and β chains, respectively. A single interchain disulphide bond connects the Aα and Bβ chains within each half molecule.

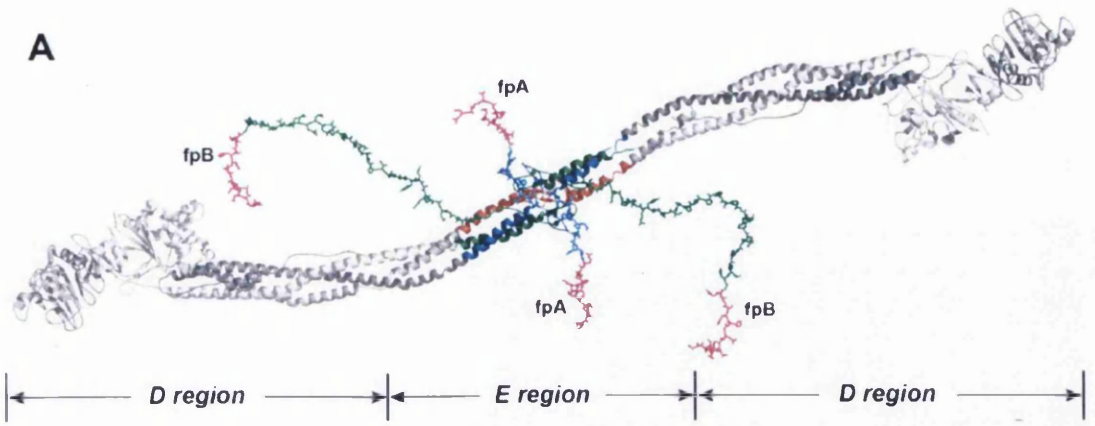

Figure 1.4. Human fibrinogen molecule

The shape of fibrinogen and its organisation into domains have been defined by a variety of physiochemical and structural techniques. Fibrinogen was one of the first biological macromolecules to be visualised by electron microscopy (Hall and Slayter, 1959). Fibrinogen was seen as an elongated trinodular molecule of about 45 nm in length and 4.5 nm in diameter with nodular regions at each end and connected by rod like strands in the middle. Subsequent studies confirmed this model.

The fibrinogen molecule consists of a central globular domain joined by two elongated connectors to two identical outer domains. This central nodule (E region) is connected to the two outer nodules, the D regions, through α-helical coiled-coils. The D region is divided into several domains, including the β and γ nodules, which constitute the C-terminal part of these chains that fold independently (Wiesel *et al.*, 1985).

Fibrinogen is a protein present at high abundance in the blood, with an average concentration of about 2.5 g/l. Under appropriate conditions, plasma will rapidly clot to form quite a stable structure mechanically. In fact, a stable gel can be formed at fibrinogen concentrations at least 100 fold lower. As a result, in a clot made from fibrinogen at a concentration of 2.5 g/l, the fibrin is only 0.25 g out of 100 ml (or g) of volume. In other words, the fibrin constitutes 0.25% of the volume in a clot, so 99.75% of the clot is liquid occupying the space between the protein polymers (Weisel *et al.*, 1985). There are large spaces between the protofibrils in the

fibres and much larger spaces between the fibres. The properties of this polymer are even more remarkable considering the small volume of material involved.

1.2.3 Fibrinogen Biosynthesis

Human fibrinogen is the product of three closely linked genes, each specifying the primary structure of one of the three polypeptide chains (Chung *et al.*, 1983; 1990). Site directed mutagenesis of fibrinogen has established the sequence of steps in fibrinogen assembly. The natural progression is from single chains to two-chain complexes to trimeric half molecules, which then dimerize to form a whole fibrinogen molecule.

Fibrinogen synthesis is stimulated by hormones such as the glucocorticoid dexamethasone or suppressed by the oestrogen estadiol-17 (Chung *et al.*, 1983; 1990). The three fibrinogen genes share a common regulatory mechanism, as indicated by the highly coordinated expression of mRNAs, such that in hepatocytes the relative proportions of mRNAs for the three chains are nearly the same (Crabtree, 1987).

Fibrinogen is one of the proteins up regulated during the acute phase response, with increases two to tenfold, while albumin levels decrease by about 50% (Crabtree, 1987). Under stressful conditions, there are a series of reactions that result in cell activation and cytokine production. Cytokines then act on other cells, resulting in an increase in production of glucocorticoids, proliferation of immune cells, and changes in the levels of plasma proteins synthesised in the liver. The up regulation of the acute phase response proteins is mediated by interleukin-6 (IL-6) (Hantgan *et al.*, 2000).

Fibrinogen is fabricated in the rough endoplasmic reticulum of the liver. The assembly of polypeptide chains into functional fibrinogen molecules has been studied extensively in several expression systems. The order in which the polypeptide chains are linked together by disulphide bonds has been determined and specific structural features that are important for assembly, such as coiled coil, have been identified (Xu *et al.*, 1996). Substitution of the cysteines with serine revealed

that the inter-chain disulfide ring at the proximal end of the coiled-coil, in addition to the disulphides between the two halves of the molecule, are necessary for assembly of the two half molecules (Zhang and Redman, 1996). Disruption of intra-chain disulphide bonds and deletions of portions of the polypeptide chains have revealed which disulfide bonds and non-covalent interactions are necessary for fibrinogen assembly.

As discussed, the primary source of plasma fibrinogen is the liver, with a steady state rate of synthesis of 1.7-5.0 g per day (Takeda, 1966). The majority of the human fibrinogen is located in the plasma, but it is also present in platelets, lymph nodes, and interstitial fluid. The half-life of fibrinogen is known to be around 3 to 5 days, but the catabolic pathway is different from the classic plasma protein pathways and is largely unknown. Nosell (1976) demonstrated coagulation and lysis accounts for only 2-3 % of fibrinogen loss in healthy individuals.

Platelets contain fibrinogen but there is controversy over its origin, and whether it is structurally and functionally distinct from plasma fibrinogen. Haidaris *et al.*, (1989) established the γ chain variants of fibrinogen do not appear to be present in platelets, and Jandrot-Perrus *et al.,* (1979) demonstrated in one patient with a heterozygous dysfibrinogen, the platelets contained only normal fibrinogen. The megakaryocytes, from which platelets originate, are a possible source of fibrinogen synthesis. However, in subjects with hypofibrinogenemia, there are also lower levels of fibrinogen in platelets, but infusion of fibrinogen results in a subsequent increase in platelet fibrinogen (Harrison *et al.*, 1989). Additionally, no fibrinogen mRNA was detected in megakaryocytes (Louache *et al.*, 1991), therefore, it appears that platelet and megakaryocyte fibrinogen arise primarily from αIIbβIII-mediated endocytosis of plasma fibrinogen and its storage in α granules.

1.2.4 Fibrin Polymerisation and clot formation

The primary stage in the development of the three-dimensional fibre network involves the activation of the fibrinogen molecule by thrombin, which removes two pairs of small peptides from the Aα and Bβ chains. Then, several non-enzymatic reactions yield an orderly sequence of macromolecular assembly steps.

Thrombin, which is produced on proteolytic cleavage of prothrombin by Factor Xa in the presence of factor V and phospholipid, is a serine protease with specificity for fibrinogen's fibrinopeptides at particular Arg-Gly bonds. This specificity arises in part because of hydrophobic and structure dependent interactions between the fibrinopeptides and thrombin's catalytic site, as well as non-catalytic binding of enzyme to substrate (Stubbs and Bode, 1993). Of the few hundred trypsin-sensitive bonds in the fibrinogen molecule, only four are preferentially cleaved by thrombin, resulting in release of 2 fibrinopeptide A and 2 fibrinopeptide B molecules.

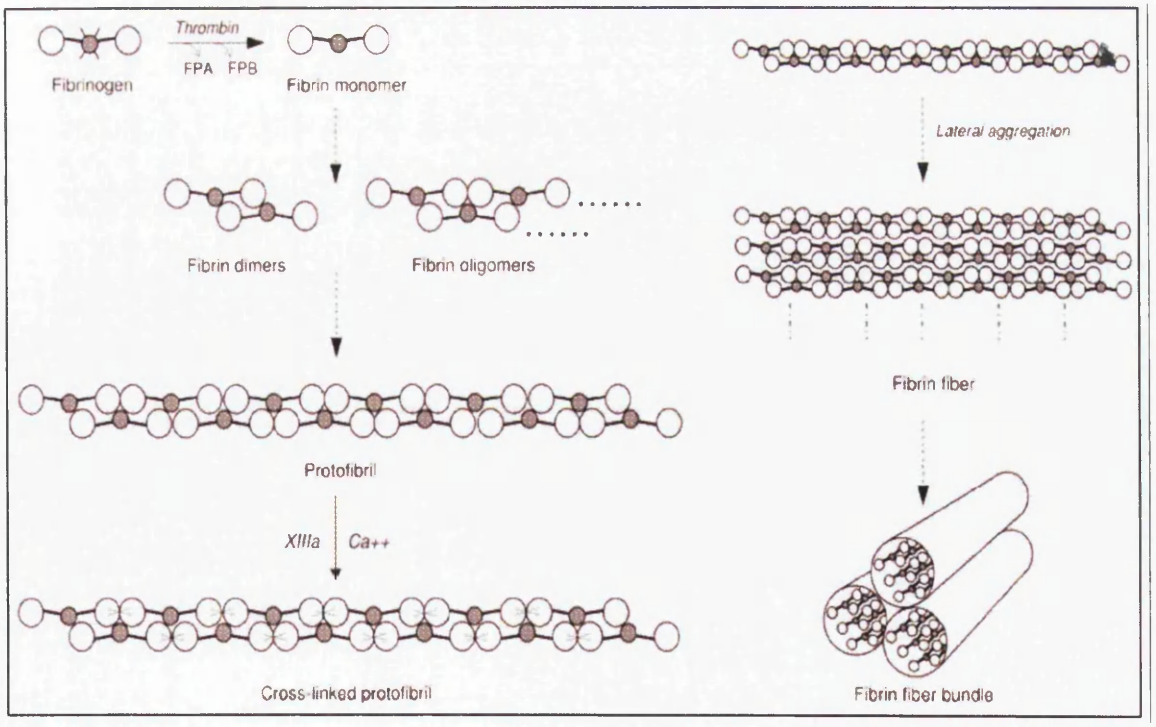

Figure 1.5. Fibrin polymerisation.

FPA is released at the fastest rate (Figure 1.6), and studies have indicated that release of FPA appears to be required for the activated molecule to be integrated in the growing polymer (Blomback *et al.*, 1978; Blomback, 1958). However, in the early stage of activation, fibrin monomer species may first be produced, which are only half activated, but these species remain monomeric until the second FPA is released at a faster rate than the first FPA. This is in conflict with other observations suggesting initial polymerisation by half-activated molecules (Meh *et al.*, 1995). At the time of gel formation (i.e. clotting time) only small amounts of FPB have been released (Figure 1.6). The release of FPB is greatly accelerated subsequent to gel formation, and this acceleration may be associated with conformational changes occurring as a result of polymer organisation. Although the fibrinopeptides constitute less than 2% of the mass of the fibrinogen molecule, their cleavage has profound consequences for the solubility of the resulting fibrin.

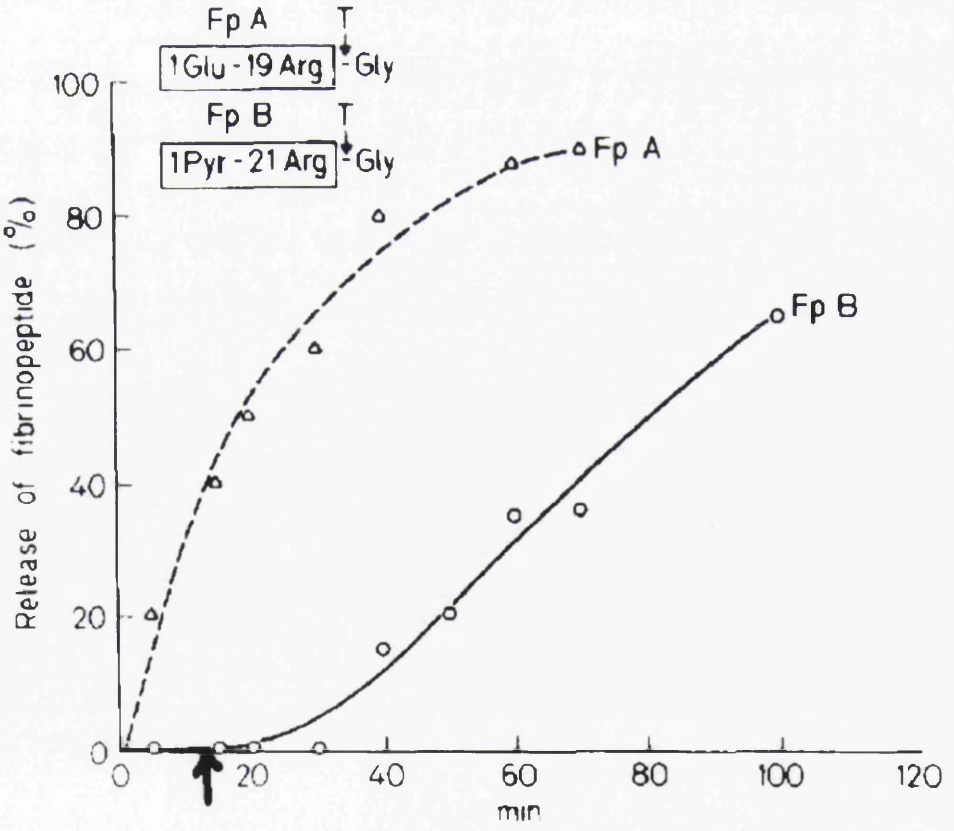

Figure 1.6. Release of fibrinopeptides A and B from bovine fibrinogen after addition of thrombin. Arrow indicates clotting time (Blomback 1996).

Polymerisation of activated fibrinogen molecules involves complementary intermolecular interactions of domains in fibrinogen after release of fibrinopeptides. Cleavage of FPA exposes binding sites in the central domain (A) that are complementary to sites (*a*) always exposed at the ends of the molecules (Doolittle, 1984). The A "knobs" consist in part of the newly exposed N-terminus of fibrin's α chain, Gly-Pro-Arg, but also include part of the Bβ chain. The *a* sites include "holes" in the C-terminal γ chain (Fig 1.4). There are also B "knobs" exposed in the middle of the molecule on cleavage of the B fibrinopeptides after polymerisation begins, these sites are complementary to "b" holes in the C-terminal β chain (Fig 1.4).

Specific interactions between the A:*a* complementary binding sites produce aggregates in which the fibrin monomers are half-staggered, since the central domain of one molecule binds to the end of the adjacent molecule (Fig. 1.5). Initially, a dimer is formed and then additional molecules are added to give a structure called the two-stranded protofibril (Medved *et al.*, 1990). As protofibrils reach a sufficient length (600-800 nm), they aggregate laterally to form a bundle of fibres (Fig. 1.5). The early protofibrils have a width about double that of a fibrinogen molecule. The intermolecular interactions that occur in lateral aggregation are specific so that the fibres have a repeat of 22.5 nm, or about half the molecular length, and a distinctive band pattern as observed by electron microscopy (Weisel, 1986a). The band pattern directly reflects the molecular structure and packing in fibrin, and indicates that fibres are paracrystalline structures with the molecules precisely aligned in the longitudinal direction, but only partly ordered in the lateral direction (Weisel, 1986a).

Blomback *et al.*, (1978) used snake venom enzymes that remove only the A fibrinopeptides to show that cleavage of the B fibrinopeptides enhances lateral aggregation, producing thicker fibres. Clots formed via cleavage of either only fibrinopeptide A or only fibrinopeptide B are made up of fibres with normal appearance, indicating that both the B knobs and the A knobs can participate in protofibril formation and neither are specifically associated with lateral aggregation (Mosesson *et al.*, 1987; Weisel, 1986b).

The αC domains enhance lateral aggregation in fibrin polymerisation and are important for the mechanical properties and stability of clots (Weisel and Medved, 2001). Experiments with purified or recombinant preparations missing either one or both of the αC domains, αC fragments, and several dysfibrinogenemias indicate that intermolecular interactions between αC domains are important for the enhancement of lateral aggregation during fibrin polymerisation (Weisel and Medved, 2001; Gorkun *et al.*, 1994).

Lateral growth of fibres seems to be limited because protofibrils in the fibres are twisted (Fig. 1.7), so that as the fibre diameter increases; they must be stretched to traverse an increasingly greater path length (Weisel *et al.*, 1987). Fibres stop growing when the energy required to stretch an added protofibril exceeds the energy of bonding. The fact that fibres are under tension accounts for the observation that fibres making up a clot are very straight under most circumstances, as observed by confocal microscopy of native fibrin clots (Fig. 1.8). Additionally, fibres being under tension are likely to have important consequences for the mechanical properties of the clot, although these consequences are still largely unknown.

Figure 1.7. Scanning electron micrograph of fibres in a fibrin clot. The surface appearance of the fibres shows that they are twisted structures. Magnification bar = 1μm (J.W. Weisel 1987).

The fibrils making up the fibres branch, leading to a complex three-dimensional branched network (Fig. 1.8). This property of branching is essential for the properties of fibrin since it leads to the production of a space filling gel.

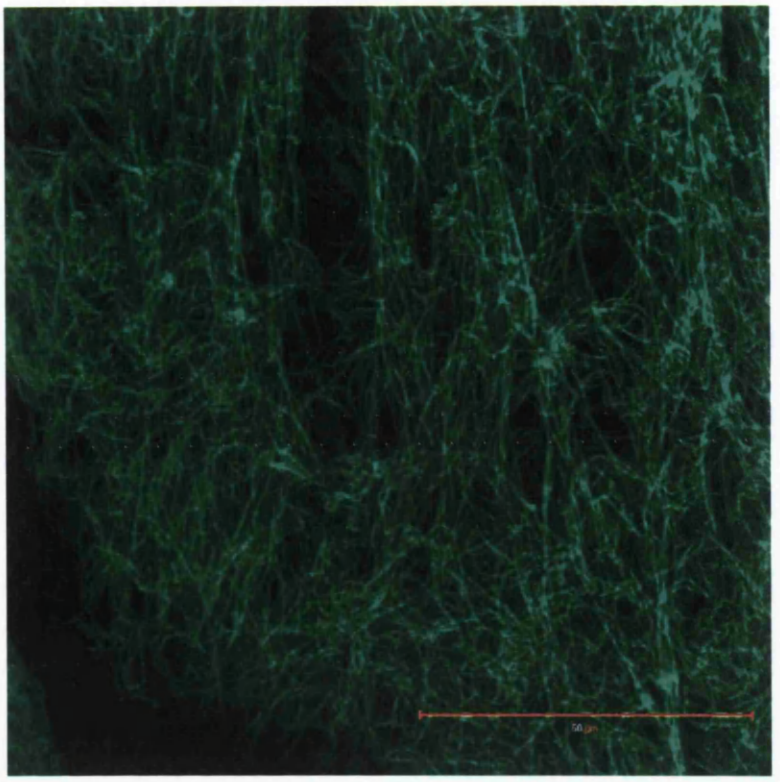

Figure 1.8. Confocal light micrograph of fibrin clot. Magnification bar = 50 μm.

The physical and mechanical characteristics of clot networks vary greatly depending on the conditions of polymerisation. As touched upon earlier, the network is further stabilised in the presence of factor XIIIa through the formation of N^{ϵ}-(γ-glutamyl)lysine isopeptide bonds (cross-links or ligations)(Lorand *et al.*, 1968; Matacic and Loewy, 1968; Pisano *et al.*, 1968).

1.2.5 Stabilising the Fibrin Structure

Blood coagulation factor XIII (FXIII) is a zymogen of tetrameric structure (A2B2) containing two potentially active A subunits (FXIII-A) and two inhibitory/carrier B subunits (FXIII-B). The clot is stabilised by the formation of covalent bonds introduced by the plasma transglutaminase, Factor XIIIa (Lorand, 2001), which is necessary to make fibrin resistant to mechanical and proteolytic insults, and hence prevent bleeding.

About half of the total Factor XIII in blood arises from platelets, which contain dimers consisting of only two A chains. The three-dimensional structure of the recombinant A chain of human Factor XIII was determined by X-ray crystallography, showing that each A chain is folded into four domains, known as the catalytic core, β sandwich, barrel, and barrel 2 (Yee *et al.*, 1994).

The 731 amino acid A subunits contain the active site cysteine, while the 661 amino acid B units serve as carrier proteins. A cellular form of FXIII that contains only two A chains exists in platelets, monocytes and macrophages. FXIII is activated by thrombin, which cleaves the peptide bond between Arg37 and Gly38 of the A subunit and releases a 37 amino acid amino-terminal activation peptide. The presence of fibrin accelerates the activation of FXIII by thrombin. In the presence of calcium, the A subunit dimer then dissociates from the B subunits and undergoes a conformational change that exposes the active site. Activated factor XIII (FXIIIa) catalyzes the formation of the γ-glutamyl-ε-lysine peptide bonds between the γ and α chains in non-covalently bound fibrin polymers. FXIIIa also incorporates the adhesive proteins, fibronectin and thrombospondin, and the antifibrinolytic protein, α-2-antiplasmin, into the fibrin clot via similar linkages. The net result is a stable clot that is relatively resistant to shear forces and fibrinolysis. The introduction of these cross-links has dramatic effects on the viscoelastic properties of fibrin (Roberts *et al.*, 1973; Mockros *et al.*, 1974). The stiffness of the clot is increased substantially and the creep or irreversible deformation is nearly eliminated.

In addition to its role in blood coagulation, FXIII also contributes to extra cellular matrix remodelling, tissue repair, and cell adhesion and migration (Siebenlist *et al.*, 2001). A recent study suggested that un-activated FXIII is capable of cross-

linking both fibrin and fibrinogen. While the physiological implications of these findings are not clear, it is possible that un-cleaved FXIII may contribute to cross linking in the early phases of fibrin clot formation (Wolberg *et al.*, 2003).

The effects of cross-linking on the mechanical stability of clots are an important part of blood clotting. The rare patients lacking Factor XIII generally have serious bleeding problems (Lorand, 2000). It is not known whether the lower stiffness or higher degree of inelastic deformation of clots without cross-links or both is responsible for the bleeding problems.

1.2.6 Calcium Binding

Calcium ions are indispensable for the structural stability and functional integrity of fibrinogen (Godal, 1960). Conformational or other structural or functional changes of the molecule accompany the removal of calcium (Blomback *et al.*, 1966; Haverkate and Timan, 1977). Fibrinogen has both strong and weak binding sites for calcium ions. High affinity binding sites for calcium are present in the C-terminal part of the γ chains, with residues Asp318, Asp 320, Gly324, Phe322, and two strongly bound water molecules providing coordination in sites with amino acid sequence homologous to the EF hand calcium binding site in calmodulin (Spraggon *et al.*, 1997; Yee *et al.*, 1997). However, the calcium binding loop γ311-336 is not a classic EF hand, but a unique structure. The dissociation constant for calcium at these binding regions is such that these sites will be fully occupied in plasma fibrinogen.

Some lower affinity binding sites are associated with interactions of the C-terminal Bβ chain with the coiled-coil backbone (Odrljin *et al.*, 1996). Other low-affinity sites are less well defined.

When Ca^{2+} binding at 10^{-4} M was followed during clotting, this revealed two sites involved (Mihalyi, 1988). The localisation of these was not possible from these experiments. However, this became apparent when the relationship of release of fibrinopeptides during clotting with thrombin and the binding of calcium was studied. It appeared that binding of calcium and release of fibrinopeptide B are

strongly related. Calcium binding was reduced, if not abolished, when the peptide remained attached to its original position. When released, a parallel calcium binding followed. This suggested that the calcium-binding site and the peptide bond cleaved by thrombin to release fibrinopeptide B must be close neighbours. Fibrinopeptide A and its release did not appear to be involved with calcium binding, but appears to be important for modulating fibrin polymerisation by enhancing lateral aggregation to form thicker fibres.

All the above facts propose that the tight structure of the N-termini of the fibrinogen molecule contain the two crucial Ca^{2+} binding sites, the polymerisation site and possibly the sites governing the conformational change of the fibrinogen molecule after thrombin action in the presence of calcium.

1.3 Effect(s) of Albumin on Fibrin Network Formation

In addition to forming fibrous clots and acting to aggregate platelets, fibrinogen is involved in other intermolecular interactions through its binding to various proteins and cells. Fibrin can interact with several cell types, including endothelial cells, smooth muscle cells, fibroblasts, leukocytes and keratinocytes. Fibrin can bind to and accumulate the cells required for the inflammatory response and for tissue repair at the site of damage. Importantly, fibrin also has the capacity to bind to several different proteins, including fibronectin, albumin, thrombospondin, von Willebrand factor, fibrulin, fibroblast growth factor-2, vascular endothelial growth factor, and interleukin-1. Binding of fibrin to these proteins often results in a change to the structure and properties of the blood clot. The importance of albumin in the evolution of the fibrin clot network is discussed here.

Torbet *et al.*, (1986) used Magnetic birefringence to monitor the kinetics of thrombin-catalyzed fibrin polymerization in model systems of increasing complexity, (i.e., fibrinogen solutions, fibrinogen/albumin mixtures) and in plasma containing free calcium, which is the physiological condition. The introduction of albumin into fibrinogen solutions was shown to shorten the lag period and enhance fibre thickness. The polymerization progress curves are sigmoidal at zero or low albumin

concentrations, but at physiological and higher concentrations, they become hyperbola-like from the end of the lag period. They conclude high albumin concentration has thus induced a change in the assembly kinetics.

Galanakis *et al.*, (1987) identified a new property of human albumin. They proposed albumin enhances formation of fine fibril (or leptofibril) structures during fibrin gelation, and by nephelometric and electron microscopic measurements, this property is independent of and synergistic with that of fibrinogen. They examined fibrin aggregation using physiologic temperatures and pH and albumin-fibrin concentration ratios below those at which the known accelerating effect on fibrin aggregation occurs. An albumin concentration dependent decrease in gel turbidity maxima was consistently demonstrable in buffers containing or lacking (2-5 mM) $CaCl_2$. Rates of fibrin aggregation as well as those of fibrinopeptide release were not affected by albumin.

Computed from wavelength dependence turbidity measurements, albumin decreased the average mass: length ratio from 8.24×10^{11} to 4.26×10^{11} Daltons/cm or from that of an approximately six to a three protofibril-thick strand. It also decreased the mean fibril radius from 48.5 to 36.4 nm but had no effect on fibril density.

Electron microscopic measurements of cross-sectional fibril widths, performed on sections of glutaraldehyde-fixed gels, disclosed differences between albumin-containing and control gels which were significant by chi 2 analysis (P greater than 0.001). Fibril groups of 7-20- and 21-40-nm width together comprised 77% of fibrils formed in the presence of albumin (n = 251) compared to 30% of controls (n = 309). Conversely, coarser fibrils of 41-60- and 61-97-nm width together comprised 23% of fibrils formed in the presence of albumin and 70% of controls.

Carr *et al.*, (1987) reported an interaction of albumin with polymerizing fibrin, resulting in a narrowing of gel fibres, utilizing turbidity techniques, the impact of human albumin on gels of human fibrin, clotted with human thrombin. The addition of albumin, at concentrations from 3 to 30 microM, to 1 mg/ml fibrin gels produced less than a 10% change in either the kinetics of turbidity increase or the subsequent fibre mass-length ratio.

With these findings, they concluded that it seems unlikely albumin imposes a physiologically significant influence on fibrin polymerization. Although, structural changes secondary to albumin-mediated enhancement of factor XIII activity remain a possibility.

A few years later Blomback *et al.*, (1990) studied hydrated fibrin gels by confocal laser 3D microscopy, liquid permeation and turbidity. The gels from normal fibrinogen were found to be composed of straight rod-like fibre elements which sometimes originated from denser nodes. In gels formed at increasing thrombin or fibrinogen concentrations, the gel networks became tighter and the porosity decreased. The fibre strands also became shorter. Gel porosity of the network decreased dramatically in gels formed at increasing ionic strengths. Shortening of the fibres were observed and fibre swelling occurred at ionic strength above 0.24.
Albumin, when present in the gel forming system, affected the formation of more porous structures with strands of larger mass-length ratio and fibre thickness confirming earlier work proposals. These types of gels were also formed in plasma. In gels formed when factor XIIIa instead of thrombin was used as catalyst for gelation, showed a completely different structure in which lumps of polymeric material were held together by a network of fine fibre strands.

In conclusion, we can state, albumin affects the lateral aggregation of fibrin, altering the thickness of the fibrin fibre in the formation of the network structure.

1.4 Mechanical Properties of Fibrin

As discussed above, the mechanical properties of fibrin are vital for its functions. In haemostasis, the clot must form a plug to stop bleeding and this structure must be strong enough to withstand the pressure of arterial blood flow. The mechanical properties of a thrombus will determine how it responds to flowing blood, including elastic or plastic deformation and embolization. Furthermore, the mechanical properties of a thrombus, determined by all the components including fibrin, will determine how it responds to treatments, such as coronary artery angioplasty. Fatah *et al.*, (1996) and Scrutton *et al.*, (1994) revealed through epidemiological studies, a relationship between myocardial infarction and clot mechanical properties. In vitro formation of fibrin clots from patients with myocardial infarction present tight and rigid fibrin network structures compared to controls. Clots that are very stiff could be more friable or clots that are more viscous or plastic could have a greater tendency to embolise, although almost nothing is known about the relationship between mechanical properties of fibrin and these pathological properties.

Embolisation of thrombi is one of the most important issues facing clinicians today. It is not known why some individuals with deep vein thrombosis or atrial fibrillation tend to embolise and others do not. The critical answers to these questions may lie in understanding the mechanical properties of fibrin.

Clinicians rely on laboratory tests to assess coagulation state of system such as thromboelastography (TEG). It is a method used widely to measure blood clot formation time, and clot elasticity. Hence, provides a rapid diagnosis of disease states and an assessment of therapeutic options. A distinct disadvantage of the use of thromboelastography is many of the parameters measured by this method have not been related to the normal viscoelastic properties used to characterise materials and have no physical meaning except in comparison with other such thromboelastography measurements.

Numerous components present in plasma and its surrounding environment can affect the properties and behaviour of the evolving fibrin networks. These factors have a great impact on fibrin's mechanical properties. The thrombin concentration

can have an effect on the clot structure, especially if the rate of generation of fibrin monomer by cleavage of fibrinopeptides becomes limiting relative to the rate of polymerisation (Blomback *et al.*, 1994; Weisel and Nagaswami, 1992). In fact, there are many factors, including calcium and chloride ion concentration, pH and other plasma proteins, that wield an influence on clot structure and mechanical properties by affecting the rates of various steps in the polymerisation process (Weisel and Nagaswami, 1992).

Fibrin is a viscoelastic polymer, which means that it has both elastic and viscous properties (Ferry, 1998). Hence, the mechanical (viscoelastic) properties of fibrin may be characterised by stiffness or storage modulus, G′ (representing solid or elastic deformation) and the loss modulus, G″ (representing viscous inelastic behaviour). These parameters will determine how the clot responds to the forces applied to it in flowing blood. For example, a stiff clot will not deform as much as a less stiff one with applied stress. A clot with a greater inelastic component will deform permanently with stress, while one with a greater elastic component will return to its original shape.

1.5 Fibrin Degradation (Fibrinolysis)

The clot acts as a temporal plug for haemostasis or wound healing, so there are natural mechanisms in the body for the efficient removal of fibrin. Various proteolytic enzymes can dissolve fibrin depending on the circumstances, but the most specific mechanism involves the fibrinolytic system. The dissolution of fibrin clots under physiological conditions involves the binding of circulating plasminogen to fibrin, and the activation of plasminogen to the active protease, plasmin, by tissue type plasminogen activator (tPA), also bound to fibrin. Plasmin cuts away a covalently linked α chain, which is not in the triple coiled region. The rather open mesh like structure of a blood clot gives plasmin relatively free access to

polymerized fibrin molecules thereby facilitating clot lysis. The components of the fibrinolytic system are schematically shown in Figure 1.9.

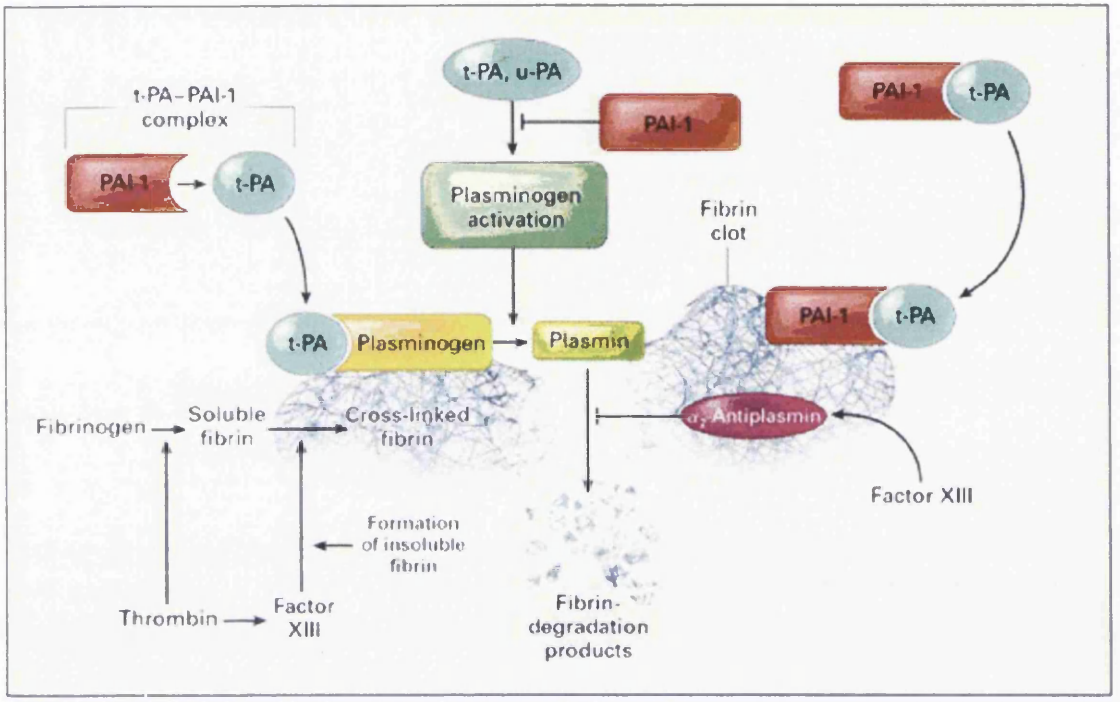

Figure 1.9. Fibrinolytic Pathway: Activation and Inhibition.

Plasmin is formed through the proteolytic cleavage of 82 kD zymogen plasminogen, a protein that is homologous to the zymogen of the blood-clotting cascade. There are several serine proteases that activate plasminogen, most notably the 54 kD enzyme urokinase, which is synthesized by the kidney and occurs as its name implies in the urine. Tissue type plasminogen activator (t-PA), a 70 kD protein, occurs in vascular tissues and activates plasminogen. In addition, activated Hageman factor, in the presence of prekallikrein and HMK activates plasminogen. Fibrinolysis is not as simple as just a zymogen and its activators. There are several inhibitors. The 70 kD glycoprotein α2-antiplasmin forms an irreversible equal molar complex with plasmin and prevents it from binding to fibrin. The α2-antiplasmin cross-links to fibrin α chains through the action of activated FSF (XIIIa) thereby making hard clots less susceptible to fibrinolysis than soft clots.

Plasminogen activators have received considerable medical attention aimed at rapidly dissolving the blood clots responsible for heart attacks and strokes. Streptokinase, a 45 kD protein produced by certain streptococci, has shown considerable utility in this regard particularly when administered together with aspirin. Despite its name streptokinase exhibits no enzymatic activity. Rather, it acts by forming a tight 1:1 complex with plasminogen that proteolytically activates other plasminogen molecules. The use of streptokinase to dissolve clots has the apparent disadvantage that it activates plasmin to degrade fibrinogen as well as fibrin thereby increasing the risk of bleeding problems, particularly strokes.

1.6 Factors Affecting Fibrin Clot Architecture

Because fibrin structure/function is one of the major final phenotypes arising from activation of the fluid phase of coagulation, it would be expected to be a synthesis of all the genetic and environmental interactions described in the coagulation cascade. However, despite the observation that individual coagulation factors have a relatively high degree of heritability, this does not appear to be the case for fibrin structure/function, wherein the major influence, appears to be environmental. Several factors influencing clot architecture have been identified within the coagulation system, including altered fibrinogen concentrations (Blomback *et al.*, 1989), genetic variations in fibrinogen and factor XIII (Ariens *et al.*, 2000), and altered concentrations of thrombin and prothrombin (Wolberg *et al.*, 2003).

However, the concentration of thrombin present at the time of gelation has the most profound physiologic influence on fibrin clot structure (Carr and Hermans, 1978; Blomback *et al.*, 1989; Blomback *et al.*, 1994). Extremely low concentrations of thrombin (<0.1 U/ml) are sufficient to cleave fibrinopeptides and catalyze fibrin polymerization. These low thrombin concentrations produce fibrin clots that are turbid and composed of thick, loosely-woven fibrin strands. Higher concentrations of thrombin produce fibrin clots that are composed of relatively thinner, more tightly-packed fibrin strands.

Variations in fibrinogen concentrations modify the polymerisation pattern and overall clot structure. Increasing fibrinogen concentration causes the lag period to become shorter, whilst the overall turbidity and maximum fibre size increases. There are more fibres present, and these fibres are longer compared to fibres formed at lower fibrinogen concentrations. The maximum rate of assembly is also increased (Roberts *et al.*, 2001). However, it is important to note that at very high fibrinogen concentrations the opposite effect may occur (Ferry and Morrison, 1947). The fact that fibrinogen concentrations can fundamentally change clot structure and properties is clearly of physiological importance and may help to explain why increased fibrinogen levels are a risk factor for cardiovascular disease.

1.7 Disorders of Fibrinogen

Several cardiovascular risk factors are associated with abnormalities in fibrinogen. As a result of the acute-phase response or through other poorly understood mechanisms, elevated plasma fibrinogen levels have been observed in patients with coronary artery disease, diabetes, hypertension, peripheral artery disease, hyperlipoproteinemia and hypertriglyceridemia. Additionally, pregnancy, menopause, hypercholesterolemia, use of oral contraceptives and smoking lead to increased plasma fibrinogen levels. Although rare, there are inherited disorders in fibrinogen. These disorders include afibrinogenemia (a complete lack of fibrinogen), hypofibrinogenemia (reduced levels of fibrinogen) and dysfibrinogenemia (presence of dysfunctional fibrinogen). Afibrinogenemia is an autosomal recessive disorder characterised by the complete absence of detectable fibrinogen. Analysis of the three fibrinogen genes in affected individuals led to the identification of several causative mutations (Brennan *et al.*, 2001). Most cases were identified to be caused by defective fibrinogen synthesis as a result of truncating mutations in the Aα chain gene.

Hypofibrinogenemia is characterised by fibrinogen levels below 100 mg/mL (normal is 250-350 mg/mL) and can be either acquired or inherited. Symptoms of

hypofibrinogememia are similar to, but less severe than, afibrinogenemia. Dysfibrinogenemias are characterised by structural changes in the fibrinogen molecule that result in detectable alterations in clotting or other functional properties of the molecule. Most congenital defects are rare but offer the opportunity to study the effects of these molecular changes on fibrinogen function. These mutations are listed and described in several reviews (Roberts *et al.*, 2001) and in addition, a database of all mutations is maintained on the website http://www.geht.org/pages/database fibro uk.html.

Molecular defects that give rise to dysfibrinogenemias are commonly caused by single base mutations that lead to the substitution of a single amino acid. Other mutations can give rise to a stop codon, resulting in a truncation of one of the chains. Finally, base deletions or additions may occur, with consequences for fibrinogen structure and function. Any such mutation can cause thrombosis, bleeding, or be asymptomatic, depending on their functional effects. Furthermore, they can affect fibrinopeptide cleavage, fibrin polymerisation, cross linking, fibrinolysis, or platelet aggregation. Since dysfibrinogenemias are discovered in a clinical setting, there are nearly always some functional effects.

The most consistent evidence that alterations in fibrin structure directly contribute to disease derives from studies of hereditary dysfibrinogenaemias. Approximately, 55% of dysfibrinogenaemias are asymptomatic and 25% are associated with bleeding tendencies. In the remaining 20%, thrombotic events with or without haemorrhage can be found. The mechanism by which the risk for pathological events is increased is still unknown and is likely to be specific for each individual defect. However, in thrombophilic dysfibrinogenaemias, common features emerge; many mutations lie within the αC domains or within the thrombin cleavage sites of the Bβ chain, leading to impaired polymerisation and structural alterations. In depth studies of the ultra structure of some of the thrombophilic fibrinogens have consistently found the formation of networks characterised by thin fibres and small pores, heightened resistance to fibrinolysis and increased clot stiffness (Collet *et al.*, 1996; Marchi *et al.*, 2000; Lefebvre *et al.*, 2004). These structural features were also found in clots formed of plasma taken from men who had suffered myocardial infarction at a young age (Fatah *et al.*, 1996).

Chapter 2

An Introduction to Rheology

2.1 Introduction

2.1.1 What is Rheology?

Rheology, defined as *"the science of deformation and flow of matter"* (Bingham, 1929), plays important roles in everyday life, examples of which may be found in areas such as food production/consumption, the formulation and use of cosmetics; and in various aspects of lubrication and tribology.

Rheology is a relatively unique branch of science, as it is one of the very few disciplines that can trace its exact date of conception. On April 29, 1929 in Columbus, Ohio, a decision was made to form a permanent association for a new discipline named rheology. The founding members included E.C. Bingham, W.H. Herschel, H. Freundlich, W. Otswald, L. Prandtl and S. Blair. Following its conception, the main areas of study focused on complex model formations (differential, integral, network, repetition, molecular models etc) and significant new theories and effects (shear flows, no slip boundary conditions, dynamic studies, thixotropy, flow instabilities) along with a vast number of other important subjects.

Rheology is principally concerned with the properties of matter that determines its behaviour when a mechanical force is exerted on it. Rheology is distinguished from fluid dynamics in that it is concerned with all three of the traditional states of matter rather than only with liquids and gases. The results of rheology provide a mathematical description of the viscoelastic behaviour of matter with significant advances been made in biorheology, in polymer rheology and suspension rheology. There has also been a significant appreciation of the importance of rheology in the chemical processing industries.

The main objectives of rheological measurement are:

- To determine the behaviour of a non-Newtonian fluid using suitably defined material functions. The aim is to seek a correlation between molecular structure and material behaviour or between material properties and observed behaviour in a practical situation.

- To predict the behaviour in non-simple flows from the results of simple rheometrical experiments.

To determine rheological measurement, the following rheological techniques are implemented:

- Material flows through a tube or between rotating surfaces.
- The variation of deformation with time under the action of forces or the variation of force with time when a body is held in a deformed state is measured.
- Oscillatory, usually harmonic forces are applied to a material and its response is measured.

2.1.2 Fundamentals of Rheology

From a rheological viewpoint, matter can be broadly described by three rheological states: the Hookean elastic solid, the Newtonian fluid and viscoelastic, and hence by the relationships between stress and strain, or strain-rate, for each state (Ferry, 1980).

2.1.3 Different Flow Properties

Flow is a term used to describe the deformation process that occurs in a material by the relative movement of adjacent points within it. A shear flow may be caused by a tangential force applied per unit area (termed the shear stress) and results in the development of a velocity gradient when the material flows (Figure 2.1). Flow may also be initiated by imparting a velocity gradient to a material and thus producing a resultant stress in the material.

The governing constitutive equation for shear stress is given by,

$$\sigma = \frac{F}{A} \qquad (\mathrm{Nm^{-2}} \text{ or Pa}) \qquad (2.1)$$

Where F is the force applied (N) and A is the area (m^2).

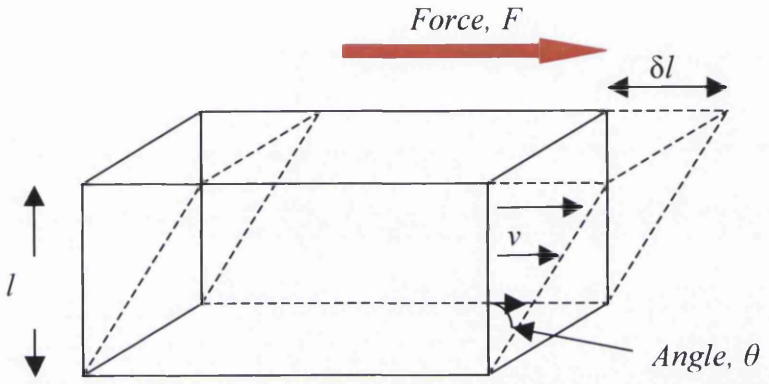

Figure 2.1. Diagram showing the formation of a velocity (v) gradient.

A constitutive equation is one that specifies the properties of the material in a manner, which is independent of the size or shape (i.e. geometry) of the body, and depends only on its material nature (Tschoegl, 1989). These equations are commonly known as 'rheological equations of state'. In order to apply these constitutive equations it is assumed that the material is both isotropic and homogeneous, incorporating no 'end-effects' (Walters, 1975).

When a body of material is subjected to a set of forces it may experience motion as a whole, or its various particles may experience motion with respect to each other. The latter situation is known as *deformation* (Tshoegl, 1989). The extent of deformation can be measured by the *strain*, which may be *reversible* or *irreversible* i.e. reversible in the sense that deformation is recoverable and hence *elastic*; whereas in *viscous* materials such deformations are irreversible.

A *simple shear strain* may be defined by dividing the relative displacement of two layers of the material by their separation (Figure 2.1) and the governing rheological equations of state for shear strain and the rate of shear strain (also termed

the *shear rate*) are given below. The shear strain, γ, and the angle of shear, θ, can be calculated using trigonometry from,

$$\gamma = \tan\theta = \frac{\delta l}{l} \tag{2.2}$$

Where the shear strain, γ, is the displacement, δl, divided by the layer separation, l.

If the deformation is sufficiently small, θ will equal γ i.e. $\theta \approx tan\ \theta$.

The rate of strain (or shear rate) is expressed as,

$$\dot{\gamma} = \frac{d\gamma}{dt} \tag{2.3}$$

The resistance to flow (also called the 'internal friction' of a material) is characterised by *viscosity*. When a shear stress is applied to a *Newtonian* fluid, the flow persists as long as the stress is applied. In contrast, for a *Hookean* solid, the application of a shear stress results in an instantaneous *deformation* of the material. Once the deformed state is reached there is no further movement; it continues as long as the stress is applied.

2.1.4 The Hookean Theory of Elasticity

In an ideal *elastic* system, the strain deformation depends only on the stress, σ, which is imparted, and *vice versa*. The corresponding strain, γ, will change instantaneously when the stress changes, and will remain constant until the stress changes further or until it is removed. The relationship between σ and γ is *Hooke's law* after Robert Hooke[1], and the constant of proportionality, *G*, is called the *elastic modulus* (or *shear modulus*),

$$G = \frac{\sigma}{\gamma} \qquad \text{(Pa)} \qquad (2.4)$$

2.1.5 The Newtonian Theory of Viscosity

If the stress applied to a material is removed after deformation has been induced, the strain may or may not return to zero. If the strain does not eventually return to zero, it is considered that flow has occurred (Whorlow, 1992). In a material presenting a purely viscous response to applied stress, the stress is proportional not to the strain, but to the rate of strain. Sir Isaac Newton[2] (1687) hypothesised that "the resistance which arises from the lack of slipperiness of the parts of the liquid, other things being equal, is proportional to the velocity with which the parts of liquid are separated from one another". The rate of strain and stress are directly proportional, with constant of proportionality being the resistance to flow, later termed the *viscosity*, η. So for a Newtonian system, the flow will continue as long as the stress is applied (Reiner, 1929).

[1] **Robert Hooke**, (18 July 1635 – 3 March 1703) was an English natural philosopher and polymath who played an important role in the scientific revolution, through both experimental and theoretical work. Hooke is known principally for his law of elasticity (Hooke's Law).

[2] **Newton, Sir Isaac** (1642-1727), mathematician and physicist, one of the foremost scientific intellects of all time. His accomplishments in mathematics, optics, and physics laid the foundations for modern science and revolutionized the world.

Thus, the shear viscosity is given by,

$$\eta = \frac{\sigma}{\dot{\gamma}} \qquad \text{(Pa.s)} \qquad (2.5)$$

A plot of σ against the shear rate is called a flow curve (or rheogram), where the gradient equals the viscosity. (Figure 2.2). For a Newtonian fluid the viscosity is independent of the shear rate and produces a straight line passing through the origin. At constant temperature and pressure, the following characteristics demonstrate Newtonian behaviour (Barnes *et al.*, 1989):

- The only stress generated in simple shear flow is the shear stress, σ.
- The shear viscosity does not vary with the shear rate, $\dot{\gamma}$.
- The viscosity is constant with respect to the time of shearing, and the stress in the liquid falls to zero immediately on conclusion of shearing. Any further shearing, however long the period of resting between measurements, will give a viscosity as previously measured.

Deviation from these characteristics is classed as *non-Newtonian* behaviour.

2.1.6 Non-Newtonian Behaviour

A non-Newtonian fluid is a fluid whose flow properties are not described by a single constant value of viscosity. The majority of process products and fluids commonly encountered in engineering show a departure from Newtonian behaviour to greater or lesser degrees. Dispersions, emulsions and polymer solutions are examples of systems which display non-Newtonian behaviour. In the vast majority of these cases, the viscosity decreases with an increase in the shear rate and such systems are termed *shear-thinning* (or pseudoplastic) but other behaviour may be encountered (see Figure 2.2).

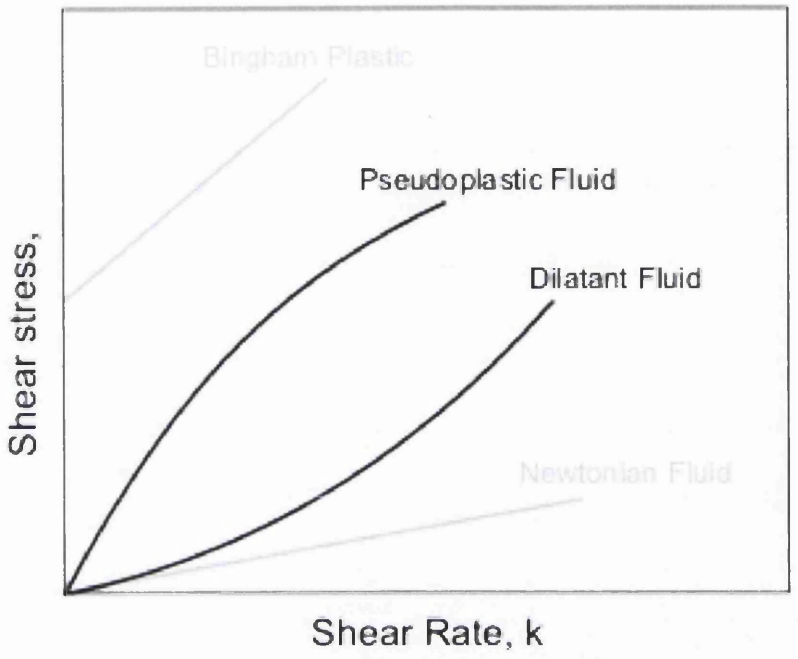

Figure 2.2. A representation of various types of flow curves.

2.2 A Rheological Perspective of Gelation

2.2.1 Definition of a Gel?

Gels are a class of materials widely used in industries and commonly encountered in our daily life. Presently, the study of gels has become an active area of research with scientists from a broad range of fields such as physics, chemistry, or biology, all working on gels of very different types. This makes it difficult to reach a consistent definition as to what constitutes a gel. This uncertainty in the definition of a gel is best described by the famous statement of Jordan-Lloyd in 1926 "the colloid condition, the gel, is one which is easier to recognize than to define".

Flory (1941; 1942) and Stockmayer (1944; 1952) reached an important milestone in the definition of a gel by attempting to include structural criteria, such as the presence of an infinite network, three-dimensional structure, coherence, and connection. Flory (1953) demonstrates that at the gel point, the effective molecular weight of a polymer solution goes to infinity. Physical interpretation suggests that at the gel point the shear viscosity extends to infinity ($\eta_0 \rightarrow \infty$) and the equilibrium modulus is 0 ($G_\infty = 0$).

The currently widely accepted topological (structural) definition of a gel is a three-dimensional network consisting of basic elements connected in some way and swollen by a substantial quantity of solvent (Guenet, 1992). This is largely consistent with the gel definition given by Hermans in 1949, "a coherent system of at least two components, which exhibits mechanical properties characteristic of a solid, where both the dispersed component and the dispersion medium extend themselves continuously throughout the whole system".

The topological definition of gels has yielded the mechanical (rheological) definition: a gel should display solid-like behaviour. The mechanical definition implies, in more scholarly terms, that a gel should be characterised by an elastic modulus at zero frequency and be self-supporting, i.e., maintaining its initial shape with time if left on its own. However the mechanical definition does not apply in the

strict sense to some of the physical gels that deform almost permanently when subjected to mechanical stress, but nobody would question their gel status and would immediately abandon the idea of a very viscous solution from their macroscopic aspects.

2.2.2 Gelation

Gelation is the process or series of processes, which leads to the formation of a gel. The importance of gelation is extensive and occurs in many areas of science, engineering, and biomedicine. It highlights the mechanism of blood clotting, and repeatedly used in developing structural engineering materials such as composites, and thin films such as paints, surface coatings, adhesives, absorbents, and sealants.

During the gelation process, a linear polymer chain crosslink's either with itself to form intramolecular cycles ('rings'), or with another chain intermolecularly to create branched chains. The size of the branched chains increases as more and more intermolecular crosslink's are formed. The molecular weight increases faster and faster and eventually becomes infinite as one of the branched chains span the whole system. This critical point for a branched chain of infinite size to appear is called the '*gel point*'. It is a transitional, metastable state between liquid and solid, which shares the rheological properties of both. The system is a liquid before cross-linking starts and remains liquid-like until the viscosity becomes infinite at the gel point. After the gel point, an equilibrium modulus develops and grows as cross-linking proceeds. A schematic of the viscosity and equilibrium shear modulus development before and after the gel point is shown in Fig. 2.3.

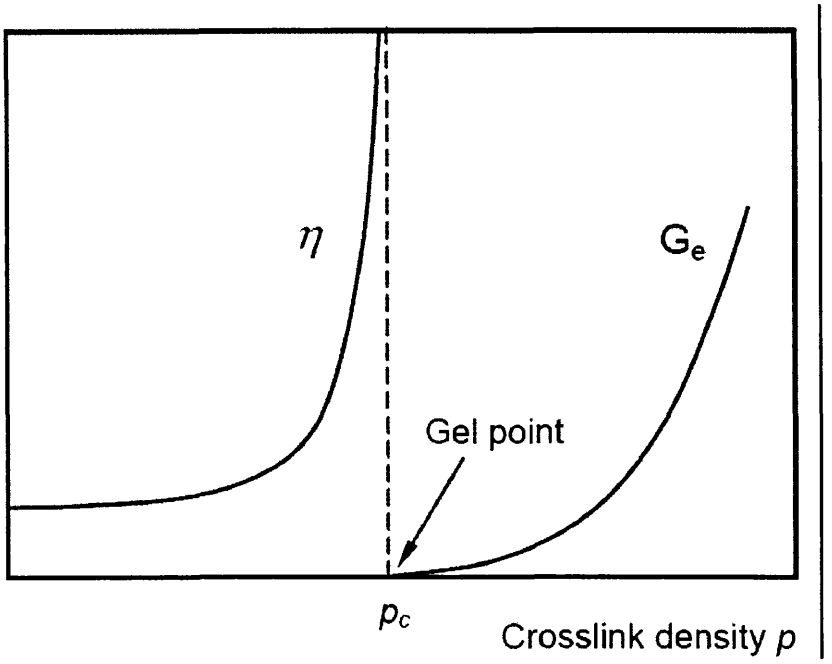

Figure 2.3. Schematic of viscosity and equilibrium shear modulus development during gelation.

The various physicochemical properties of gels are strongly related to the structure of cross-linking polymer chains and bridging sites, and the network structure is an essential factor in the characterisation of the intrinsic properties of gels. The study of dynamic process of network formation (gelation) is, therefore, quite important for revealing the structure and properties of the gel, since the structure of a three-dimensional network is dependent on the kinetics of junction formation. Many studies have been conducted on various aspects of gelling systems of flexible polymers.

A liquid such as water may be sufficiently described as a Newtonian fluid and an ideal elastic solid may be described as Hookean. The process of gelation usually involves a rheological transition, from a Pre Gel viscoelastic liquid to a Post Gel viscoelastic solid. The mechanical microstructure of a system changes from one in which, initially, only a short-range connectivity is present, to one in which structural self-similarity is sample spanning (Carnali, 1992). The gel point as discussed by Winter and Chambon (1986) represents a unique state for the material as it describes the very first moment in time that viscoelastic *solid like* behaviour is observed. Prior

to the Gel Point, the system is a '*sol*' as it is soluble in good solvents. Beyond the Gel Point the material is a '*gel*'. Numerous studies of its rheological properties have been undertaken and these have contributed to the following glossary of terms which are regularly used to define some rheological properties of gelling systems and which will be used throughout the remainder of this Thesis.

Gel Time, t_{gel} – this is defined as the time taken to reach the Gel Point.

Gelation Time, t – this is defined as the time elapsed during the gelation of the gelling system. When the system reaches its Gel Point, the Gelation Time is equivalent to the Gel Time, by definition.

Gel Temperature, T - this is the temperature at which the gelation experiment is conducted. Most experiments are conducted under isothermal conditions and in these cases the Gel Temperature remains constant throughout the experiment.

Critical Gel Temperature, T_{gel} - this is defined as the temperature at which the gelling system would take infinite time to reach the Gel Point. Therefore, a system undergoing gelation at the Critical Gel Temperature will equilibrate at its Gel Point. In the case of physical gels, if the temperature is higher than the Critical Gel Temperature, then the system will never gel, i.e. it will never reach a Gel Point.

Regardless of the type of gelation, the fundamental characteristic remains the same, i.e. there is a transition between the 'sol' state and the 'gel' state, which can be identified in a number of ways, one of which is to study variation in the rheological behaviour of the material in relation to the gel point.

The work herein is concerned with the gel point and its accurate identification for the bio gel fibrinogen by appropriate rheological techniques. This is a matter of considerable scientific and medical interest as the understanding of the gelling properties and mechanisms for many bio-gels are unknown.

2.3 *Theory of Linear Viscoelasticity*

The word 'viscoelastic' means the simultaneous existence of viscous and elastic properties in a material. It is not unreasonable to assume that all real materials are viscoelastic, to varying degrees, in that they exhibit both elastic and viscous responses to applied stress. Linear viscoelasticity implies that the ratio of applied stress to strain for any shear history as a function of time alone, and is independent of stress magnitude (Van Wazer *et al.*, 1963); and each stress applied to a material produces a strain which is independent of that produced by any other stresses. Hence, in the limit of infinitesimal deformation, viscoelastic behaviour can be described by linear differential equations with constant coefficients. Such behaviour is termed linear time-dependent or linear viscoelastic (Ferry 1980). Many materials display linear time dependent behaviour under small strain deformation i.e. below the Linear Viscoelastic Limit. This may be described in terms of the *Boltzmann Superposition Principle*, which states the total strain experienced by a material is equal to the sum of all the changes induced in the material by the applied stress, throughout its history. The development of the mathematical theory of linear viscoelasticity is based on this principle, which may also be expressed in terms of the following linear constitutive equation (Ferry 1980),

$$\sigma(t) = \int_{-\infty}^{t} G(t-t')\dot{\gamma}(t')dt' \qquad (2.6)$$

Where G (t) is the stress relaxation modulus and the integration is performed over all past times, t′, up to the current time, t.

Physically, what occurs when a stress or strain is applied to a material is that structural rearrangements take place within it. The time required for these rearrangements can be either relatively short or relatively long depending on the types of structure involved i.e. orientation of bonds, types of bonding etc. Structural rearrangements on a local scale (involving short-range interactions) are relatively rapid but occur more slowly over long ranges. If a materials structure changes so

rapidly that the time for these changes are negligible compared to the timescale of the experiment, then a purely viscous response would be observed and the energy associated with the deformation is dissipated as heat. However, when the material rearrangements take a long time in relation to the timescale of the external stimulus, then an elastic response is perceived. If the energy associated with the deformation is stored, then it may be recovered elastically upon release of the applied force. Thus, a given material can behave like a solid or a liquid on the time scale of the deformation process.

The scaling of time in rheology is described by means of the 'Deborah number' defined by Prof. Markus Reiner (1969). The Deborah number is a dimensionless number, used in rheology to characterise how "fluid" a material is. Even some apparent solids "flow" if they are observed long enough; the origin of the name, coined by Prof. Markus Reiner, is the line "The mountains flowed before the Lord" in a song by prophetess Deborah recorded in the Bible (Judges 5:5). The idea is that *everything flows if you wait long enough, even the mountains*! Formally, the Deborah number is defined as the ratio of a relaxation time, characterizing the intrinsic fluidity of a material, and the characteristic time scale of an experiment (or a computer simulation) probing the response of the material. The smaller the Deborah number, the more fluid the material appears.

The Deborah number, N_D, is defined as,

$$N_D = \frac{\tau_{mat}}{\tau_{exp}} \tag{2.7}$$

where τ_{mat} and τ_{exp} are the material and experimental times respectively.
Small Deborah numbers correspond to situations where the material has time to relax (and behaves in a viscous manner), while high Deborah numbers correspond to situations where the material behaves rather elastically.

Sinusoidally varying perturbation of a material about a 'rest state' is one of the most common ways by which the relative contribution of the viscous and elastic components of a materials response to applied stress can be simultanously resolved. This refers to a technique whereby the stress or strain is applied in a harmonically time-varying sinusoidal oscillation.

2.3.1 The Significance of Linearity

So far we have considered elastic behaviour and viscous behaviour in terms of the laws of Hooke and Newton. These are linear laws, which assume direct proportionality between stress and strain, or strain rate, whatever the stress. Within this linear framework, an extensive range of rheological behaviour can be accommodated. However, this framework is incredibly restrictive. The range of stress over which materials behave linearly is invariably limited, and the limit can be quite low. In other words, material properties such as shear modulus and viscosity can change with the applied stress.

In most rheological experiments concerning the measurement of viscoelastic behaviour, it is enviable (and generally necessary) to ensure that measurements are conducted within the Linear Viscoelastic Range, LVR, of the material and in which the theory of Linear Viscoelasticity may be invoked (Ferry, 1980).

Non-linear effects, and their importance, have been recognised since the early days of rheology. Such effects include the plasticity of paints (Bingham and Green, 1925), "structure viscosity" of colloidal solutions (Otswald, 1925), the Non-Newtonian viscosity of polymer solutions (Reiner et al, 1933), and investigations of thixotropic behaviour of several materials (Freundlich, 1935). It is also important to appreciate that non-linear rheological phenomena may occur for a variety of reasons. Malkin (1995) proposed to classify three distinguished levels of non-linearity in rheological behaviour of materials.

There is a group of phenomena, which originate as a consequence of finite elastic deformations. This is weak non-linearity related to equilibrium properties of a

matter. This level is characterised by permanent material constants and unchanging relaxation properties of a medium.

The second level can be characterised as strong non-linearity. It is related to reversible structure changes, developing in time and connected with changes in relaxation properties of a matter. This group of effects can be treated as kinetic phenomena.

Finally, the third level of non-linearity is connected with breaking or phase transitions induced by deformations. This leads to the most severe consequences and can be treated as effects of thermodynamic nature.

When applying dynamic testing, such as oscillatory shear techniques, the transition from classical linear to non-linear viscoelastic response is dependent on strain amplitude. Linear viscoelastic response (LVR) is observed during small amplitude oscillatory shearing, while non-linear viscoelastic response is observed during finite strain amplitude oscillatory shearing (Ferry 1980). The strain amplitude for the onset of non-linear viscoelastic response varies for different materials and is termed the materials critical strain, γ_c, which determines the range of the LVR. In the case of controlled stress rheometry, it is necessary to find the LVR in terms of a maximum permissible stress to achieve a linear response, termed the critical stress, σ_c.

2.3.2 Determination of the Linear Viscoelastic Range

The linear viscoelastic range of transient systems such as gelatin can prove extremely difficult to find. The classical method for determining a materials linear viscoelastic range involves measuring G′ whilst increasing the stress/strain in a stepwise manner (stress/strain sweep) and documenting any sudden change (this being outside the linear viscoelastic range) in the phase angle of the material over a specific range of stresses/strains. However it must be stressed that such criterion cannot be applied to transient systems, such as gelling systems to the reality that the

dynamic moduli, G′ and G″, are time-dependent, subsequently it is then difficult to analyse G′ as a function of applied stress/strain alone as the rheological properties of the material change during the time required to perform a stress/strain sweep. However it can also be said that the material is most susceptible to non-linear effects at the pre-gel regime so a study of the material above the critical gel temperature may perhaps give a crude upper limit estimation of the stress or strain applicable for the material to be in the linear viscoelastic range. It was found appropriate that the linear viscoelastic range could be maintained for stress/strain of no more than 20 %. The work established here, limited stress/strains to 10 % where possible to ensure the linear viscoelastic range.

2.4 Dynamic Testing

2.4.1 Small Amplitude Oscillatory Shear

Dynamic mechanical measurements that involve the application of an oscillatory stress or strain provide a process to examine the viscous and elastic behaviour of a viscoelastic material simultaneously. Small amplitude oscillatory shear involving an imposed stress of angular frequency, ω, will result in a harmonic strain response proportional to the stress amplitude, and with phase lag, δ, relative to the stress, which is independent of the applied stress amplitude (Ferry, 1980). Since stress is directly proportional to strain for a Hookean solid, a sinusoidal stress wave produces a strain wave, which is in phase with the stress wave. Conversely, for a Newtonian liquid, stress is directly proportional to strain rate, and a sinusoidal stress wave produces a strain wave, which are 90° out of phase (i.e. in quadrature, by $\pi/2$ radians).

Figure 2.4 shows a controlled harmonic shear stress,σ applied to a linear viscoelastic system resulting in a harmonic strain response waveform with a phase lag, δ to the stress.

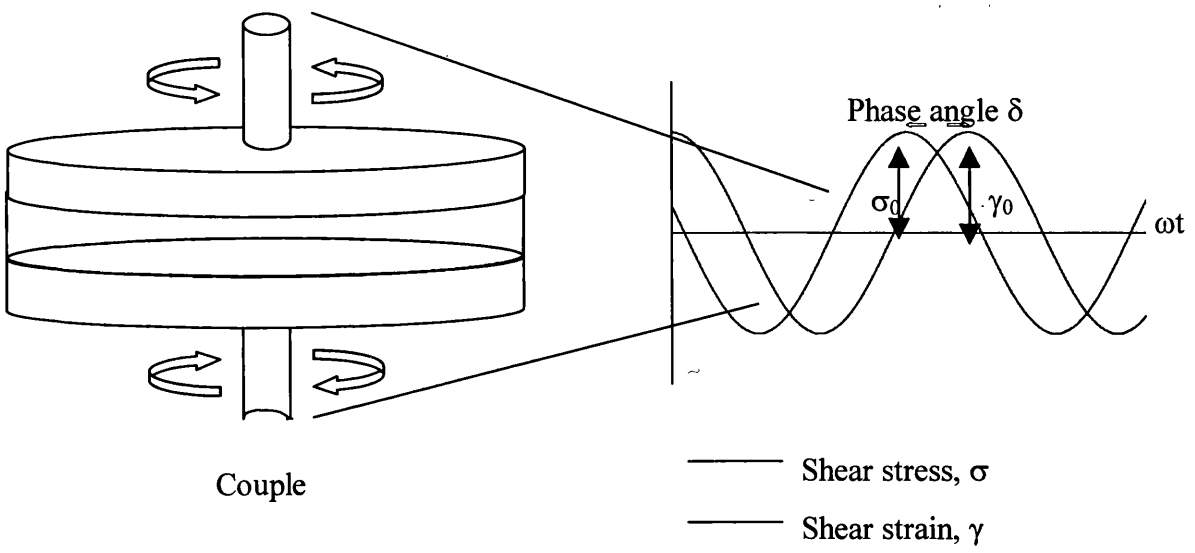

Figure 2.4. Oscillatory shear strain out of phase with an applied shear stress, by a phase angle, δ as a function of dimensionless time, ωt.

Considering Figure 2.4, if the stress excitation varies as,

$$\sigma = \sigma_0 \cos \omega t \tag{2.8}$$

where σ_0 is the maximum stress amplitude (Pa), ω is the angular frequency (rad s^{-1}), and t is the time (s).

Then for a Hookean solid, the strain response, γ, will vary as,

$$\gamma = \gamma_0 \cos \omega t \tag{2.9}$$

For a Newtonian liquid, the strain response, γ, will vary as,

$$\gamma = \gamma_0 \sin \omega t \tag{2.10}$$

where γ_0 is the maximum strain amplitude.

In response to an imposed small amplitude oscillatory shear stress, within the linear regime, viscoelastic materials produce a corresponding sinusoidal strain wave with a phase lag behind the stress wave by more than 0°, but less than 90° (as shown in Figure 2.4). *The phase difference* is denoted by the *phase angle,* δ.

Hence,

$$\gamma = \gamma_0 \cos\left(\omega t - \frac{\pi}{2}\right) = \gamma_0 \sin \omega t \tag{2.11}$$

The harmonic shear stress and harmonic shear strain can be expressed as complex quantities,

$$\sigma^* = \sigma_0 e^{i(\omega t)} \tag{2.12}$$

and

$$\gamma^* = \gamma_0 e^{i(\omega t - \delta)} \tag{2.13}$$

where $i = \sqrt{-1}$ and $e^{i\delta} = \cos\delta + i \sin\delta$ and δ is in radians. A complex shear modulus, G* may be defined as,

$$G^* = \frac{\sigma^*}{\gamma^*} = \left(\frac{\sigma_0}{\gamma_0}\right) e^{-i\delta} \tag{2.14}$$

where

$$G^* = G' + iG'' \tag{2.15}$$

G′ and G″ represent the real and imaginary parts of G* respectively.

G′ is the *storage modulus* (Pa), and is defined as the stress in phase with the strain in a sinusoidal shear deformation, divided by the strain. G′ represents the magnitude of the elastic component of a material and is a measure of the energy stored and recovered per cycle of sinusoidal deformation.

G″ is the *loss modulus* (Pa), and is defined as the stress 90° out of phase with the strain divided by the strain in a sinusoidal deformation. G″ represents the magnitude of the viscous component of a material and is a measure of the energy dissipated per cycle of sinusoidal deformation.

For viscoelastic systems,

$$\gamma = \gamma_0 \cos(\omega t - \delta) \tag{2.16}$$

Using simple trigonometric relations, equation (2.16) yields,

$$\gamma = \gamma_0 \cos\delta \cos\omega t + \gamma_0 \sin\delta \sin\omega t \tag{2.17}$$

$\gamma_0\cos\delta$ is the amplitude of the component of strain in phase with the stress, alternatively $\gamma_0\sin\delta$ is the component of strain in quadrature with the stress.
G′ and G″ can be defined thus,

$$G' = \left(\frac{\sigma_0}{\gamma_0}\right)\cos\delta \tag{2.18}$$

and

$$G'' = \left(\frac{\sigma_0}{\gamma_0}\right)\sin\delta \tag{2.19}$$

By definition,

$$\tan\delta = \left(\frac{G''}{G'}\right) \tag{2.20}$$

where tan δ is known as the loss tangent

Phase relationships may also be expressed in terms of the dynamic complex viscosity, η*,

$$\eta^* = \eta' - i\eta'' \tag{2.21}$$

thus

$$\eta' = \frac{G''}{\omega} \tag{2.22}$$

and

$$\eta'' = \frac{G'}{\omega} \tag{2.23}$$

η′ is the dynamic viscosity which is defined as the stress in phase with the rate of strain, divided by the rate of strain in a sinusoidal deformation.
η″ is the stress 90° out of phase with the rate of strain, divided by the rate of strain in a sinusoidal deformation.
These are related to the complex shear modulus, G*, as,

$$G^* = \omega\eta'' + i\omega\eta' \tag{2.24}$$

This theory provides a basis for the interpretation of linear viscoelasticity.

2.5 *Gel Point Theory*

In simplistic terms, a gelling system can be described as developing from an initial Newtonian liquid pre-gel state, characterised by a Newtonian viscosity, μ, to an elastic solid, post-gel state, characterised by an elastic modulus, G, via an intermediate transitional critical gel state. However this representation is fundamentally limited and can be improved by the addition of viscoelastic liquid and viscoelastic solid states that are found directly before and after the gel state.

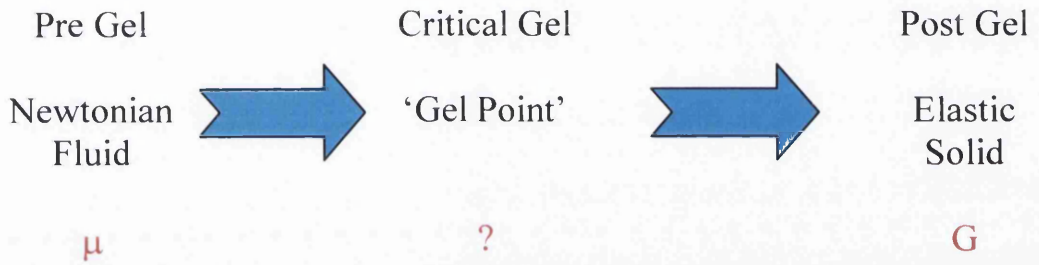

Figure 2.5. Simple rheological representation of gelation.

However this Model is in no way a sufficient or realistic representation of the true gel system. Although with the addition of the viscoelastic states that border the critical gel region, plus a description of the critical region itself the system will become more realistic.

As gelation proceeds and the gelling system approaches the gel point, the zero shear rate viscosity, η, increases until, at the gel point, it diverges to infinity. At the gel point, the relaxation time also diverges to infinity but the equilibrium modulus G_e is still zero (Winter, 1989). Beyond the gel point, at increased extents of reaction when the newly formed macroscopic network structure begins to coexist with the remaining molecules, the equilibrium modulus becomes non-zero. Thereafter, the equilibrium modulus proceeds to increase steadily as the network stiffness increases until it reaches a maximum plateau value as the reaction ceases. A schematic diagram indicating the variation in the physical properties with time during gelation is presented in Figure 2.3 (Lipshitz and Macosko, 1976).

Malkin (1992) gave a suitable model that would give a suitable representation of a gelation process by describing viscoelastic solid and viscoelastic liquid behaviour of a material which would take into account multiple associated relaxation times and strengths. The new model expands upon simple models such as the Maxwell model giving:

$$G^*_{(\omega)} = G_e + \sum_{i=1}^{K} G_i \frac{i\omega\tau_i}{1+i\omega\tau_i} \qquad (2.25)$$

Where τ_1 and G_i are associated pairs of relaxation times and strength's respectively, from which G′ and G″ may be calculated.

$$G'_{(\omega)} = G_e + \sum_{i=1}^{K} G_i \frac{(\omega\tau_1)^2}{1+(\omega\tau_1)^2}$$

$$G''_{(\omega)} = \sum_{i=1}^{K} G_i \frac{\omega\tau_1}{1+(\omega\tau)^2}$$

In this way the basic Newtonian liquid – critical gel – elastic solid gelation model is extended to a more detailed model, however a complete rheological representation of gelation requires that the critical gel be modelled (Winter and Chambon 1987).

2.6 *Critical Gel Behaviour – Winter-Chambon Gel Equation*

During gelation, a material changes from one in which only short-range connectivity is present to one in which structural self-similarity is sample spanning. The point at which connectivity first spans the entire sample is the *Gel Point*. A polymer at the Gel Point is characterised by a limiting behaviour for both the viscoelastic liquid in the Pre Gel and viscoelastic solid in the Post Gel region. Its molecular weight distribution (or polydispersity) is infinitely broad and a critical gel consists of many different species of molecular clusters (such as precursor molecules or monomers and oligomers). The largest cluster spans the entire sample size and is identified by an infinite relaxation time and an infinite molecular weight. Prior to the gel point, the system is a 'sol' as it is soluble in good solvents. Beyond the gel point, the material is a 'gel'. As a result, critical gels have unusual rheological properties, in the sense that they behave neither wholly like solids nor liquids. Their distinguishing feature is the macroscopic molecular structure that permeates the whole volume of a sample of material.

The most rigorous and widely accepted definition of the sol-gel transition in rheological terms arises from the seminal studies of the gelation of polydimethylsiloxane and polyurethane chemical-gel systems by Winter and Chambon (1986, 1987). That work demonstrated that the sol-gel transition is characterised by power-law behaviour of the time dependent, linear, shear stress relaxation modulus, G (t) that tends to infinity at the Gel Point. Such behaviour is frequently observed in studies of relaxation processes in complex materials near a critical state;

$$G_{(t)} \propto t^{-\alpha} \qquad (2.26)$$

Where $0 < \alpha < 1$ over several decades of time.

Cross-linking polymers at the sol-gel transition have been suggested as model systems for studies of algebraic decays (Schiessel and Blumen, 1995) and a widely used model for the description of the sol-gel transition is based on the percolation model (Scanlan and Winter, 1991). From theories of gelation which describe cluster

growth processes, a power law cluster number distribution, N_M, at the Gel Point in terms of cluster mass, M, is predicted (Scanlan and Winter, 1991);

$$N_M \propto M^{-\tau_p} \tag{2.27}$$

where

τ_p is the polydispersity index

Further, the cluster radius, R_c, is also a power law at the Gel Point with the exponent of fractal dimension, d_f, such that;

$$R_c \propto M^{\frac{1}{d_f}} \tag{2.28}$$

Thus, the stress relaxation exponent, α, has been expressed by several authors in terms of fractal dimension. The most simplistic relationship of Muthukumar (1985) and Cates (1985) for a mono-disperse solution of polymers, for which Rouse dynamics prevail, gives;

$$\alpha = \frac{d_f}{d_f + 2} \tag{2.29}$$

For an arbitrary fractal dimension, in the range $1 \leq df \leq 3$, this model restricts the stress relaxation exponent to $1/3 \leq \alpha \leq 3/5$. Muthukumar and Cates (1986) applied this to the analysis of experimental results obtained for polyethylene. Muthukumar (1989) introduced corrections for the polydispersity of the critical gel, by incorporating a polydispersity index, τ_p, into Equation 2.29, to give a stress relaxation exponent of;

$$\alpha = \frac{d_f(\tau_p - 1)}{(d_f + 2)} \tag{2.30}$$

which, if the fractal dimension is arbitrary and $1 \leq d_f \leq 3$, is restricted to $3/5 \leq \alpha \leq 1$.

Following studies of the influence of excluded volume, Hess *et al.*, (1988) suggested that cluster growth models using rigid bonds may not properly describe the dimensions of the critical gel. Assuming the excluded volume to be completely screened, the prediction for a polydisperse material becomes;

$$\alpha = \frac{d(d+2-2d_f)}{(2(d+2-d_f))} \tag{2.31}$$

Where

d is the Euclidean dimension of the embedding space,

Which for partial screening of the excluded phase predicts values of the stress relaxation exponent in the range $0 \leq \alpha \leq 1$ for the physically acceptable fractal dimension range of $1 \leq d_f \leq 3$.

Scanlan and Winter (1991) have reported experimentally determined values of stress relaxation exponent, α, ranging from 0.18, for crystallising polypropylene to 0.92, for a blend of the medium chain length prepolymer PS442 and an inert Poly(dimethylsiloxane) polymer PS042. This work and related studies has established the validity of the Winter-Chambon Gel Equation (as it is now known), a power law stress relaxation model characterising the relaxation modulus at the Gel Point,

$$\alpha(t) = S\int_{-\infty}(t-t')^{-\alpha}\dot{\gamma}(t')dt' \tag{2.32}$$

The power law relaxation of G(t) at the Gel Point can now be represented by,

$$G(t) = St^{-\alpha} \tag{2.33}$$

where

S is the strength of the three-dimensional gel structure

α is the network stress relaxation exponent ($0 < \alpha < 1$)

This equation provides a theoretical basis for the determination of gel point by oscillatory shear testing. For oscillatory shear data $G'(\omega)$ and $G''(\omega)$ can be obtained from the relaxation modulus G(t) [Equation 2.6] as follows:

$$G'(\omega) = \omega \int_0^\infty G(t)\sin(\omega t)dt \tag{2.34}$$

$$G''(\omega) = \omega \int_0^\infty G(t)\cos(\omega t)dt \tag{2.35}$$

It is important to note that the Gel Equation is restricted to small strains, in accordance with the requirements of linear viscoelastic theory. In the frequency domain, the dynamic moduli can be related as in Equations 2.34 and 2.35 and at the Gel Point $G'(\omega)$ and $G''(\omega)$ are proportional to ω^α. The Kramers–Kronig relation (Kramers 1926; Kronig 1927) states that one should be able to calculate the real (G′) part from complete knowledge of the imaginary (G″) part and *vice versa*, as the same parameters define both. This relationship is restricted to the region of power law frequency dependence and is only valid if either $G'(\omega)$ or $G''(\omega)$ is known over the entire frequency range ($0 < \omega < \infty$).

The relation yields,

$$\frac{G'(\omega)}{\omega^2} = \frac{2}{\pi}\int_0^\infty \frac{G''(x)/x}{\omega^2 - x^2} \tag{2.36}$$

And the complex modulus, G^* of the critical gel is given by:

$$G^*(\omega) = \Gamma(1-n)S(i\omega)^n \tag{2.37}$$

With G'(ω) and G''(ω) being related by:

$$G'(\omega) = \frac{G''(\omega)}{\tan\left(\frac{n\pi}{2}\right)} = \frac{\pi}{2\Gamma(n)\sin\left(\frac{n\pi}{2}\right)} S\omega^n \tag{2.38}$$

Where

Γ denotes the gamma function that is related to the phase angle δ by,

$$\tan\delta(\omega) = \frac{G''(\omega)}{G'(\omega)} = \tan\left(\frac{n\pi}{2}\right) \qquad 0 < \alpha < 1 \tag{2.39}$$

Thus in the linear viscoelastic response, both the storage modulus and the loss modulus of the critical-gel display a power law dependence (with an equal relaxation exponent, n) on the frequency of oscillation. As a result the phase angle δ has frequency *independence* at the gel point (Winter and Chambon, 1986; Winter, 1987; Cuvelier and Launay, 1990; Carnali, 1992). For systems in which n = ½ (δ = 45°), the crossover of G' and G'' may be used to determine the gel point.

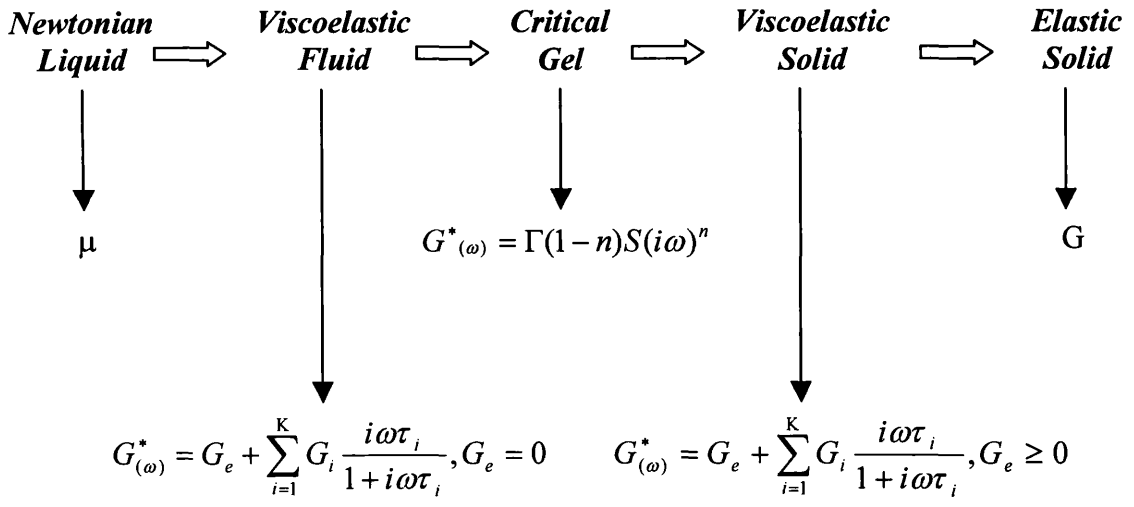

Figure 2.6. The Winter-Chambon Critical Gel Model.

The Winter-Chambon critical gel model presents the opportunity to study exponents of a gelling system at the gel point providing a valuable insight into the structural rearrangements and mechanical response of a wide range of gels. This definition of the Gel Point, developed using the Winter-Chambon model will be used throughout the remainder of this Thesis, to be exploited using rheometrical techniques.

Chapter 3

Rheological Characterisation of Fibrin-Thrombin Gel Formation

3.1 Significance of viscoelasticity in Fibrin Clots

Fibrin gels are the main structural scaffolds of the haemostatic plug or 'clot' formed in vertebrate blood coagulation, a process involving significant changes in viscoelasticity. Some of these changes have been associated with pathologies such as myocardial infarction (MI), peripheral vascular disease, cancer and diabetes, and have stimulated studies of the rheological properties of coagulating blood, particularly their viscoelastic properties (Scrutton *et al.*, 1994; Chmiel *et al.*, 1990). Viscoelastic properties are among the most sensitive measures of fibrin polymerization and clot structure and there are numerous examples of their physiological importance (Weisel, 2004). The connection between disease and clot properties has been reported in terms of an increased incidence of MI in patients with elevated levels of plasma fibrinogen, which results in less deformable clots (Scrutton *et al.*, 1994). After MI, fibrin clots have reduced permeability and a lower fibre mass-to-length ratio (Fatah *et al.*, 1996). There are independent associations between permeability and the extent and severity of coronary artery stenosis and also of fibrinolytic activity. Patients with severe coronary artery disease have more rigid clot structures and an elevated fibre mass-to-length ratio (Greilich *et al.*, 1994).

The goal of relating the viscoelastic properties of fibrin gels to their microstructure using complementary rheological and morphological studies has been an area of significant activity (Ryan *et al.*, 1999; Thurston and Henderson, 1992). The three-dimensional network of fibrin fibres formed in vivo constitutes the primary micro structural basis of a blood clot (Ferri *et al.*, 2002) and the time required for conversion of fibrinogen into a clot network is an important clinical parameter called the 'clotting time' (CT). This term is often used synonymously with the term 'Gel Point' in studies of fibrin gels (Blomback and Bark, 2004) and it is evidently important to consider the rheological significance of the Gel Point insofar as it defines the transition between a (pre-gel) viscoelastic fluid and a (post-gel) viscoelastic solid. The key point in the context of blood coagulation is that the fibrin clot is required to perform a haemostatic function and the properties of a viscoelastic *solid* are necessary in order to perform this function. It follows that rheometrical

detection of the Gel Point provides a basis for assessing the clotting time in terms of the establishment of an *incipient* clot.

Quantitative correlations between the structural features of clots and their rheology have not been made, partly due to the difficulty of quantitatively analysing the morphology of the often-complex fibrin networks. Many rheological studies have attempted to use the rheometrical detection of a Gel Point (GP) as a basis for assessing the clotting time (CT) of blood. However, it is important to distinguish between those techniques, which provide absolute values of viscoelastic properties, under conditions where the length scales and timescales of deformation are controlled, and other (usually less sophisticated) techniques, which provide more qualitative assessments of rheological changes during coagulation. In particular it is necessary to consider how the choice of rheological technique can have a significant impact on the assessment of clotting time.

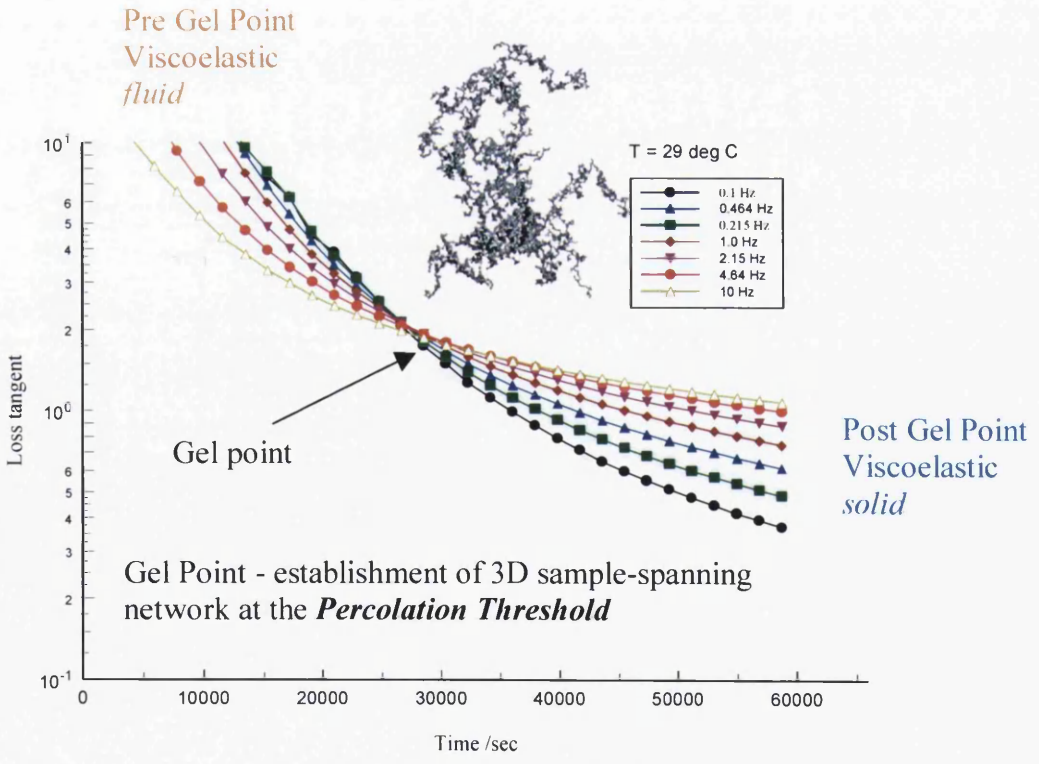

Figure 3.1. Defining the gel point and relationship to fractal dimension, d_f.

In various disease states, such as atherothrombotic vascular disease, prothrombotic processes reportedly lead to an increased density of fibrin strands in blood clots, thereby creating a more "compact" network structure (Isogai *et al.*, 1973). In studies of whole mature blood clots it has been observed that such "tight" (or "compact") clot structures are associated with several pathological states (Scott *et al.*, 2004). Thus the ability to characterize the microstructure of clots formed under pathological conditions has potential relevance to the diagnosis of various diseases.

In the present work, we study the mechanical properties of fibrin gel structures using rheological techniques, and where appropriate provide a quantitative basis for the characterisation of incipient clots based on a fractal description of their microstructure (fig. 3.1).

3.2 Characterisation of Fractal Microstructure

Fractal geometry has been extensively utilised in medicine and biology to characterise branching network structures and polymerising gel-networks, including those formed in fibrin-thrombin gels (Losa *et al.*, 2002). The percolation theory of gelation and polymerisation provides a means of analysing the fractal characteristics of the sample-spanning fibrin network cluster formed at the sol-gel transition (Goldenfeld and Goldbart, 1992). For a length scale $L >> \varepsilon$ the polymerising system is macroscopically homogeneous whereas for $L << \varepsilon$ the sample-spanning network cluster is a 'self-similar' 'fractal' object whose mass M scales with ε as $M \sim \varepsilon^{df}$ where d_f is known as the fractal dimension of the network.

Many rheological studies have investigated fibrinogen-thrombin gels (e.g. Ferry and Morrison, 1947; Jamney *et al.*, 1983; Scrutton et al., 1994), however, they have been confined to measurements of the evolution of viscoelasticity (in terms of elastic modulus, G', and loss modulus, G'') at a single frequency. These measurements present information on the evolving mechanical properties of the gel but no previous rheological study has attempted to relate the viscoelastic properties of fibrin-thrombin gels to the fractal characteristics of their underlying microstructure. Such work has however been reported for incipient clots formed in

samples of human blood (Evans *et al.*, 2008a, 2008b). An analysis of the viscoelastic data obtained at the Gel Point of samples of whole blood drawn from healthy individuals indicates that normal blood has a clearly defined value of d_f within a narrow range, which represents an index of clotting in health. The microstructure of the incipient clot is characterized by a fractal dimension d_f= 1.74 (+ 0.07) which is commensurate with that reported to arise in other biological systems which involve disordered branching fractal structures.

3.3 *Determination of Rheological Characteristics in Small Amplitude Oscillatory Shear*

3.3.1 *Frequency Sweeps*

The rheometrical procedure known as a frequency sweep involves the measurement of rheometrical functions G′ and G″ over a desired frequency range in a series of (single frequency) sequential tests. In these tests the frequency usually decreases from a maximum value stepwise manner (however it can be started from a minimum and increased). Frequency sweeps can however take a long time to produce one sweep through the whole range of frequencies (depending on the range). This in itself can lead to the phenomena of Mutation Number.

3.3.2 *Mutation Number*

When dealing with transient or time dependent materials, such as gelling systems, error may be introduced into the measurement due to the materials instability. Single point measurements must span a time period equal to that over which the material can respond to the imposed stress or strain (Mours and Winter, 1994). Therefore the material must be stable or at least 'quasi-stable' to produce meaningful rheological measurements. In a frequency sweep, data is obtained by shearing the material at different frequencies sequentially; systematic error is

introduced due to the fact that the material is changing with time. Winter *et al.*, (1988) define the dimensionless Mutation Number, N_{mu}, for quantifying the change of a dynamic rheological property during the frequency sweep of experiment as

$$N_{mu} = t_{\exp} \frac{1}{G} \frac{\partial G}{\partial t} \tag{3.1}$$

Where

t_{exp} is the duration of the experiments

G may be replaced with any rheological parameter chosen

Mours and Winter (1994) define a characteristic time constant for the change in the material as the mutation time λ_{mu} where

$$\lambda_{mu} = \left[\frac{1}{G} \frac{\partial G}{\partial t} \right]^{-1} \tag{3.2}$$

The dimensionless Mutation Number can be combined with the Deborah Number, N_{De}, (Reiner, 1969),

$$N_{De} = \frac{\tau_d}{t_{\exp}} \tag{3.3}$$

Where

τ_d is the materials dominant relaxation time constant

To give a third dimensionless group,

$$N_{De} N_{mu} = \frac{\tau_d}{\lambda_{mu}} \tag{3.4}$$

Mours and Winter (1994) conclude that the sample can be considered 'quasi-stable' if $N_{De}N_{mu} << 1$, whilst a detailed relaxation model of the materials transient properties is required if $N_{De}N_{mu} > 1$ since the sample changes during the relaxation process. Examinations of the equations given above conclude that t_{exp} must be kept to a minimum for reliable data. In a study of the gelation of model polyurethanes, Mours and Winter (1994) identified $N_{mu} < 0.15$ as a cut-off point below which the sample could be assumed to be 'quasi-stable' i.e. in that study t_{exp} was required to be a minimum of seven times smaller than N_{mu}. This has implications for all rheological techniques applied to non-equilibrium systems, including Gel Point determination by oscillatory shear testing.

This requirement has prompted advances in the development of a frequency-multiplexing technique known as Fourier Transform Mechanical Spectroscopy, FTMS (Malkin *et al.*, 1984; Holly *et al.*, 1988).

3.4 Fourier Transform Mechanical Spectroscopy

Fourier Transform Mechanical Spectroscopy (FTMS) is a frequency 'multiplexing' technique, which combines several harmonics of varying frequencies to produce a composite non-sinusoidal waveform. In a controlled stress rheometer torque waveforms incorporating various oscillation frequencies are presented to the test material simultaneously, but the dynamic consequences of each are analysed separately using an appropriate Fourier analysis. In principle therefore, multi-frequency data may be obtained in a single test using FTMS.

In its most widely implemented form FTMS was developed by Holly *et al.*, (1988) using a controlled strain rheometer. It was revealed that multiple frequency values of the dynamic moduli could be acquired successfully in a single test for non-reacting polymeric liquids and a cross-linking polydimethylsiloxane (PDMS) gelling system. They concluded that FTMS had advantages over conventional frequency sweep methods (which require measuring dynamic properties for each individual

frequency) when dealing with *transient* systems due to the decrease in time of the rheological experiment, t_{exp}. For frequency sweep experiments:

$$t_{exp} = \sum_{f=f_f}^{f=f_h} \frac{\xi_f}{f} \qquad (3.5)$$

Where

ξ is the number of cycles per measurement at a frequency f

f_f is the lowest or fundamental frequency in the test (Hz)

f_h is the highest frequency in the test (Hz)

f is the frequency including all frequencies ranging from f_f to f_h (Hz)

For FTMS

$$t_{exp} = \frac{\xi_{f_f}}{f_f} \qquad (3.6)$$

Comparing the equations 3.5 and 3.6 it is evident that FTMS has considerable time saving qualities. FTMS is a potentially useful tool in attempts to detect the instant of gelation (the gel point). In terms of the Winter-Chambon gel equation, the gel point can be detected by a frequency independent phase angle. Therefore the multiple frequency capabilities of FTMS make it in principle the ideal technique for gel point determination. FTMS has also been applied to other gelling systems (In and Prud'homme, 1993, Malkin *et al.*, 1992) and the technique was successfully implemented to achieve dynamic properties at multiple frequencies in a single test for a model viscoelastic fluid (Davies and Jones, 1994).

3.4.1 Theory of FTMS

The basic aspects of FTMS were originally implemented on a controlled strain rheometer by Holly *et al.*, (1988); however the technique can be readily applied to controlled stress rheometers by simply exchanging strain γ with stress σ. In FTMS on a controlled stress rheometer the material is subjected to an oscillator stress σ.

$$\sigma = \sum_{i=1}^{m} \sigma(\omega_i) = \sum_{i=1}^{m} \sigma_i \sin \omega_i t \qquad (3.7)$$

Where

m is the number of frequency components

σ_i is the stress amplitude of the i^{th} component (Pa)

ω_i is the i^{th} angular frequency component (integer multiples of the fundamental frequency ω_f) (rad s^{-1})

The resulting complex strain response is recorded and broken down into its individual frequency components using an appropriate Fourier analysis (by the Fast Fourier Transform, FFT). From this the viscoelastic parameters $G'(\omega_i)$, $G''(\omega_i)$, and hence phase angle $\delta(\omega_i)$ can be calculated from the individual values of stress and strain at each individual frequency ω_i. A more comprehensive account of FTMS testing with inertial considerations is given in Davies and Jones (1994).

3.4.2 *Boltzmann Superposition Theory*

The Boltzmann Superposition Theory that highlights the Theory of Linear Viscoelasticity states that the total strain experienced by a material is equal to the sum of all the changes induced in the material by an applied stress throughout its past history (Ferry 1980). It follows that the total stress or strain, which is experienced by a material under FTMS testing, is equivalent to the sum of the individual stresses or strains associated with each constituent applied harmonic frequency of the composite FTMS waveform.

Figure 3.2 shows the result of combining three harmonic stress waveforms of frequency A, B and C with equal amplitude to give a composite stress waveform of varying amplitude. The maximum amplitude of which is almost 3 times greater than that of the individual constituent component waveforms.

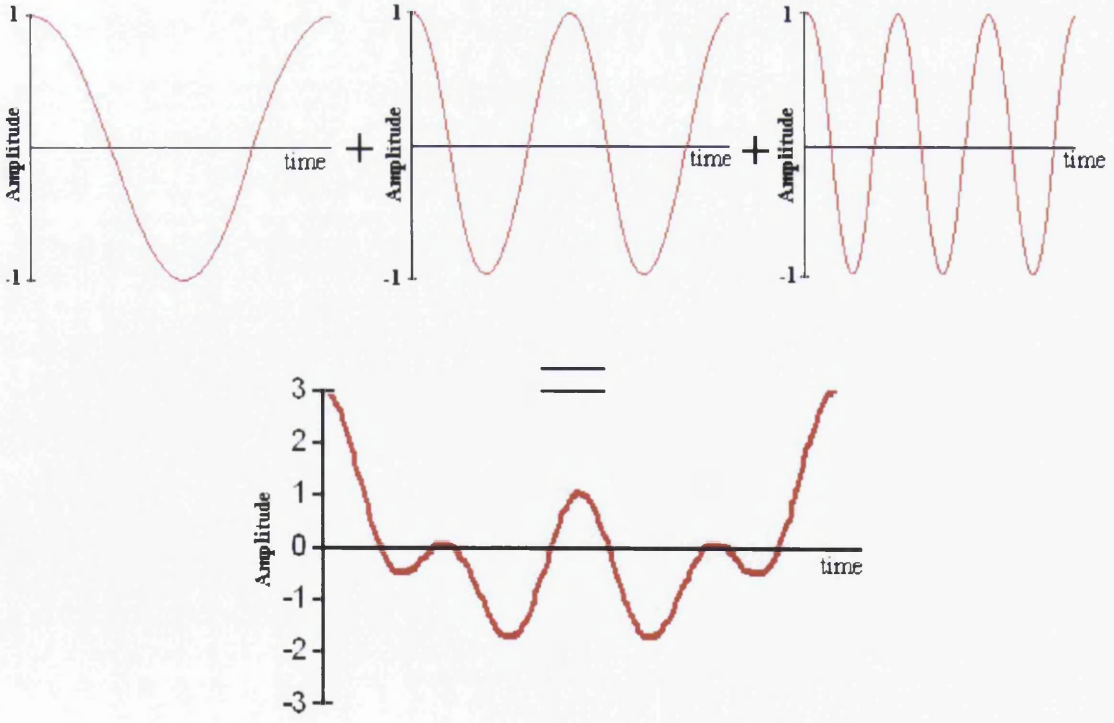

Figure 3.2. Graphical representations illustrating three single frequencies signals combined into one FTMS.

Given that FTMS is only valid in the Linear Viscoelastic Range, the total stress σ (or total strain γ) must not exceed the critical stress σ_c or the critical strain γ_c respectively. This will limit the number of harmonics that can be used in a single FTMS test because each individual component waveform will contribute a value of strain γ_i and these strain values must be of a certain magnitude to be resolvable for accurate measurements.

3.5 Controlled Stress Rheometry

Controlled Stress Rheometers are more appropriately termed controlled torque rotational rheometers, in which a test material is sheared between solid surfaces using an appropriate combination of rotating plates, cones or cylinders. A controlled stress dynamic test refers to an experiment in which the applied torque varies harmonically with time. Controlled stress rheometry employs non-resonant oscillations ('forced vibrations') to achieve experimentally determined values of torque and displacement, which, under appropriate conditions, may subsequently be converted to stresses and strains for the calculation of the viscoelastic parameters of interest.

Controlling the torque and measuring the resulting displacement is one of the earliest rotational rheometerical techniques for investigating a material's steady shear properties (Van Wazer *et al.*, 1963), however, in order to provide a comprehensive characterisation of viscoelastic properties, it is generally necessary to operate in dynamic or oscillatory mode. Jones *et al.*, (1984) reported that Controlled Stress Rheometers can be modified to operate in oscillatory mode and such instruments which subject a sample to small amplitude oscillatory shear, have been developed and used to study a wide range of systems such as oils (Conrad *et al.*, 1995), emulsions (Pal, 1997; Guerrero *et al.*, 1998), inks (Fernandez *et al.*, 1998) and gels (Carnali, 1992; Rueb and Zukoski, 1997; Rodd *et al.*, 2001).

3.5.1 TA Instruments AR-G2 Controlled Stress Rheometer

The controlled stress instrument used in the experimental work reported in this Thesis was a TA Instruments AR-G2 Controlled Stress Rheometer. The rheometer is equipped with Rheology Advantage Software, which includes Universal Analysis 2000 data analysis software. The rheometer (See Figure 3.3) consists of several key components, which are described below.

3.5.2 Mode of Operation

Rheological tests were conducted using an AR-G2 Controlled Stress Rheometer fitted with a double-gap (rotor o.d. 43.92 mm, i.d. 40.76 mm, stator i.d. 40.00 mm, cylinder immersed height 59.50 mm) measuring system for additional torque sensitivity. The system was maintained at the test temperature by means of a peltier temperature control system fitted to a recirculating water bath. In addition, a vapour hood was fitted to minimise any effects due to sample evaporation. Prior to each rheological test, the requisite volume of sample was transferred to the rheometer's measuring geometry, the sample being cooled ('quenched') as rapidly as possible to the test temperature (typically taking approximately 10 seconds).

Figure 3.3. TA Instruments AR-G2 Controlled Stress Rheometer.

3.5.3 Geometries

The geometry used throughout the investigation was the double gap viscometer (Fig 3.4). Moore and Davies (1956) developed the double gap viscometer; it doubles the effective cylinder surface area and greatly reduces the area of the base of the cylinder.

Furthermore, as the gap at the bottom was made equal to the mean annular gaps the shearing conditions were approximately uniform throughout the fluid being tested. Moore and Davies arranged that,

$$R_2/R_1 = R_4/R_3 \tag{3.8}$$

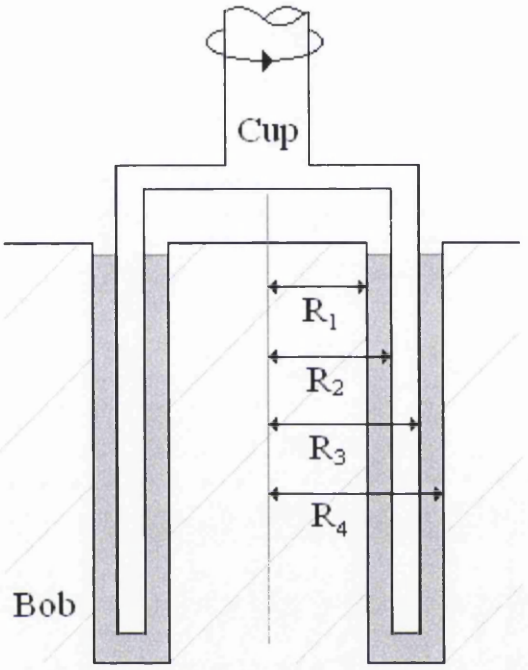

Figure 3.4. Schematic diagram illustrating a cross section of the Double Gap Viscometer Geometry.

So that the shear stresses at the two inner surfaces, σ_1 and σ_3, were equal and those at the two *outer* surfaces, σ_2 and σ_4, were also equal. Full analysis of this statement can be found in *Rheological Techniques by R.W. Whorlow section 3.2 page 140 (1980).* The uniform shearing conditions are not the only advantage of the double gap viscometer possibly its most important advantage is the large surface area it offers compared with other geometries. The increased surface will enhance the sensitivity of the measured response of the fluid obtained by the rheometer, making the double gap viscometer ideal for system where low torques must be applied. A disadvantage

of the geometry is that with certain materials the system can be difficult to clean, plus it can be problematic to prevent evaporation of liquid from the sample.

3.6 Experimental Considerations of Controlled Stress Rheometry

Here we consider the limitations of controlled stress rheometry, which serve to complicate the conversion of experimental values of torque and displacement to stress and strain, respectively. These limitations involve,

- End Effects and Edge effects
- Inertial effects
- Wall slip effects
- Effects of viscous heating
- The material's Mutation Number

3.6.1 End Effects and Edge Effects

End effects or edge effects may occur for a variety of reasons depending on the type of geometry employed. The conditions at the outer edge of the cone and plate are important because any stresses near the edge contribute substantially to the measured torque. Hence, the major problems of edge effects for cone and plate geometries are that the outer surface of the material is in contact with the atmosphere. This can lead to evaporation or formation of a skin, which considerably alters the composition and properties of the sample at the edge. However, this can be eliminated by the addition of silicon oil acting as a vapour hood (Boger and Ramamurthy, 1969). Other edge effects may be due to surface tension or the influence of the 'concentric cylinder' part of the geometry. Griffiths and Walters (1970) showed that this latter type of edge effects has negligible influence on rheological measurements when employing a cone of angle less than 4 degrees.

End effects may occur at both ends of the cylinder in Couette type geometries. Any fluid below the inner cylinder will exert a torque on the geometry. This can be eliminated by the design of a cone end (such as the Mooney-Ewart type) or minimised by employing a recessed inner cylinder. The recessed bob traps air, which transfers essentially no torque to the fluid (Macosko, 1994). The top end of the inner cylinder introduces other end effects. To eliminate these effects, it may be necessary to cover the top of the cylinder. Also any evaporation or skin forming effects may be minimised by application of non-volatile oil.

3.6.2 Inertial Effects

There are two types of inertial forces to consider those due to the instrument and those due to the sample.

Instrumental Inertia

If the force-sensing element has perceptible motion, or if the force and displacement are measured at the same surfaces, motion of the apparatus must be specifically taken into account. In a controlled stress rheometer, where measurements are performed at the surface, it is convenient to discuss the mechanical impedance, Z^*_M, or the complex ratio of force to velocity of a moving element. This includes contributions from the surface in contact with the sample, but also the inertia, elastance, and frictance of the moving element itself (Ferry 1980).

Neglecting sample inertia, analysis of the equation of motion for driving with a sinusoidal force gives a simple expression for the mechanical impedance of the moving element:

$$Z_M^* = \frac{F^*}{\upsilon} = R_M + iX_M = R_M + i\left(\omega M - \frac{S_M}{\omega} - \frac{S_M^0}{\omega}\right) \qquad (3.9)$$

Where

F*is the complex force (N)

υ is the velocity of the moving part (m s^{-1})

R_M is the frictance of the sample (kg s^{-1})

X_M is the mechanical resistance (kg s^{-1})

M is the mass of the moving element (kg)

S_M is the elastance of the sample (N m^{-1})

S^0_M is the elastance in the axial direction of the mechanism, which supports and centres the moving element (N m^{-1})

Whence

$$G' = \frac{\left(-\omega X_M + \omega^2 M - S_M^0\right)}{b} \tag{3.10}$$

$$G'' = \frac{\omega R_M}{b} \tag{3.11}$$

Where

b is a geometrical form factor (m)

There are certain restrictions for the above equations. S^0_M should be small compared to S_M and sets a low frequency limit. At high frequencies the $\omega^2 M$ term in equation 3.9 may become dominant and only inertia of the element will be measured. This sets a high frequency limit for the rheometer as resonant frequency is approached.

The instrumental inertial forces are calibrated prior to experiments and a correction factor is introduced by the rheometer software to correct the applied torque. Also to reduce instrument inertia lightweight geometries made of acrylic were used.

Sample Inertia

Conversion of the experimentally determined forces and displacements to the stresses and strains experienced by the sample depend on whether the inertia of the sample has to be considered. There are two limiting cases:

(a) *Gap loading limit* – the sample is sheared between closely spaced surfaces and the sample inertia is considered negligible. Cone and plate geometries exploit the gap loading condition therefore inertial forces in the sample are ignored.

(b) *Surface loading limit* – the driven surface is immersed in a volume of sample sufficiently large enough to effectively eliminate interference from reflecting shear waves (Schrag, 1977). The surface-loading limit represents a limit where sample inertia must be considered. Schrag (1977) examined a criteria for this gap loading condition and stated in order to perform high precision dynamic rheological measurements it is essential that,

The Controlled Stress Rheometer exploits the gap loading condition therefore inertial forces are ignored. This assumption is acceptable if,

$$\rho << \frac{G'}{h^2 f^2} \quad \text{Or} \quad \rho << \frac{G''}{h^2 f^2} \quad \text{(Ferry, 1980)} \qquad (3.12)$$

Where

ρ is the sample density (kg/m^3)

h is the sample thickness, either the distance between the plates or the distance between the concentric cylinders (m).

Schrag (1977) examined a criteria for this gap loading condition and stated in order to perform high precision dynamic rheological measurements, it is essential that,

$$\frac{\lambda_s}{h} \geq 40 \qquad (3.13)$$

Where

λ_s is the shear wavelength of the wave propagated through the viscoelastic medium (m).

And from Whorlow (1992),

$$\lambda_s \approx \sqrt{\frac{G'}{\rho f^2}} \quad \text{for highly elastic systems} \qquad (3.14)$$

These equations set an upper limit on the gap size in dynamic rheological measurements.

3.6.3 Wall Slip

The no-slip condition between a fluid and a solid boundary in contact with the fluid is one of the most classical assumptions in continuum fluid mechanics. For Newtonian fluids, the assumption of no-slip at a fluid-wall interface leads to good agreement with experimental observations. However, rheologically complex fluids are known to violate the no-slip boundary condition when certain critical conditions are exceeded (Barnes, 1995). It is called 'wall slip' when the no-slip condition is invalid.

The analysis of small amplitude oscillatory measurements invokes the assumption that the sheared sample is homogeneous and that the sample adjacent to the geometry's solid surface moves with the velocity of that surface. Discrepancies here produce 'true slip', that is, a discontinuity in velocity at the wall, which could be due to the material not adhering to the geometry surface sufficiently. It is generally associated with the flow instabilities occurring during extrusion (Kalika and Denn, 1987).

In systems, such as polymer solutions, gels, concentrated suspensions, emulsions, semisolid materials and foams, true slip does not occur. In these systems, wall slip is considered to occur through an 'apparent slip' caused by large velocity gradients in a thin region adjacent to the wall, where the viscosity is low because of a reduced concentration of the suspended phase (Aral and Kalyon, 1994; Jana *et al.*, 1995). A shear rate gradient may cause particles to migrate away from the wall or plate surface developing a low viscosity layer near the cylinder surfaces of a concentric cylinder (Macosko, 1994; Barnes, 1995). Slip effects in viscometers or rheometers can usually be coped with if they are confined to very thin layers, and no gross changes occur in the bulk of the fluid.

The proposed method to eliminate the wall slip at the fluid-wall interface is to alter the surface roughness of the wall. Many workers have used roughened plates or grooved surfaces to prevent wall slip. This produces uncertainty in the plate gap (or cone angle) due to the assumption that the material in the grooves does not flow and the tops of the ridges form the effective boundary surface (Whorlow, 1992). In some cases, the physicochemical nature of the wall can be altered to reduce repulsion effects by the absorption of certain chemical species (Hatzikiriakos and Dealy, 1991).

A common procedure for detecting wall slip is that proposed by Yoshimura and Prud'homme (1988a). Repeating measurements at the same frequency and strain but at different plate separations or cone angles will produce consistent values of the derived dynamic moduli if slip is absent. In the presence of slip, not only will the derived dynamic moduli become dependent on the geometry but also the stress or

strain response waveform will become non-linear. Yoshimura and Prud'homme (1988b) simulated a simple model of slip to understand these non-linear waveforms by using a linear viscoelastic model to represent the bulk fluid rheology, so that non-linearities arise from slip effects alone. They show that wall slip produces non-linear but symmetric waveform responses, which appear as 'flat topped' sinusoids. Therefore wall slip may also be detected by the presence of any additional harmonics in the sinusoidal response, providing the rheology of the material is linear. In this work, low values of stress and strain are required for the experiments to ensure the material remains in the linear viscoelastic range, hence large velocity gradients in the test material will be absent.

3.6.4 Viscous Heating

When a material is sheared it is inevitable that some of the work will be dissipated as heat (viscous heating). This shear-induced heating gives rise to an increase in temperature within the material (Walters, 1975). As the viscosity of most materials has high temperature dependence, this increase in temperature can give rise to significant errors. However due to the temperature control systems found on both rheometer's viscous heating should not be present.

3.6.5 Mutation Number

See section 3.3.2.

3.7 Rheological Characterisation of Fibrin Network Formation

3.7.1 Materials

Purified, plasminogen-depleted human fibrinogen at least 95 % clottable, and human thrombin were obtained from Enzyme Research Laboratories, UK.
The fibrinogen and thrombin were made up to stock solutions of 45 mg/ml and 50 NIH Units/ml, respectively by gradual addition to Tris Buffered Saline, TBS, (20 mM Tris, pH 7.4, and 0.9% NaCl, Sigma Aldrich, UK) and left to fully dissolve in a water bath at 37 °C. After hydration, the stock solutions were dispersed into small vials and stored at -80°C until required. One part TBS (at 10 times the working concentration) was added to 9 parts 4.5% w/v Human albumin (Zenalb®, Bio Products Laboratories, UK) to make a final stock solution of 4.05 % human albumin in 20mM Tris.

3.7.2 Problems in Measuring Gel Points of Fibrin Networks

Initial experiments soon presented the difficulty of acquiring good rheological data. It became apparent that numerous variables would have a significant effect on the retrieval of realistic data. Sample loading (discussed below) and temperature were paramount for retrieving good rheological data. The experiments were run at a low temperature of 10°C to reduce any loss of thrombin activity and to increase the viscosity of the sample to help with obtaining accurate results. Initial experiments were carried out in simple deionised water solutions (instead of the albumin/TBS solution), precipitation of the fibrinogen became a significant problem, due to the water insoluble nature of the material, especially on mixing. TBS was added to the deionised water to remove the problem of precipitation of the fibrinogen solutions in water but obtainable gel point data became a severe problem, once again due to low G′ (t) values at the gel points, leading to the rheometer not having the resolution to obtain meaningful data. Finally

albumin was introduced; albumin has a number of effects on fibrin network production that would help in producing good gel point data (see section 1.3).

3.7.3 Sample Loading

Sample loading plays a significant role in the experiment of fibrin gels due to the physical nature of the gelling system. The pre gel mixture containing the thrombin must be loaded into the rheometer geometry quickly especially during *fast* experiments. The sample is made at 10°C and the rheometer should be pre-cooled to this temperature before loading can begin. The temperature of the rheometer is controlled by a water bath cup (AR-G2 controlled stress rheometer). It is also imperative to load the sample slowly and deliberately in a uniform manner to remove the risk of air bubbles and ensure all geometry surfaces will be well *wetted.* It is also essential that exactly 6.6 ml of the sample is added to the geometry (total volume is in excess to reduce chance of bubbles when removing sample from preparation container). Once the sample is loaded into the bottom cup geometry the top bob geometry must be swiftly brought into contact with the sample solution. Due to the use biological materials and thus risk of contamination safety precautions must be observed, wearing goggles and gloves must be worn when in contact with the material.

3.7.4 Determination of the Linear Viscoelastic Range

As discussed in Chapter 2, determining the linear range of a transient system can prove extremely difficult. A conventional procedure as outlined in section 2.3.2 for finding a material's linear viscoelastic range involves monitoring G′ whilst increasing the stress in a stepwise manner i.e. a stress sweep. This method allows us to observe non-linear effects in the pre-gel regime to locate a crude upper limit estimation of the maximum stress obtainable in experimentation whilst still maintaining the linear viscoelastic fluid regime. It was found that the linear

viscoelastic range could be maintained for torques of no more than 15 micro Nm. The work found herein limited torques to below this value.

3.7.5 Dynamic Rheological Measurements

The rheological properties of the fibrin network formation were measured using the TA Instruments AR-G2 Controlled Stress Rheometer. Rheology Advantage Software equipped on the rheometer computer was used to run the dynamic rheological measurements (frequency sweeps and FTMS experiments). The geometry used throughout the study was the double gap viscometer (Figure 3.4).

Rheological measurements were performed with the rheometer operating in oscillatory mode, with an imposed stress of 0.03 Pa in the linear viscoelastic domain. The stock fibrinogen solutions were diluted to the required concentration (see below) with the stock albumin solution. This solution was treated with the appropriate volume of 1 M $CaCl_2$ (Sigma Aldrich, UK) to make a final $CaCl_2$ concentration of 0.005 M. Fibrin polymerisation was initiated at room temp by the addition of thrombin at various concentrations ranging from 0.0025 to 0.01 NIH Units/ml to various fibrinogen concentrations (see text). All samples were placed within the instrument immediately after the thrombin was added to allow the clot to form between the instrument plates. The evolution of the viscoelastic properties of the fibrin gels were examined by successive frequency sweeps at four frequencies between 0.2 and 2 Hz. The storage modulus (G'), a measure of the elastic energy stored during the deformation imposed by one oscillation of the rheometer, was calculated by TA Instruments Rheometer Software and used as a measure of clot rigidity. The loss modulus (G''), which reflects the energy dissipated by the clot during deformation, was also recorded and used to calculate the loss tangent ($\tan \delta = G''/G'$), the ratio of energy lost to energy stored in a cyclic deformation. These rheological characteristics allowed us to monitor the evolving rheological behaviour of the fibrin network formation, and also presented a rigorous method in the detection of the gel point. By plotting the loss tangent, $\tan \delta$, as a function of time at the various frequencies, a frequency independent phase angle may be established.

The point at which the data crosses over corresponds to the Gel Point, in terms of the Winter-Chambon Gel Equation.

3.8 Results and Discussion

3.8.1 Gelation Time

Figure 3.1 shows the evolution of viscoelasticity as a function of time at different frequencies for fibrin clot formation. The gelation time (t_g = 1029 s for fig 3.1) is defined by the intersection of the different frequencies as mentioned above. The same type of curve is observed for all fibrin gels at varying fibrinogen and thrombin concentrations.

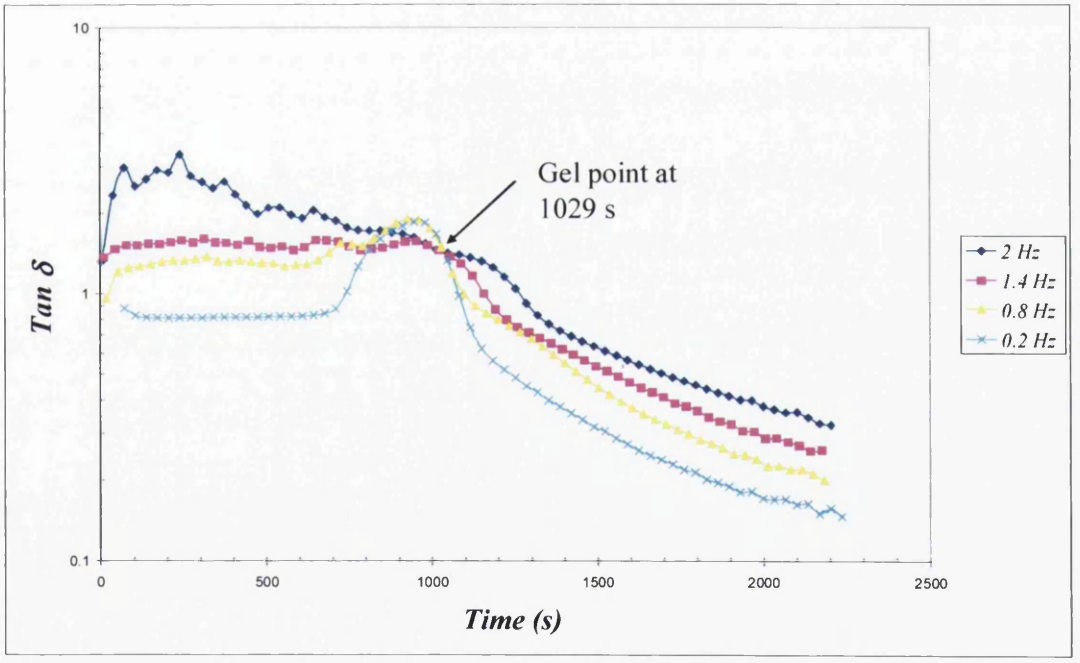

Figure 3.5. Results of oscillatory shear measurements of the loss tangent, tan δ, during fibrin clot formation (fibrinogen: 6 mg/ml, thrombin: 0.0025 NIHU/ml, $CaCl_2$: 0.005 M).

In this early, pre-clot viscoelastic fluid stage of gelation (prior to the establishment of the incipient clot); G′ varies from 0.038 to 0.166 Pa over the oscillatory frequency range. The frequency dependence of tan δ decreases progressively as gelation

proceeds, becoming frequency independent as the incipient clot is established as a sample-spanning cluster at the GP, where tan $\delta = 1.5$ (Figure 3.5, corresponding to $\delta = 56°$). A rapid increase in elasticity follows the establishment of the incipient clot in this post-GP regime, behaviour that is characteristic of a viscoelastic solid.

3.8.2 Influence of Gel Composition on Gel Point

Interestingly, many experimentally controllable parameters, such as the fibrinogen, thrombin, $CaCl_2$, or salt concentration have a major influence on the polymerisation process, and hence clot architecture.

Effect of Thrombin

The rheological behaviour of fibrin gels at varying concentrations of thrombin was studied at consistent fibrinogen concentrations of 8 mg/ml and 0.005 M Ca. The viscoelastic properties for clots formed at several thrombin concentrations illustrate markedly different values with respect to both the storage modulus, G′ and the loss modulus, G″ (fig 3.7).

Thrombin Conc. (NIHU/ml)	Gel point (°)	Clotting time (s)	G' @ GP (Pa)
0.0025	53.4	849	0.2
0.005	49.6	507	0.25
0.0075	47.4	330	0.27

Table 3.1. Properties of incipient clots in fibrinogen-thrombin systems.

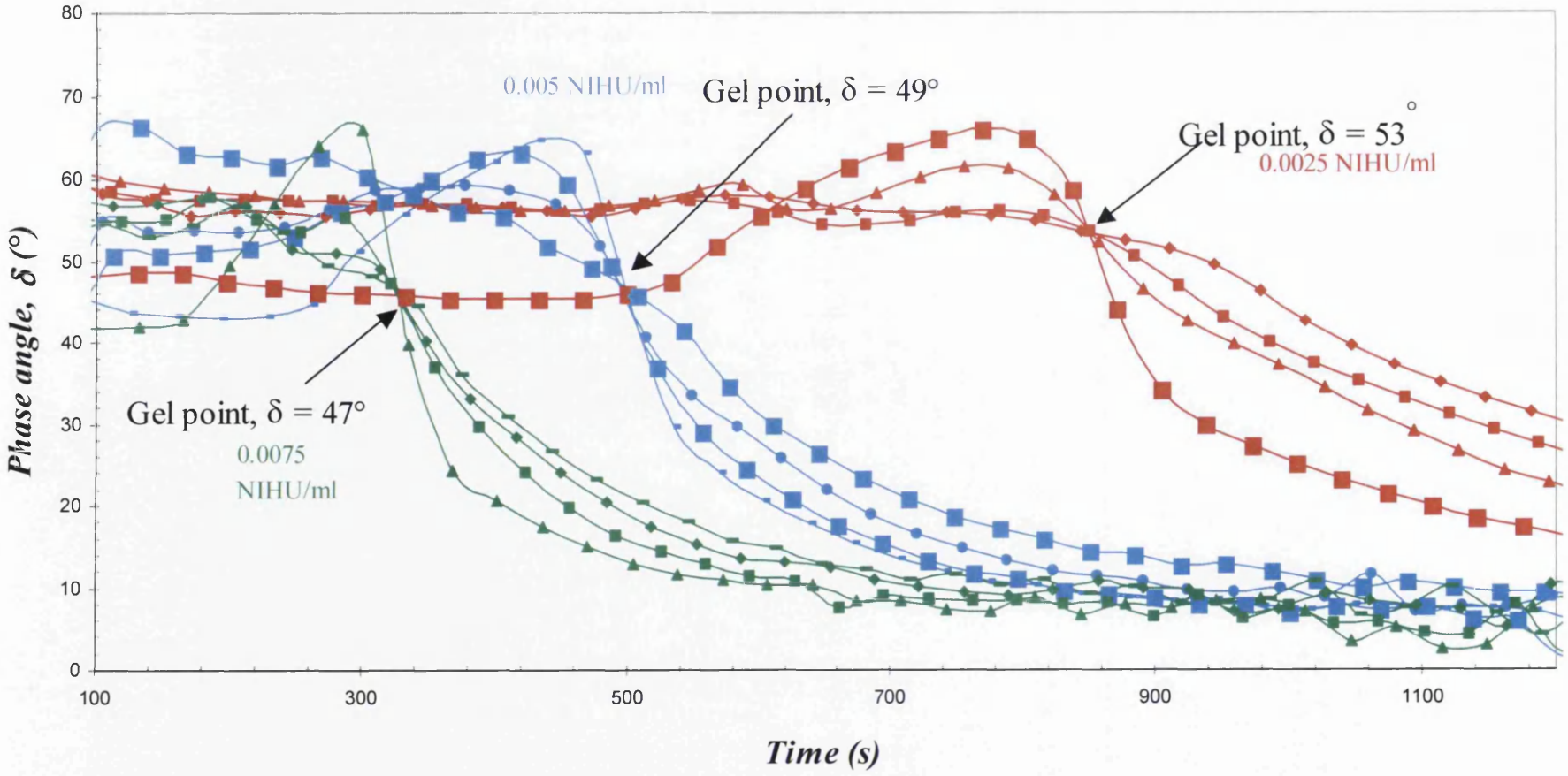

Figure 3.6. Effect of thrombin on gel point for fibrinogen-thrombin systems. (Fibrinogen concentration 8 mg/ml; 0.005 M $CaCl_2$).

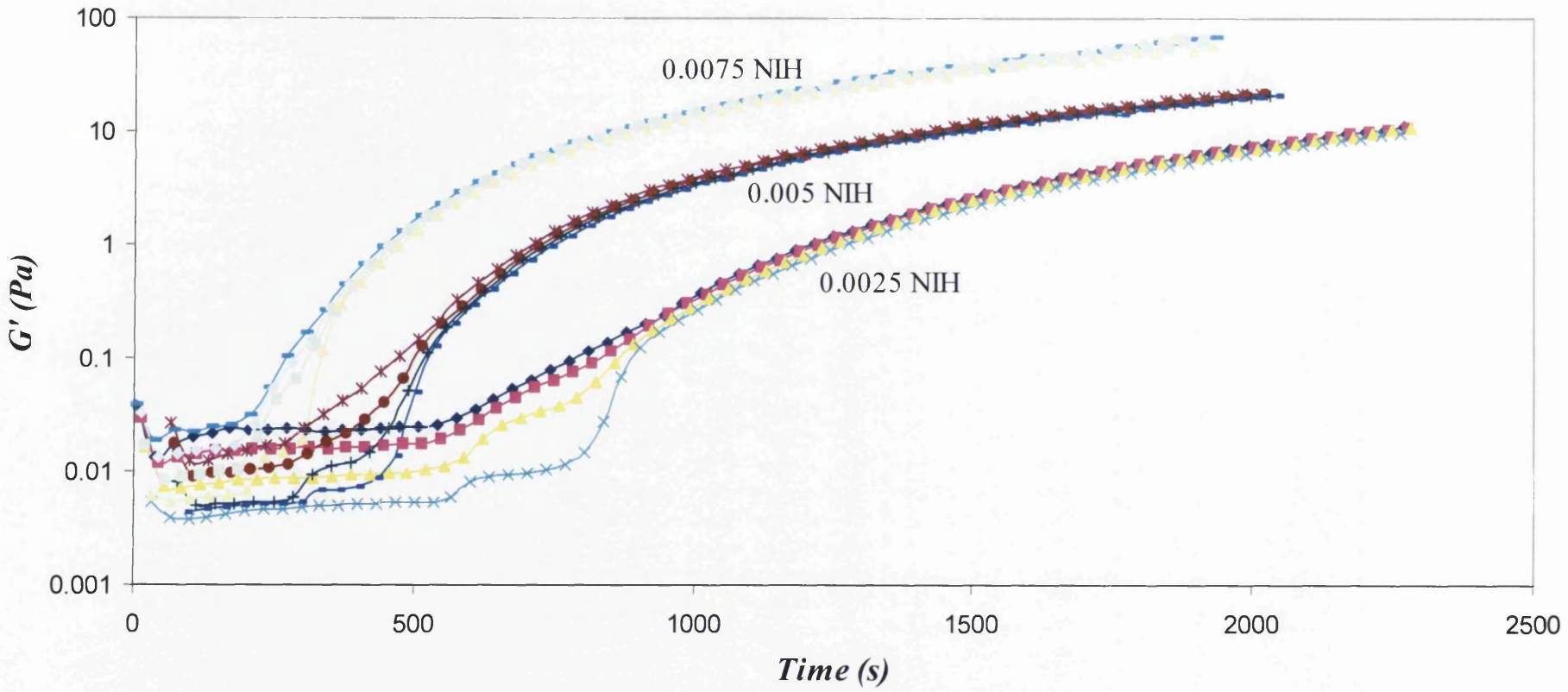

Figure. 3.7. Evolution of elasticity (G′) in Fibrin Gels at different concentrations of Thrombin. (Fibrinogen concentration 8 mg/ml; 0.005 M $CaCl_2$).

The results exhibit a good example for supporting our understanding how fibrin structure relates to the mechanical properties of a clot. G′ for a fibrin clot made with addition of thrombin at 0.0075 NIHU/ml, was about eight times higher than that of the fibrin clots made at 0.0025 NIHU/ml. Although the mechanisms responsible for the elasticity of fibrin clots are not entirely known (Ferry, 1988), in general, an increase in G' could arise from an increase in the number of branch points or an increase in the stiffness of the fibres (Gerth *et al.*, 1974; Jamney *et al.*, 1991). Clotting times decreased dramatically from 849 seconds for thrombin concentrations at 0.0025 NIHU/ml, to 330 seconds for thrombin concentrations of 0.0075 NIHU/ml (table 3.1).

Effect of Fibrinogen

Various concentrations of fibrinogen were used to prepare the gel (Figure 3.8 and 3.9). In contrast to variation in thrombin concentration, the kinetics of gel formation is not directly dependent on fibrinogen concentration (Fig. 3.9); gelation time only decreases from 340 s to 312 s when fibrin concentration is doubled. However, the storage modulus (G') of the gel increases with the fibrinogen. After the sol-gel transition, the storage modulus evolves towards values of 150 Pa with a 12 mg/ml fibrinogen concentration (Fig. 3.8).

3.8.3 Effects of Network Structure on Clot Rigidity

Definite increases in clot rigidity (*G'*) were obtained as fibrinogen concentrations were raised (Figure 3.8). The increased incidence of myocardial infarction in patients with elevated levels of plasma fibrinogen has been attributed, in part, to the less deformable clots formed at these concentrations (Scrutton et al., 1994), but the densely packed structures observed at higher substrate levels may also

contribute to limited fibrinolysis. The small degree of change in fibre diameters and lengths exhibited in this fibrinogen range (Chapter 6) indicates that the most probable cause for the bolstered clot rigidity at higher substrate levels is not the changes in fibre structure, but rather the increased density of fibres resulting from the greater total mass of protein. This difference of structure can be evaluated by the determination of the fractal dimension, which is discussed in the following section.
In contrast, modifications of fibre structure were most likely responsible for the variances in rigidity observed in clots formed with changing thrombin levels. The observed increase of clot stiffness with increasing levels of thrombin has also been demonstrated by other investigators (Kaibara and Fukada, 1971; Kaibara, 1973; Marx, 1988).

With regard to fibrinolysis in general, Collet *et al.*, (2000, 2003) discovered that fine fibrin gels are dissolved at a slower rate than coarse gels even though thin fibres are cleaved at a faster rate than thick ones. This was attributed to the enormously higher number of thin fibres in fine fibrin gels compared to the lower number of thick fibres in coarse gels. Thus, besides the thickness of the fibres, fibrin network architecture may play an important role in fibrinolysis. Taking together the review of the literature and the results of our study, a single preparation parameter obviously is not responsible for gel turbidity and stability, rather a combination of different parameters. In our study, although the interaction of the preparation parameters is still far from being fully elucidated, at least ranges for certain parameters could be identified in which the production of stable fibrin gels is possible.

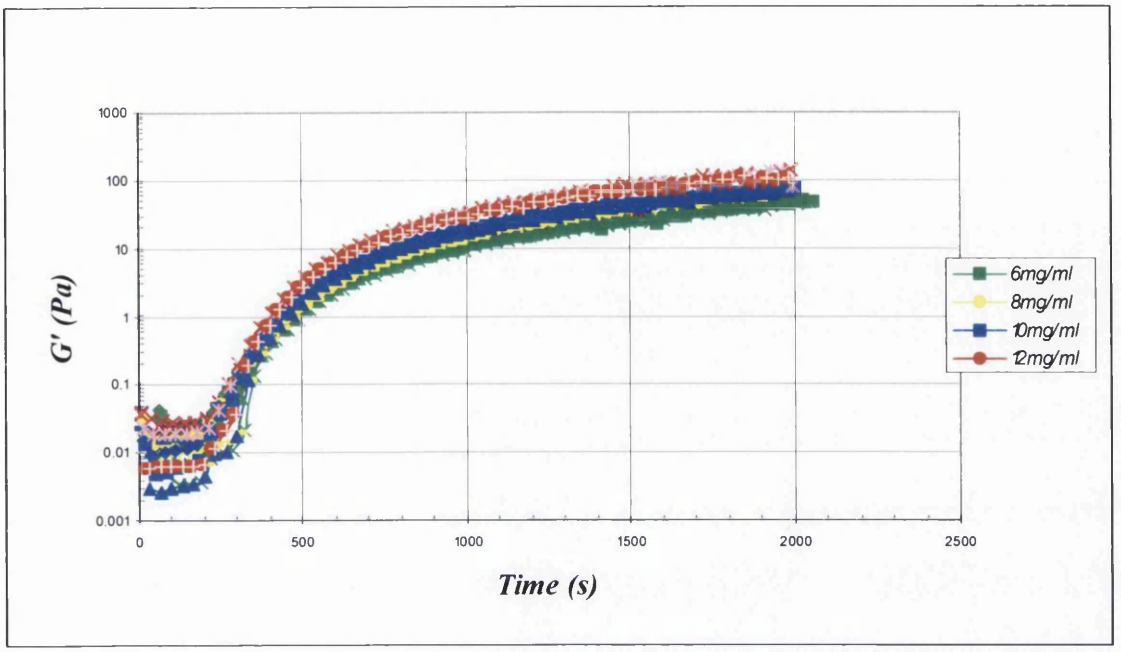

Figure 3.8. Evolution of elasticity in Fibrin Gels at different concentrations of fibrinogen (mg/ml). (Thrombin: 0.0075 NIHU/ml, Ca: 0.005 M).

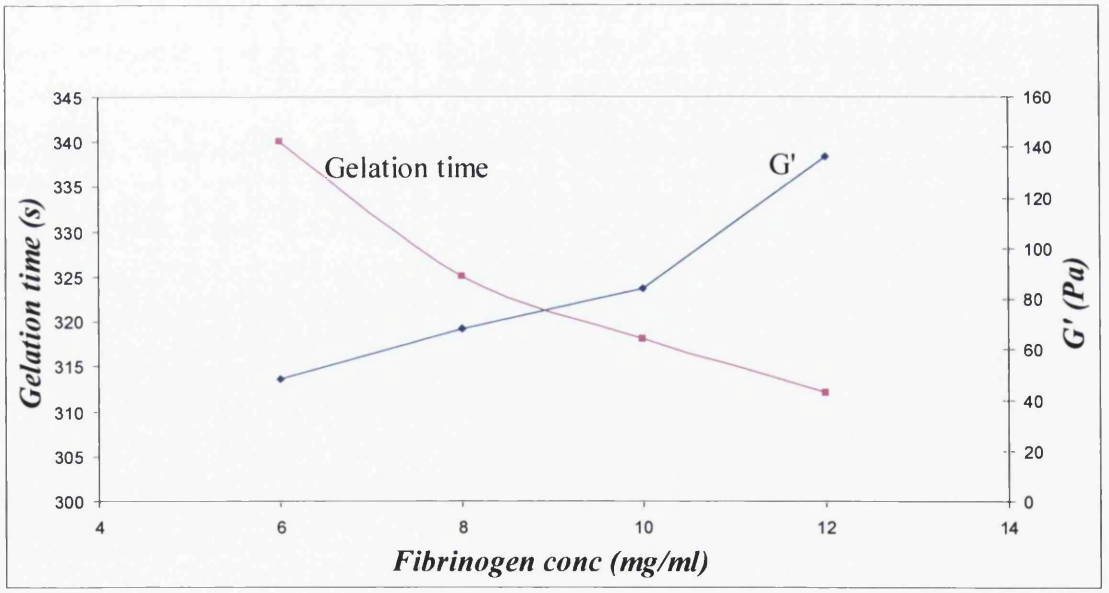

Figure 3.9. Storage modulus, *G'* (Pa) and Gelation time (s) as a function of fibrinogen conc. (mg/ml).

3.9 Characterisation of incipient clots based on a fractal description of their microstructure

In addition to providing a basis for the *detection* of incipient clot formation, the present GP analysis also suggests a possible basis for the characterisation of incipient clots, based on a fractal description of their microstructure. The need for such a basis is well established as studies of the conversion of fibrinogen to fibrin under varying conditions of ionic strength, fibrinogen and hydrogen ion concentrations have shown that the Gel Point is the parameter of overriding significance in determining clot structure (Blomback, 2004). The particular significance of quantifying the structural complexity of the incipient clot is that there is evidence that fibrin polymers formed *after* the GP are incorporated into the general architecture of the existing network, i.e. they do not form *de novo* networks within fluid spaces of the original (i.e. incipient) network (Blomback and Okada, 1982, 1983; Blomback, 2004).

These ideas, which have been expressed in other areas of gel formation as 'decorating' or 'dressing' the network, accord with theoretical studies of gels formed by heterogeneous (fractal) networks of branching colloidal fibres and the analysis of network structure, which is represented in part by a fractal dimension, may be useful for understanding the physical properties of clots formed under various physiological conditions (Takahashi *et al.*, 2003).

3.9.1 Results and Discussion

For determining the fractal nature of fibrin thrombin systems in this perspective, it is useful to recall that the value of the viscoelastic stress relaxation exponent α in the Gel Equation is a sensitive measure of the degree of branching in a gel and has been related to the fractal dimension of the sample-spanning network formed at the GP (Muthukumar and Winter, 1986). All values of α in the range $0 < \alpha < 1$ are possible for a fractal dimension d_f in the physically acceptable range $1 \leq d_f \leq$

3. Such behaviour is widely observed in chemical, physical and colloidal gels, including fibrin gels.

Fib Conc. (mg/ml)	*Frequency independent phase angle, δ (°)*	*Gel time, t_{gel} (s)*	*Stress relaxation exponent, α*	*G' at max time 2000 s (Pa)*	*G' @ GP (Pa)*	*Fractal Dimension, d_f*
6	56.1	1020	0.62	3	0.1	1.84
8	53.4	849	0.59	8	0.2	1.88
10	51.3	730	0.57	30	0.25	1.91
12	49.5	684	0.55	24	0.3	1.93

Table 3.2. Rheological and fractal characteristics of fibrin gels initiated at thrombin concentration 0.0025 NIH units/ml.

Fib Conc. (mg/ml)	*Frequency independent phase angle, δ (°)*	*Gel time, t_{gel} (s)*	*Stress relaxation exponent, α*	*G' at max time 2000 s (Pa)*	*G' @ GP (Pa)*	*Fractal Dimension, d_f*
6	51.2	340	0.56	35	0.25	1.92
8	49.6	500	0.55	22	0.3	1.94
10	48.3	450	0.53	56	0.31	1.96
12	47.1	480	0.52	70	0.36	1.97

Table 3.3. Rheological and fractal characteristics of fibrin gels initiated at thrombin concentration 0.005 NIH units/ml.

Fib Conc. (mg/ml)	*Frequency independent phase angle, δ (°)*	*Gel time, t_{gel} (s)*	*Stress relaxation exponent, α*	*G' at max time 2000 s (Pa)*	*G' @ GP (Pa)*	*Fractal Dimension, d_f*
6	48.2	340	0.53	48	0.26	1.96
8	47.4	325	0.52	68	0.27	1.97
10	46.1	318	0.51	84	0.28	1.98
12	44.9	312	0.49	136	0.38	2.01

Table 3.4. Rheological and fractal characteristics of fibrin gels initiated at thrombin concentration 0.0075 NIH units/ml.

Figure 3.5 shows a typical experimental result relative to the variations of tan δ near the sol-gel transition as a function of time at different frequencies. As described above, the gel point is derived by the intersection of the curves corresponding to different frequencies. For $t < t_g$ the decrease of tan δ with time can be explained by an enhancement of the elasticity due to the formation of clusters. At $t = t_g$, tan δ is independent of frequency and the value gives the relaxation exponent. The structural information near the sol-gel transition is derived from the relaxation exponent and the fractal dimension as described in the theoretical section in Chapter 2. Determination of the fractal dimension presents the opportunity to evaluate the differentiation in structure for fibrinogen-thrombin systems. These variations in the fractal characteristics of fibrin thrombin systems at varying concentrations of fibrinogen and thrombin are presented in table 3.2, 3.3 and 3.4. Figure 3.10 shows the results of sequential frequency sweep measurements (0.2, 0.8, 1.4 and 2 Hz) of fibrin-thrombin gels formed under a concentration of thrombin of 0.0025 NIH Units/ml. The figure illustrates the influence of fibrinogen concentration on characterising incipient clots based on a fractal description of their microstructure. The evolution of viscoelasticity recorded during gelation is shown in terms of the time dependence of phase angle δ. The initial response is characteristic of an elasticoviscous fluid, with increasing frequency of oscillation causing δ to decrease. In this early stage of gelation (prior to establishment of the GP), G' at 2 Hz is less than 0.02 Pa. The frequency dependence of δ decreases progressively as fibrinogen is polymerized to insoluble fibrin, with δ attaining a characteristic frequency independent behaviour ($\delta = 56.1°$ corresponding to $\alpha = 0.62$ for fibrin-thrombin gel at 6 mg/ml fibrinogen) as the GP is established. A rapid increase in G' follows the establishment of the GP and in this post-GP regime δ increases with increasing frequency of oscillation, behaviour which is characteristic of a viscoelastic solid.

Further tests were conducted on a series of gels systems at varying thrombin concentrations (table 3.2, 3.3, 3.4 and Fig 3.11). These results show similar features to the previous thrombin concentration insofar that the GP is characterized by the attainment of a frequency independent phase angle and prior to the GP, δ decreases with increasing frequency and post-GP, δ increases with increasing frequency.

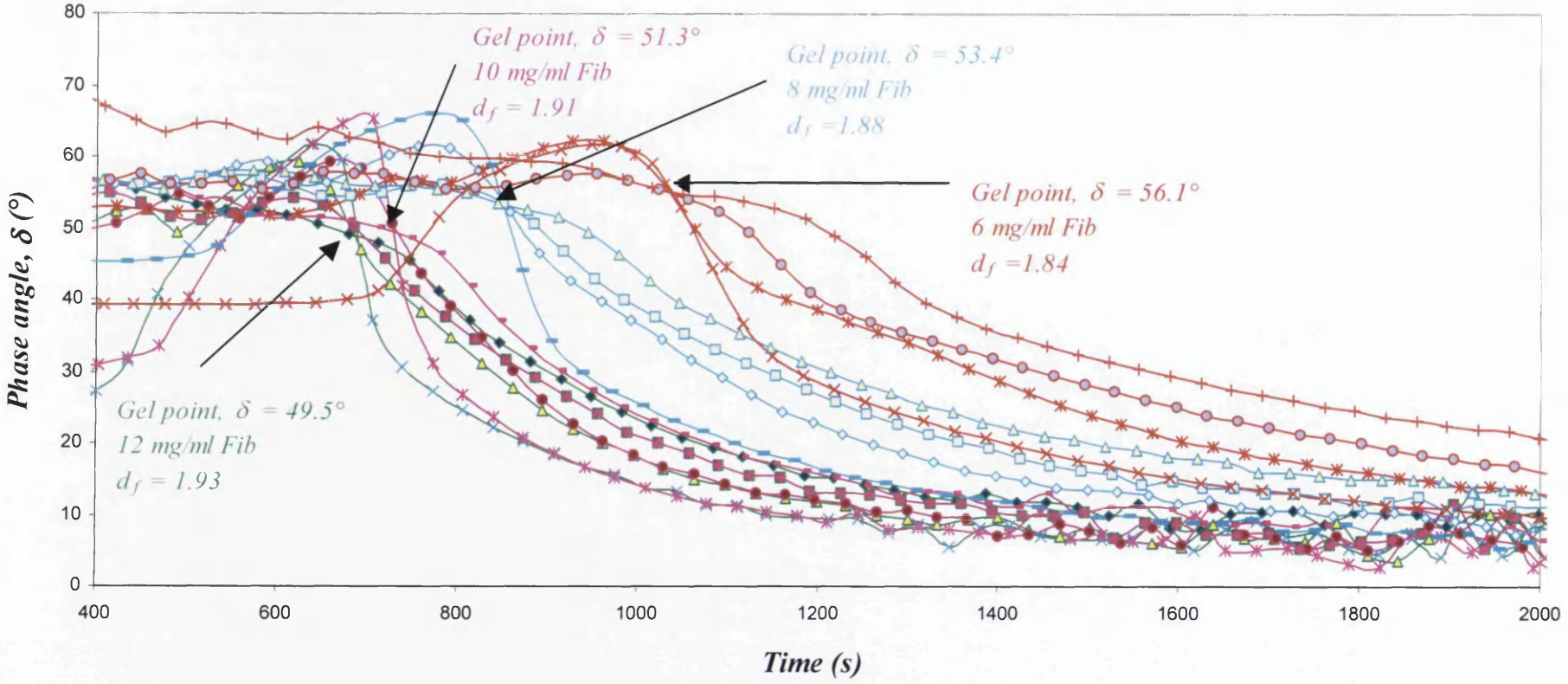

Figure 3.10. Effect of fibrinogen concentration on fractal microstructure of fibrin gels. (Thrombin concentration = 0.0025 NIH units/ml).

However, it is evident that the effect of increasing thrombin and fibrinogen concentrations forms gels with a decrease in gel time, t_{gel}, and a decrease in the frequency independent phase angle and α. The results exhibit subtle structural differences with variation of thrombin and fibrinogen concentration. Hence, a fibrinogen and thrombin dependent relationship is revealed for the structural characteristics of fibrin-thrombin gel systems. Higher fibrinogen and thrombin concentration lead to a higher d_f value for the critical gels. This suggests that the cluster space is more densely occupied for gels at higher concentrations of fibrinogen and thrombin.

These results show that by varying the amount of available thrombin and also fibrinogen we can produce fibrin-thrombin gels, which exhibit self-similar features at the GP with marked differences in fractal dimension.

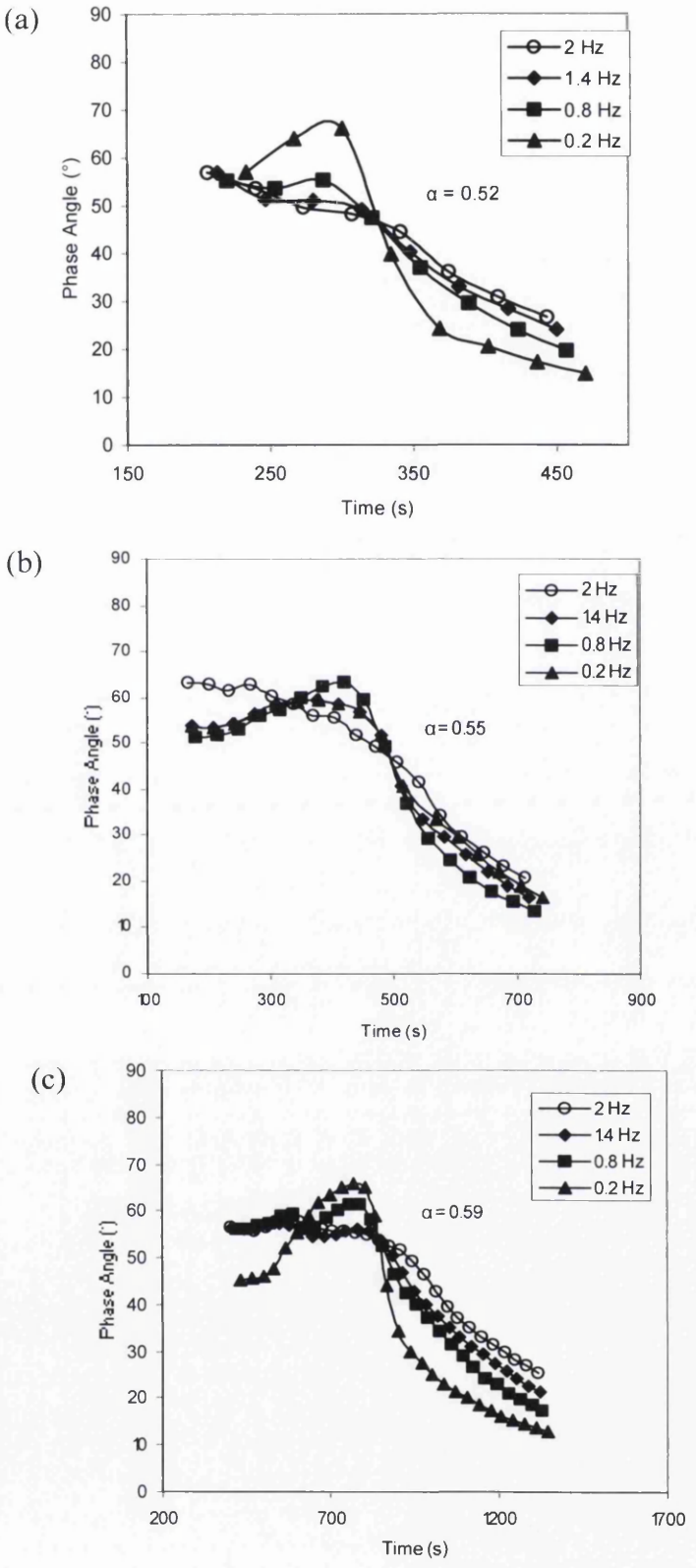

Figure 3.11. Results of frequency sweep measurements of fibrin-thrombin gels formed by the addition of thrombin at concentrations of (a) 0.0075 NIH Units/ml, (b) 0.005 NIH Units/ml, and (c) 0.0025 NIH Units/ml.

3.9.2 Conclusions

The work reported in this paper is the first to identify the Gel Point of coagulating fibrin clot networks in terms of the Chambon–Winter Gel Point criterion and to use it (i) as the basis for the rheometrical detection of the establishment of the incipient clot and (ii) as the basis of characterising its fractal microstructure. The GP delineates between the pre-GP elasticoviscous fluid behaviour of coagulating fibrin gels and its post-GP viscoelastic solid behaviour. Only in the post-GP phase can the requisite haemo*static* function of the clot be performed and it follows that the establishment of the incipient clot is defined unambiguously in terms of the gel point. The results provide a means of systematically investigating pathologically induced differentiation in their micro structural features, by exploiting relationships between the viscoelastic stress relaxation exponent α and the fractal dimension of the incipient clot gel network cluster.

Small amplitude oscillatory shear measurements have the advantage of providing information on the continuous evolution of the structure. The results exhibit the influence of experimentally controllable parameters such as fibrinogen and thrombin concentrations on the polymerisation process and hence the final fibrin network architecture. Hence, results of these experiments show that fibrin clot rheological behavior is regulated by fibrinogen and thrombin concentration. Increased fibrinogen concentrations elevate clot rigidities through the establishment of greater fibre and branch point densities. The high rigidities exhibited by clots that display this type of network morphology appear to result from a balance between a high degree of branching and thicker fibres, characteristics that both enhance network rigidity but are antithetical, since more branching leads to thinner fibres and thicker fibres yield less branching. Rearrangements in clot structure that lead to losses of elastic energy during deformation appear to be more common in clots having thicker fibres.

This work supports the hypothesis that the self-similar (fractal) stress relaxation behaviour recorded at the GP of samples of coagulating blood (Evans *et al.*, 2008c) is associated with the microstructural characteristics of the incipient blood clot's fibrin network. Following our assessment of the suitability of sequential

frequency sweeps for the detection of the GP, we conclude that the gel time must be at least an order of magnitude greater than the time taken to perform each frequency sweep in order to obtain an accurate measure of the stress relaxation exponent α, and hence a reliable estimate of the incipient clot's fractal dimension d_f.

In the present work the values of d_f obtained for fibrin-thrombin gels formed with high and low levels of thrombin are bounded by those associated with widely reported gel formation mechanisms, namely reaction limited cluster-cluster aggregation (RLCCA, d_f = 2.05) and diffusion limited cluster-cluster aggregation (DLCCA, d_f = 1.8), respectively. The results support the findings of the confocal microscopy study reported in Chapter 6 and work by Bateman *et al.*, 2005, insofar as the value of d_f increases with increasing levels of thrombin.

However, it is important to note that all other studies in this area to date refer to the inferred fractal characteristics of a fully formed, mature gel. The present study is the first to report modification of the fractal characteristics of incipient clots.

Chapter 4

Fractal Analysis as a Tool for Quantifying Fibrin Clot Networks

4.1 Introduction to Fractals

While the term 'fractal' is still relatively unknown today by the general public, paradoxically, everyone has an intuition of this concept. Fractal geometry has become indispensable in the understanding of many phenomena since its inception by Mandelbrot in 1975. Its popularity rests in the promise of a deeper understanding of complex, chaotic and disordered systems, which have resisted conventional geometrical attempts to model them.

The term *fractal* (from Latin *fractus* - irregular, fragmented) applies to objects in space or fluctuations in time that possess a form of self-similarity and cannot be described within a single absolute scale of measurement (figure 4.1). Fractals are recurrently irregular in space or time, with themes repeated like the layers of an onion at different levels or scales.

Figure 4.1. Fractal aggregate formed by diffusion limited cluster aggregation (DLCA).

The concept of fractal geometry (Mandelbrot, 1982; Falconer, 1990) has proved useful in describing structures and processes in experimental systems (Takayasu, 1990; *Fractals in Science,* 1994). It provides a framework that can quantify the structural complexity of a vast range of physical phenomena.

A well-known example of a fractal system is the shape of a coastline. Two pictures of a coastline on two different scales look the same; it is difficult to tell which scale belongs to which picture. This means the coastline is scale-invariant or, equivalently, has no characteristic length scale (Bunde and Havlin, 1994). Other examples include features of mountains, clouds, rivers, the vascular system and other biological structures.

Fractal geometry has evoked a fundamentally new view of how both nonliving and living systems result from the coalescence of spontaneous self-similar fluctuations over many orders of time and how systems are organized into complex recursively nested patterns over multiple levels of space.

4.2 Self-similarity and Fractal Geometry

The key idea in fractal geometry is self-similarity. An object is self-similar if it can be decomposed into smaller copies of itself. Thus self-similarity is the property in which the structure of the whole is contained in its parts. A system or structure can be anything that has more than one part. The system is said to be dynamical when systems states, including the relationships (interactions) between its parts (elements), change with time. Rules that describe these changes are called dynamics. If the interactions are non-linear, i.e. if the result of action of one element onto another is not directly proportional to the action itself, the system is said to show nonlinear dynamics. For example, in classical mechanics the result of a force acting onto a body is an acceleration of the body proportional to the acting force because body's mass is constant and does not depend on the body's velocity, whereas in relativistic mechanics this is not true since body mass does depend on its velocity.

Simple systems with nonlinear dynamics often generate very random-like characteristics known as *chaos*. The paradox of chaos is that it is *deterministic* i.e. results from a dynamic that is not govern by laws of probability. Because of extreme sensitivity to initial conditions and systems parameters, chaotic systems may seem to behave completely randomly. But there is an order underlying such behaviour. For

example, random numbers from a computer generator appear to lack any degree of order, when in fact the numbers are produced in a very ordered and deterministic fashion. Probability of a random number generator producing the string "1010..." is exactly the same as the probability of any other particular string with half 1's, half 0's. Both strings have the same statistics and thus the same probability of occurrence, although one is regularly patterned and other is not. Randomness is relative and context dependent, the definition of randomness "lacking all order" has no real meaning. Unlike random systems, systems governed by deterministic chaos may be rather easily controlled. Methods of nonlinear dynamics and deterministic chaos theory provide tools for analysing and modelling chaotic phenomena and can supply us with effective quantitative descriptors of underlying dynamics and of systems fractal structure.

Dynamical systems move towards one or more attractors, which can be thought of as the systems equilibrium states in the systems phase space. Systems that give rise to deterministic chaos have chaotic or strange attractors. Here chaos theory intimately relates to fractal geometry since strange attractors turn out to be fractals. But building up the phase space for a system poses several problems – the data characterizing the system (e.g. amplitudes of a signal produced by the system in consecutive moments of time) have to be embedded in the properly chosen multidimensional space. On the other hand, processes in chaotic systems often produce structures or signals that are fractal in real space or in time, respectively.

Fractal dimension is a measure of how 'complicated' a self-similar figure is. In a rough sense, it measures 'how many points' lie in a given set. A plane is 'larger' than a line, while Sierpinski triangle (Fig 4.2) sits somewhere in between these two sets. On the other hand, all three of these sets have the same number of points in the sense that each set is uncountable.

Somehow, though, fractal dimension captures the notion of 'how large a set is'. Fractal geometry can be considered as an extension of Euclidean geometry. Conventionally, we consider integer dimensions which are exponents of length, i.e., surface = length^2 or volume = length^3. The exponent is the dimension. Fractal geometry allows for there to be measures which change in a non-integer or fractional

way when the unit of measurements changes. The governing exponent d_f is called fractal dimension.

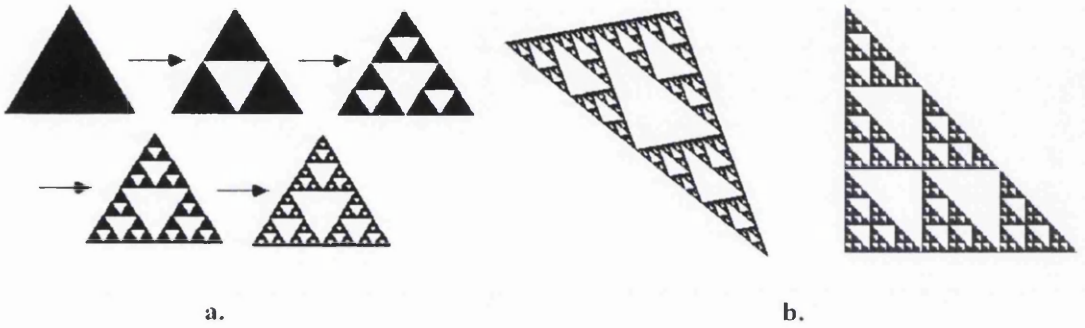

a. b.

Figure 4.2. Sierpinski triangles - concept of self-similarity and calculation of D by similarity method. a) Creation of Sierpinski triangle, S, by subsequent iterations, $S_n \rightarrow S_{n+1}$. In an iteration, from each black triangle in S_n the triangular piece of S_{n+1}, congruent with the whole S_n, is 'produced'; each of 3 congruent pieces of S_{n+1} produced this way is exactly ½ the size of the given piece in S_n itself. So, fractal dimension of S is 1.58.

Fractal objects possess a characteristic revealing more fine structure as the object is magnified, similarly like morphological complexity means that more fine structure (increased resolution and detail) is revealed with increasing magnification. Fractal dimension measures the rate of addition of structural detail with increasing magnification, scale or resolution. The fractal dimension, therefore, serves as a quantifier of complexity.

Ideal points have Euclidean dimension of 0, ideal lines of 1, and perfectly flat planes of 2. However, a collection of real points have a dimension greater than 0, real lines greater than 1, and real surfaces greater than 2 etc. At each level, as the dimensions of an object increase, the complexity of the object increases, it becomes more area filling from 1 to 2, more volume filling from 2 to 3 (Smith *et al.*, 1989). Euclidean or non-fractal (points, lines, circles, cubes, etc.) may be viewed as fractal

objects with the lowest complexity (integer fractal dimensions) within their respective dimension domains (0 to 1, 1 to 2, etc.)

Natural objects are often rough and not well described by the ideal constructs of Euclidean geometry (Smith *et al.*, 1989). The similarity method for calculating fractal dimension works for a mathematical fractal, which like Sierpinski triangle is composed of a certain number of identical versions of itself. It is not true for natural objects. Such objects show only *statistical self-similarity* (Kraft).

Deterministic fractals can be easily constructed using computer algorithms. In order to quantify the fractal dimensionality of an object, a simple two-dimensional common deterministic fractal, namely the Koch curve (after Helge von Koch) can be considered (Figure 4.3). Von Koch's curve comes from an iterative process bearing on the modifications of a segment of a straight line in accordance with a predetermined unchangeable rule. At each iteration, the central third of each segment of the straight line (initiator) is replaced by two identical segments angled at 60° (the generator). From this process appears a curve with surprising properties whose infinite length within a limited surface is not the least.

The Koch curve also demonstrates the self-similarity of fractal images as any change in scale will show more detail as magnification is increased but will not lose detail if the magnification is decreased. Fractal analysis is then the procedure that compares the size of the outline or mass of the object for each scale of the measurement. This can be done using disks or squares. If this change of size is constant with change of scale on a double logarithmic plot, the form approximates a fractal and the gradient of the line through these points is proportional to the fractal (self-similarity) dimension.

The gradient is mathematically defined by,

$$d_f = \frac{\log N(e)}{\log(1/e)} \qquad (4.1)$$

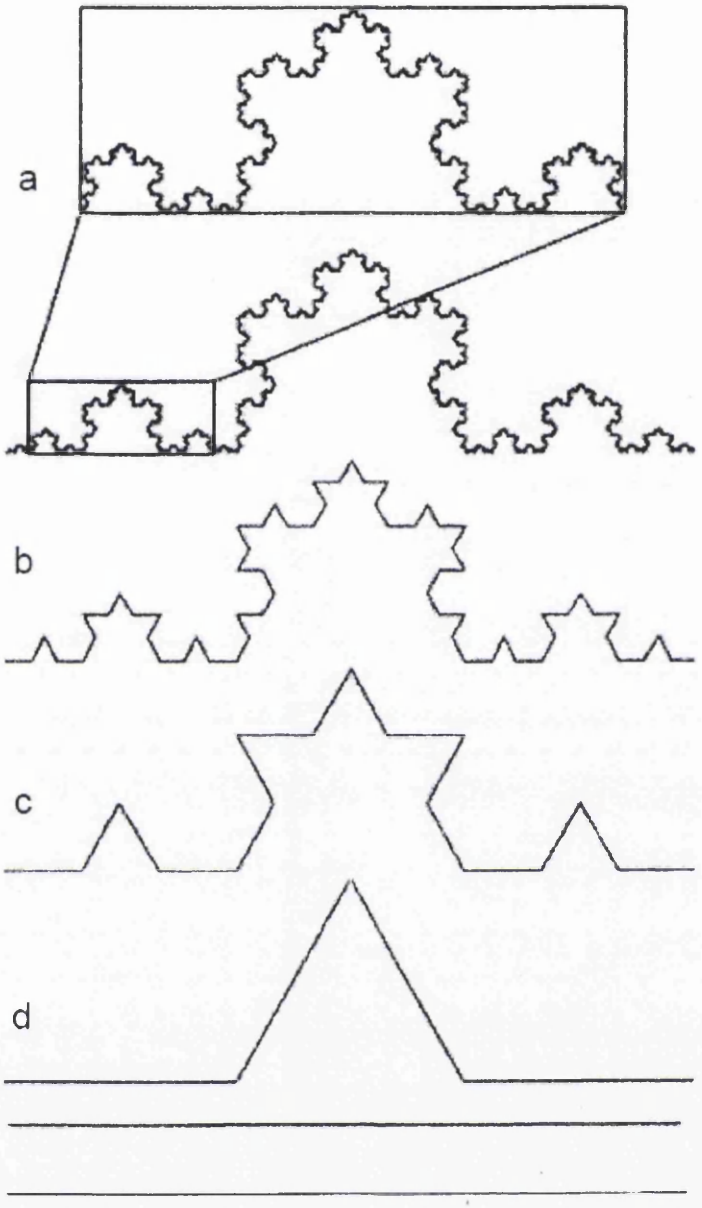

Figure 4.3. Von Koch curve (a) Initiator; (b) Generator; (c) Von Koch after numerous iterations; (d) Self-similarity illustrated on Von Koch curve.

which, transforms into $N(e)^D = 1$, a power law relationship, where the exponent 'd_f' is the fractal dimension (for the Koch curve, $d_f = 1.246$). The mathematical definition of the fractal states that the size of the image scales indefinitely by a constant proportion. The fractional part of the exponent indicates the complexity of the object. If the fractional part of the exponent is 0, d_f would be equal to 1 and equal to the Euclidean dimension for a line. If the line becomes more space filling the fractional part of the exponent increases towards 2.

Complexity is another common term used to describe the surface irregularities or the intricacy of a branching structure. d_f indicates whether the structure contains a degree of self-similarity, which in turn can be an indication of the underlying biological process that leads to the observed pattern. Self-similarity, as Mandelbrot (*The Fractal Geometry of Nature,* 1982) points out, is a simple design principle that can be independent of genetic determination and only dependent on a consecutive scaling with changes of magnitude. The dimension exponent can indicate how a structures branches scale from the parent to the daughter branches as can be observed in the lung bronchi for instance (Bassingthwaighte *et al.*, 1994).
d_f can also be an indicator of how space filling a structure is. If d_f has a value of 1.2 then the structure is not as space filling as if d_f was 1.4. Thus the feature that makes fractal analysis interesting is measuring the range of the statistical self-similarity across scaling levels and the associated estimate of d_f. Statistical self-similarity can be an indicator of a growth process in tubular structures such as blood vessels, lung bronchi or neurons. The fractal dimension thus brings about a quantitative approach of parameters, which until now have been rather abstract, such as heterogeneity, irregularity or complexity.

4.3 Measurement of Fractal Dimensions

A large number of different types of fractal dimensions have been described (Mandelbrot, 1982) but many are only applicable to pure mathematical fractal objects. Random fractal models are widely used to mimic fractal systems in nature but the general methods presented above to deduce fractal dimensions cannot be applied directly as random structures cannot be exactly mapped onto themselves after dilation or contraction. Instead, an average or statistical self-similarity is estimated. Indeed, several techniques exist among which is box-counting, meant for assessing fractal dimension (d_f) on the basis of fractal images.

4.3.1 Box-Counting Estimation Method

The box dimension is defined as the exponent d_f in the relationship:

$$N(d) = \frac{1}{d^{d_f}} \tag{4.2}$$

where N(d) is the number of boxes of linear size d necessary to cover a data set of points distributed in a two-dimensional plane. The basis of this method is that, for objects that are Euclidean, equation (4.2) defines their dimension. One needs a number of boxes proportional to 1/d to cover a set of points lying on a smooth line, proportional to $1/d^2$ to cover a set of points evenly distributed on a plane, and so on.

This dimension is sometime called grid dimension because for mathematical convenience the boxes are usually part of a grid. One could define a box dimension where boxes are placed at any position and orientation, to minimize the number of boxes needed to cover the set. It is obviously a very difficult computational problem to find among all the possible ways to cover the set with boxes of size d the configuration that minimizes N(d). Also, if the overestimation of N(d) in a grid dimension is not a function of scale (i.e., we overestimate N(d) by, say, 5% at all box

sizes d), which is a plausible conjecture if the set is self-similar, then using boxes in a grid or minimizing N(d) by letting the boxes take any position is bound to give the same result. This is because a power law such as (eq.4.2) is such that the exponent does not vary if we multiply N(d) or d by any constant.

In practice, to measure d_f one counts the number of boxes of linear size d necessary to cover the set for a range of values of d; and plot the logarithm of N(d) on the vertical axis versus the logarithm of d on the horizontal axis (Figure 4.4). If the set is indeed fractal, this plot will follow a straight line with a negative slope that equals $-d_f$. To obtain points that are evenly spaced in log-log space, it is best to choose box sizes d that follow a geometric progression (e.g., d = 1, 2, 4, 8,...), rather than use an arithmetic progression (e.g., d = 1, 2, 3, 4,...).

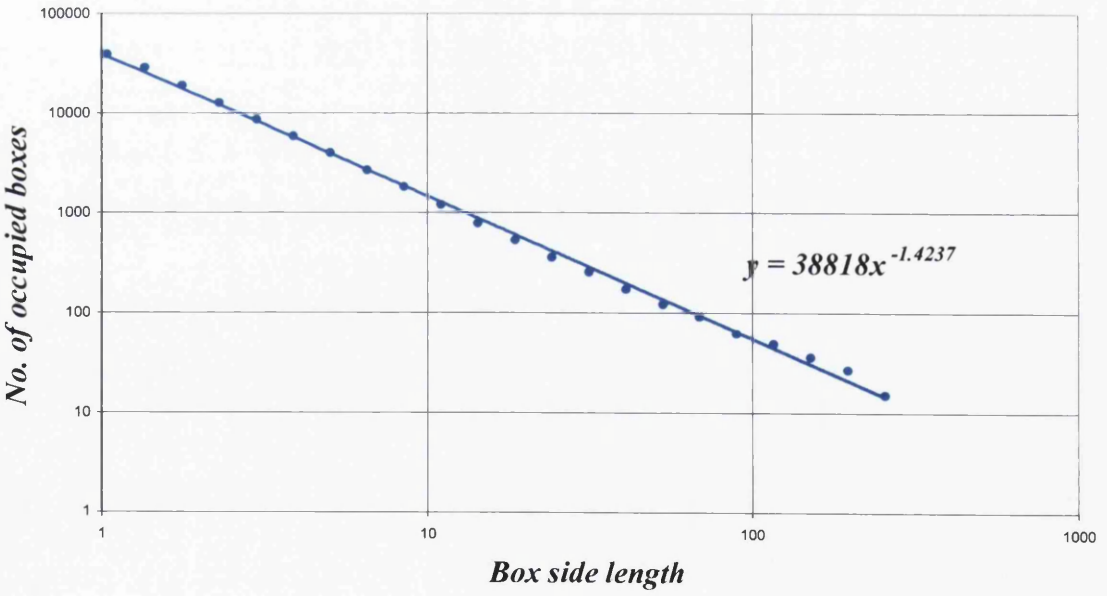

Figure 4.4. Logarithmic plot of number of occupied boxes, N(d) versus box side length, d.

A choice to be made in this procedure is the range of values of d. Trivial results are expected for very small and very large values of d. A conservative choice may be to use as the smallest d ten times the smallest distance between points in the set, and as the largest d the maximum distance between points in the set divided by ten. Alternatively, one may exceed these limits and discard the extremes of the log-log plot where the slope tends to zero. In theory, for each box size, the grid should be overlaid in such a way that the minimum number of boxes is occupied. This is accomplished in Benoit by rotating the grid for each box size through 90 degrees and plotting the minimum value of N (d).

The fractal dimension thus brings about a quantitative approach of parameters that until now have been rather abstract, such as heterogeneity, irregularity or complexity.

4.3.2 Information Dimension Estimation Method

This fractal dimension is often encountered in the physics literature, and is generally different from the box dimension. In the definition of box dimension, a box is counted as occupied and enters the calculation of N(d) regardless of whether it contains one point or a relatively large number of points. The information dimension effectively assign weights to the boxes in such a way that boxes containing a greater number of points count more than boxes with fewer points.

The information entropy I(d) for a set of N(d) boxes of linear size d is defined as:

$$I(d) = -\sum_{i=1}^{N(d)} m_i \log(m_i) \qquad (4.3)$$

where m_i is:

$$m_i = \frac{M_i}{M} \tag{4.4}$$

where M_i is the number of points in the i^{th} box and M is the total number of points in the set.

Consider a set of points evenly distributed on the two-dimensional plane. In this case, we will have

$$N(d) \approx \frac{1}{d^2} \qquad m_i \approx d^2 \tag{4.5}$$

so that (4.3) can be written as

$$I(d) \approx -N(d)\left[d^2 \log(d^2)\right] \approx -\frac{1}{d^2}\left[2d^2 \log(d)\right] = -2\log(d) \tag{4.6}$$

For a set of points composing a smooth line, we would find

$$I(d) \approx -\log(d) \tag{4.7}$$

Therefore, we can define the information dimension D_i as in:

$$I(d) \approx -D_i \log(d) \tag{4.8}$$

In practice, to measure D_i one covers the set with boxes of linear size d keeping track of the mass m_i in each box, and calculates the information entropy *I(d)* from the summation in (eq.4.3). If the set is fractal, a plot of *I(d)* versus the logarithm of *d* will follow a straight line with a negative slope equal to $-D_i$.

The information dimension differs from the box dimension in that it weighs more heavily boxes containing more points. To see this, let us write the number of occupied boxes *N(d)* and the information entropy *I(d)*, in terms of the masses m_i contained in each box:

$$N(d) = \sum_i m_i^0 \qquad (4.9)$$

$$I(d) = -\sum_i m_i \log(m_i)$$

The first expression in (eq.4.9) is a somewhat elaborate way to write N(d), but it shows that each box counts for one, if $m_i > 0$. The second expression is taken directly from the definition of the information entropy (4.3). The number of occupied boxes, N(d), and the information entropy I(d) enter on different ways into the calculation of the respective dimensions. Hence from Eq (4.9);

$$D_b \leq D_i \qquad (4.10)$$

The condition of equality between the dimensions (4.10) is realized only if the data set is uniformly distributed on a plane.

4.4 The Limitations of Fractal Analysis

It is important to appreciate the fractal notion must be adapted whenever it is applied to natural shapes. Unlike mathematical fractals, natural objects are not the result of construction by iteration. While for ideal fractals no basic length exists which can be used as a unit, whereas, in real systems a smallest length (a) always exists, which is the linear size of the elementary particle of the system. In this kind of object, self-similarity arises only if the linear size of the object 'L' being studied is much greater than 'a'.

Hence, in most practical cases, the fractal can only be defined in a limited scale range. Within these boundaries, the experimental points in log-log plots, which characterise the fractal dimension, often present some fluctuations or discrepancy with respect to a straight line. In this situation, it is sometimes difficult to be sure of the fractality of the object observed. From here on, the size effect must be kept in mind.

Therefore, the fractal dimension must be considered as a relative measure rather than an absolute one.

4.5 Fractal Models for Gelling Systems

Martin and Adolf (1991) quoted "in the race to understand the curious structural and dynamical transformations that occur near the sol-gel transition, investigators have discovered that the incipient gel, that fluid formed just at the sol-gel transition, is a viscoelastic intermediate between the liquid and solid state and a paradigm of fractal structure and fractal time". The scientific fascination with the sol-gel transition has thus transcended practical applications.

The relaxation exponent α in the Gel Equation has been related to a fractal dimension, d_f, in terms of various theories of gelation and cluster growth (Scanlan and Winter, 1991). The latter have invoked several different aggregation models to

investigate the fractal attributes of different gel structures. It is appropriate to briefly review the main features of the principal forms of aggregation models and the main theoretical descriptions of gelation processes.

4.5.1 The Diffusion Limited Aggregation Model (DLA)

Witten and Sander (1981) formulated the diffusion limited aggregation model (DLA), which refers to a simple growth algorithm in which individual particles are added to a growing cluster through a diffusion-like process. Starting from any suitable cluster *seed* fixed in d-dimensional space, a new particle is launched at a random position far away from the cluster and undergoes Brownian motion. When the randomly walking particle contacts the cluster, it is stopped and incorporated to the cluster at its contacting position. This process of launching a random walker and adding it to the cluster on its first contact is repeated until the cluster has reached a desired number of particles. The DLA model generates strongly ramified clusters with a complex geometry. Figure 4.5 illustrates a fully developed DLA cluster. The fractal dimensions published for off-lattice, i.e. hexagonal, triangular lattice etc which generate more realistic structures (Meakin, 1988b), DLA are $d_f \cong 1.71$ for $d = 2$, and $d_f \cong 2.5$ for $d = 3$ (Bunde and Havlin, 1994).

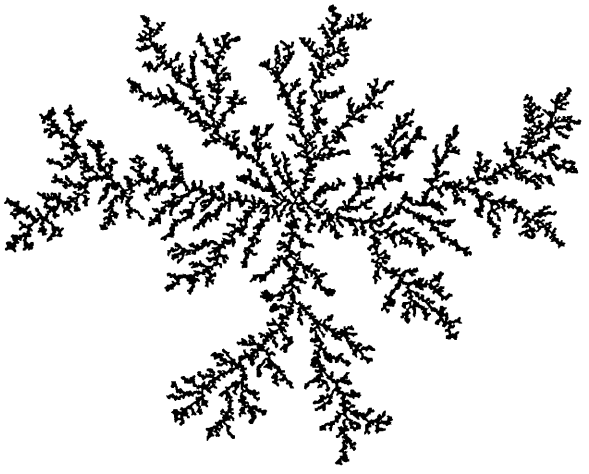

Figure 4.5. Two-dimensional Diffusion Limited Aggregation (DLA) cluster.

4.5.2 *Diffusion Limited Cluster-Cluster Aggregation (DLCA)*

The diffusion limited cluster-cluster aggregation (DLCA) model consists of no unique seed or growth site. Figure 4.6 presents four stages of DLCA at various times during a 2-D computer simulation (Meakin, 1988b) in which a chosen concentration of particles randomly diffuse on a lattice. Whenever two (or more) clusters touch each other, i.e. when they are nearest neighbours on the lattice, they stick together permanently and thus form a new larger cluster. In this way, a variable array of cluster sizes can be produced, the number of clusters invariably decreasing. At longer times, larger and larger clusters are created and randomly branching aggregates emerge in the system, until finally a single macroscopic cluster is formed (Meakin, 1983; Kolb, 1984). The structures developed using DLCA models are less compact than DLA, with $d_f \cong 1.4$ in $d = 2$, and $d_f \cong 1.8$ in $d = 3$ (Bunde and Havlin, 1983).

4.5.3 *Reaction Limited Cluster-Cluster Aggregation (RLCA)*

In reaction-limited cluster-cluster aggregation (RLCA), a small repulsive barrier must be crossed before the aggregating clusters can contact each other and become irreversibly joined. This means that on average many encounters between clusters must take place before a bonding event occurs and the clusters are able to explore all possible bonding configurations (or at least a representative sample of them) before a new bond is formed. The RLCA model requires that the attractive particle-particle interaction potential must be greater than kT (the activation energy or bond formation energy), in order for aggregation to take place. Herein, a probability factor (sticking probability) is introduced as the fraction of particles that overcome the potential barrier and aggregate (Meakin, 1983b). A high sticking probability produces faster growth and *vice versa.*

An exponential growth of the cluster radius is associated with RLCA and the resulting fractal dimensions are higher than obtained in the DLCA models i.e. the

structures formed are more compact with $d_f \cong 1.56 \pm 0.3$ for $d = 2$, and $d_f \cong 2.0 \pm 0.1$ for $d = 3$ (Meakin, 1988).

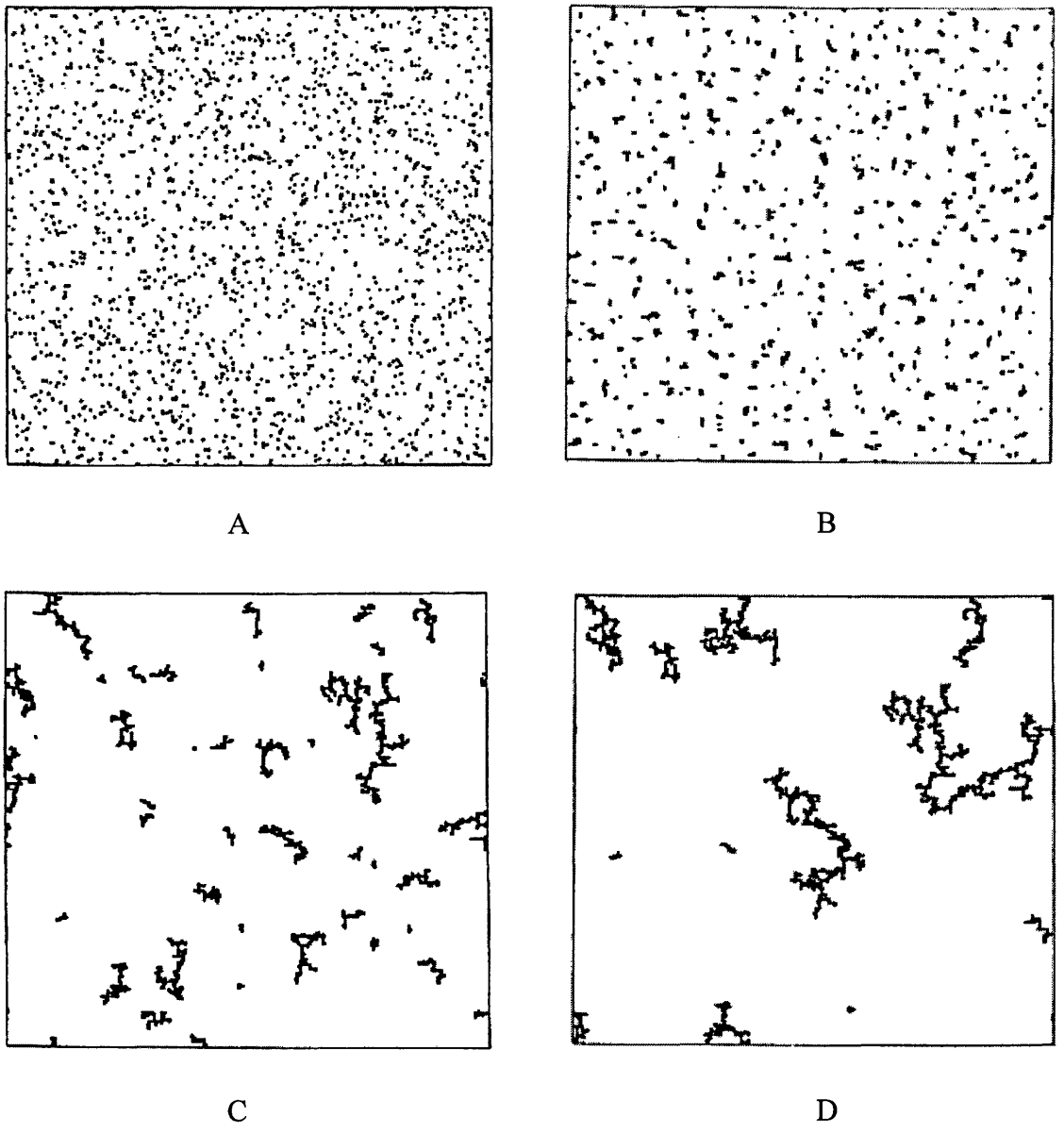

Figure 4.6. Four stages in computer simulation showing monomers evolving into large fractal clusters by diffusion limited cluster-cluster aggregation (Meakin, 1988).

4.6 Theory of Gelation

There are two main theories of gelation, namely, the classical mean-field theory of Flory (1941) and Stockmayer (1943) and the percolation theory. Both entail a power law scaling relationship for the divergence of the static properties (i.e. molecular weight and size) of the polymeric species at the gel point.

4.6.1 Classical Theory

In the mean field theory of gelation (the classical theory developed by Flory, 1941 and Stockmayer, 1943), gelation is modelled as a branching process of multifunctional monomers. The branching process is described as random cross-linking of multifunctional monomers on the Bethe lattice (or Cayley tree) as shown in Fig. 4.7. On the Bethe lattice, each black dot is a multifunctional monomer with functionality, $f \geq 3$, and a bond is formed between monomers with the probability, p. The mean field theory assumes that the probability p for bond formation is the same between any pair of monomers and no intramolecular bonds are allowed. The second assumption excludes the formation of rings or cycles within the branched macromolecule.

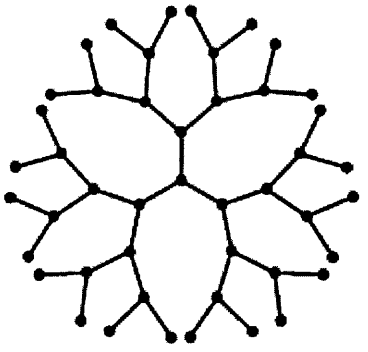

Figure 4.7. Branching process of multifunctional monomers (functionality = 3) on the Bethe lattice. Each monomer is modelled as a black dot, and cross-linking is formed between monomers with probability p.

The probability that a bond is formed equals the overall extent of reaction of all the functional groups (fraction of the functional groups that have reacted). The gel point in the mean field theory is defined as the critical extent of reaction, p_c, at which the molecular weight diverges, $M_w \rightarrow \infty$.

All gelation models yield unique scaling relations as a power law in the relative extent of reaction, $\varepsilon = (p_c - p)/p$ for structural (mean cluster size, size distribution) and physical (viscosity, modulus) properties near the critical point. However, different models yield different values for the critical exponents and different relations among them. The power law behaviour predicted by the Flory-Stockmayer (FS) theory for extents of reaction, $p < p_c$, (where p_c is the critical extent of reaction) are,

$$M_w \propto \varepsilon^{-k} \qquad (4.11)$$

And

$$R_z \propto \varepsilon^{-\upsilon} \qquad (4.12)$$

Where

$\varepsilon = |p_c - p|$

M_w is the average molecular weight

R_z is the typical cluster radius (or correlation length)

In the FS theory, the predicted exponents are $k = 1$ and $\upsilon = 0.5$. Also, scaling predictions for the steady-state viscoelastic properties G_e and η_0 can be shown as,

$$G_e \propto \varepsilon^{z} \qquad \text{for } p > p_c \qquad (4.13)$$

$$\eta_0 \propto \varepsilon^{-s} \qquad \text{for } p < p_c \qquad (4.14)$$

In which z = 3, and s = 0, which implies the viscosity is not predicted to diverge, growing only logarithmically near the gel point (Hodgson and Amis, 1990).
The relationship between the exponents z and s with the stress relaxation exponent, α can be defined as (Winter, 1987),

$$\alpha = \frac{z}{(s+z)} \qquad (4.15)$$

Where, for the FS theory, α = 1 (for z = 0 and s = 0).

The principle shortcoming of the FS theory is that for branched clusters, $d_f = 4$ i.e. the mass, M, increases as R^4 for d = 3, and d_f becomes larger than the space dimension, hence therefore unphysical (Hess *et al.*, 1988). Thus, a more refined model for the sol-gel transition was proposed independently by Stauffer (1985) and de Gennes (1979), titled the 'Percolation Theory'.

4.6.2 The Percolation Theory

Percolation theory was first introduced by Broadbent and Hammersley (1957) to describe diffusion in disordered media and concerns the permeation threshold. The percolation idea was later adapted to the gelation process by de Gennes (1976) and Stauffer (1976) and was suggested to possibly give a better description of gelation than the classical statistical methods, since the mean field assumption of no intramolecular reactions is avoided.

A percolation model is a collection of points distributed in space, certain pairs of which are said to be adjacent or linked. Whether or not two points are adjacent is governed by a random mechanism, the details of which depend on the context in which the model is used. Two basic types of mechanism may be distinguished. The points may have fixed positions and random linkages made between them or the positions may be random and the linkages determined by a rule which depends on the positions. The resulting models are known as bond percolation and site

percolation respectively (Figure 4.8), the terminology coming from applications in solid-state physics. In both cases, structures of connected points can be defined (clusters), in a way that it is possible to create a path between any two points of the cluster.

Site percolation theory assumes a lattice of sites (bond percolation theory assumes a lattice of bond links), which are either occupied or empty. The probability that a site is occupied by a particle is P_r, and the probability that a site is vacant is 1-P_r. In terms of gelation, P_r is proportional to the extent of reaction. When P_r is increased, the average size of the clusters increases and at a critical concentration (or extent of reaction), P_c, a large cluster emerges which connects opposite edges of the lattice (corresponding to the gel point). This critical concentration is also known as the *percolation threshold*, at which an infinite cluster is established, where the term 'infinite' is used in the sense that the cluster is *sample-spanning* and its size diverges when the lattice size is infinite. If P_r increases further, the density of the infinite cluster increases, as more and more sites become part of the infinite cluster, and hence the average size of the finite clusters decreases.

The percolation threshold, P_c depends explicitly on the type of lattice considered. For example, in a square lattice, $P_c \approx 0.59$, whereas if a triangular lattice is used, $P_c \approx 0.5$ (for bond percolation, $P_c \approx 0.5$ and 0.35 for square and triangular lattices respectively).

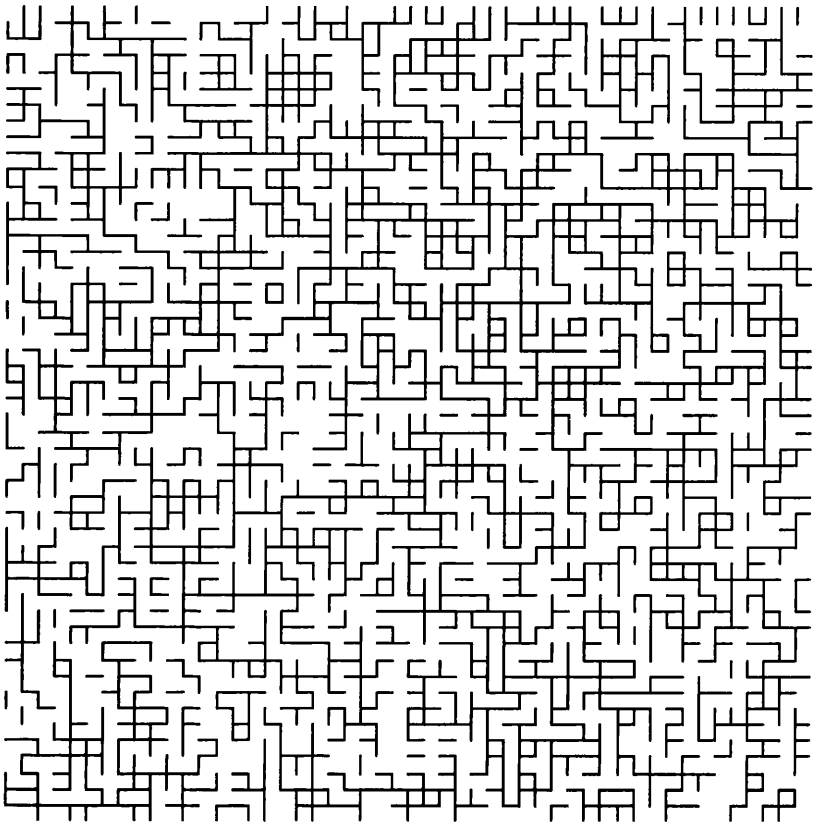

Figure 4.8. Detail of bond percolation on the square lattice in two dimensions with percolation probability, $p_r = 0.51$.

Fractal dimensions are independent of the type of lattice but are dependent on the dimension, d, where $d_f \cong 1.9$ for $d = 2$ and $d_f \cong 2.5$ for $d = 3$. Stauffer (1985) accounts a number of possible lattice arrangements and their respective percolation thresholds.

The FS theory may be viewed as a mean field version of the percolation model, hence Equations 4.11 to 4.14 also determine the characteristics of the percolation model, where $\varepsilon = |p_c - p| \equiv |P_c - P_r|$. However, the percolation model predicts different values for the exponent's k, υ, z and s, depending on the specific model assumptions used to describe the experimental results (Martin et al, 1988; Mours and Winter, 1996).

For a system obeying Rouse dynamics (Rouse, 1953; Edwards and Muthukumar, 1984), in terms of rigid chains and hydrodynamic screening with the excluded volume effect dominant, d_f and α have been found to be related by,

$$\alpha = \frac{d}{d_f + 2} \tag{4.16}$$

Muthukumar (1985) and Cates (1985) derived an expression for the relaxation exponent, α in terms of the fractal dimension for a monodisperse solution of polymers using flexible chains,

$$\alpha = \frac{d_f}{d_f + 2} \tag{4.17}$$

Following studies of the influence of excluded volume, Hess *et al.*, (1988) suggested that cluster growth models using rigid bonds may not properly describe the dimensions of the critical gel. Assuming the excluded volume to be completely screened, the prediction for a polydisperse material becomes (Muthukumar, 1989),

$$\alpha = \frac{d(d + 2 - 2d_f)}{(2(d + 2 - d_f))} \tag{4.18}$$

Where

d is the Euclidean dimension of the embedding space

This suggests that the sol-gel transition is not a pure percolation process but a combination of percolation and either partial or full extent of screening, depending on the nature of the polymer system.

4.7 Fibrin Clot Structures Quantified by Fractal Analysis

4.7.1 Clot Structure and Clot Quality

Thrombo-embolic disease, and coagulation abnormalities, account for a large number of deaths in Western society. This number is expected to grow considerably over the next 25 years (ageing). These outcomes are a careful balance between thrombotic and fibrinolytic tendencies. Disease states have a direct influence on ***'clot quality'*** and ***'clot structure'*** with significant effects on clinical outcome, in terms of morbidity and mortality. Abnormalities in coagulation directly affect the quality of clot structure.

Within this field, no rigorous quantitative basis exists for defining what is meant by clot 'quality'/'structure'. So the question is asked, how we interpret a 'good, bad, tight, loose, open, coarse, dense' etc clot. Thus no quantitative basis exists for relating clot 'quality'/'structure' to the mechanical (viscoelastic) properties of clots.

Clinicians rely on laboratory tests to assess coagulation state of system such as thromboelastography (TEG). It is a method used widely to measure blood clot formation time, and clot elasticity. Hence, provides a rapid diagnosis of disease states and an assessment of therapeutic options. A distinct disadvantage of the use of thromboelastography is many of the parameters measured by this method have not been related to the normal viscoelastic properties used to characterise materials and have no physical meaning except in comparison with other such thromboelastography measurements.

To interpret the relationship between coagulation and clot structure, investigators have used SEM to look at clot compactness and quality. With these SEM images (e.g. Fig. 4.9), researchers have counted individual fibrin strands in the network to correlate abnormal coagulation with clot strength and rigidity. This data lacks objective assessment, the clot may appear to have increased denseness of fibrin fibres but this does not relate to improved clot quality or strength.

How do we determine what is a 'bad' or 'good' clot in terms of pathological illness and treatment options?

(a) 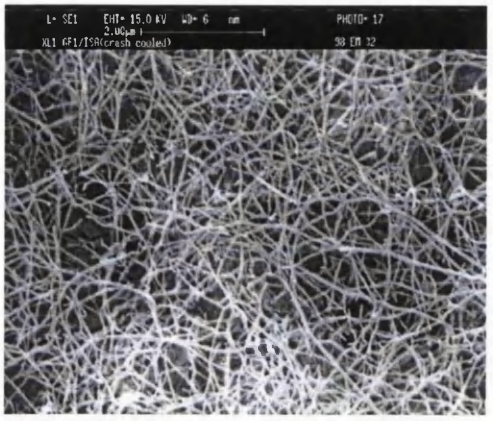

(b) 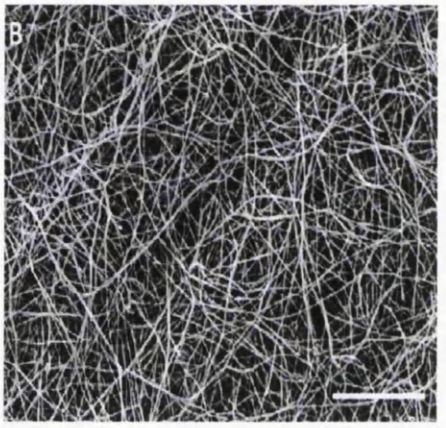

(c) 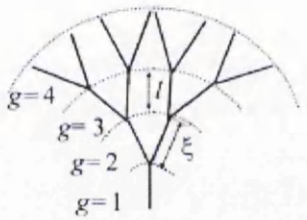

Figure 4.9 (a, b). Fractal nanofibre network in an organo-gel (Liu & Sawant, Appl. Phys. Lett. 2001), (c) Fibrin gel network (John Wiesel).

Laser scanning confocal microscopy provides a basis for performing a *fractal analysis* as a quantitative basis for defining clot quality and clot structure. The experimental methods involve following the mechanical properties of a gelling system up to and beyond the gel point.

As mentioned above, fractal geometry is well established in many areas of biomedical research as fractal patterns are intimately connected to natural optimisation principles in both dynamical processes and structure formation. It will present a framework for the quantification of structural complexity. The measurements will allow us to monitor the evolution of structure and mechanical

properties over many hours, or days, following the attainment of the Gel Point. No other researchers have used such advanced techniques to study the bio gel systems at physiologically relevant concentrations or temperatures.

In the present work, a dynamic approach using confocal microscopy is implemented to visualise fibrin clot networks and several forms of fractal analysis are investigated for quantifying structural complexity. This issue is now explored in the following sections.

Chapter 5

Optical-based Characterisation of the Fractal Structure of Fibrin Clot Networks

Introduction

The technique of laser scanning confocal microscopy has become a fundamental tool in biology and the biomedical sciences, as well as in materials science due to attributes that are not readily available using other traditional optical microscopy (Pawley, 1995; Sheppard and Shotton; 1997, Padock 1999; Diaspro 2002; Matsumoto, 2002; Müller, 2002). LSCM represents one of the most significant advances in optical microscopy ever developed, primarily because the technique enables visualisation deep within both living and fixed cells and tissues. The technique also affords the ability to collect sharply defined optical sections from which three-dimensional renderings can be created. The application of a wide array of new synthetic and naturally occurring fluorochromes has made it possible to identify cells and sub-microscopic cellular components with a high degree of specificity amid non-fluorescing material.

The basic concept of confocal microscopy was originally developed by Marvin Minsky in 1955 when he was a postdoctoral student at Harvard University (Minsky, 1988). Minsky sought to image neural networks in unstained preparations of brain tissue and was driven by the desire to image biological events as they occur in living systems. Minsky's invention would perform a point by point image construction by focusing a point of light sequentially across a specimen and then collecting some of the returning rays. By illuminating a single point at a time, Minsky avoided most of the unwanted scattered light that obscures an image when the entire specimen is illuminated at the same time. Additionally, the light returning from the specimen would pass through a second pinhole aperture that would reject rays that were not directly from the focal point. The remaining desirable light rays would then be collected by a photomultiplier and the image gradually reconstructed using a long-persistence screen. To build the image, Minsky scanned the specimen by moving the stage rather than the light rays. This was to avoid the challenge of trying to maintain sensitive alignment of moving optics. Minsky's invention resumed largely unnoticed, due most probably to the lack of intense light sources necessary for imaging and the computer horsepower required to handle large amounts of data.

Following Minsky's work, in 1967, M. David Egger and Mojmir Petran (Egger and Petran, 1967) fabricated a multiple-beam confocal microscope in the late 1960s that utilised a spinning (Nipkow) disk for examining unstained brain sections and ganglion cells. Continuing in this area, Egger went on to develop the first mechanically scanned confocal laser microscope, and published the first recognisable images of cells in 1973 (Davidovits and Egger, 1973). During the late 1970s and the 1980s, advances in computer and laser technology, coupled to new algorithms for digital manipulation of images, led to a growing interest in confocal microscopy (Amos and White, 2003).

Modern confocal microscopes have kept the key element of Minsky's design, the pinhole apertures and point-by-point illumination of the specimen. Advances in optics and electronics have been incorporated into current designs and provide improvements in speed, image quality, and storage of the generated images. Confocal microscopy offers several advantages over conventional wide-field optical microscopy. These include the ability to control depth of field, elimination or reduction of background information away from the focal plane (that leads to image degradation), and the capability to collect serial optical sections from thick specimens. The basic contribution to the confocal approach is the use of spatial filtering techniques to eliminate out-of-focus light or glare in specimens whose thickness exceeds the immediate plane of focus. There has been a vast explosion in the popularity of confocal microscopy in recent years (Pawley, 1995; Paddock, 1999; Diaspro, 2002; and Matsumoto, 2002). This growth is due in part to the relative ease with which extremely high-quality images can be obtained from specimens prepared for conventional fluorescence microscopy, and the growing number of applications in cell biology that rely on imaging both fixed and living cells and tissues. In fact, confocal technology is proving to be one of the most significant advances ever achieved in optical microscopy.

5.1 Principles of Confocal Microscopy

The principle of LSCM is diagrammatically presented in Figure 5.1. Coherent light emitted by the laser system (laser excitation source) passes through a pinhole aperture that is situated in a conjugate plane with a scanning point on the specimen which in turn is focused by an objective lens into a small focal volume within a fluorescent specimen. A mixture of emitted fluorescent light as well as reflected laser light from the illuminated spot is then recollected by the objective lens. A beam splitter separates the light mixture by allowing only the laser light to pass through and reflecting the fluorescent light into the detection apparatus. After passing a pinhole the fluorescent light is detected by a photo-detection device (photomultiplier tube (PMT) or avalanche photodiode) transforming the light signal into an electrical one which is recorded by a computer.

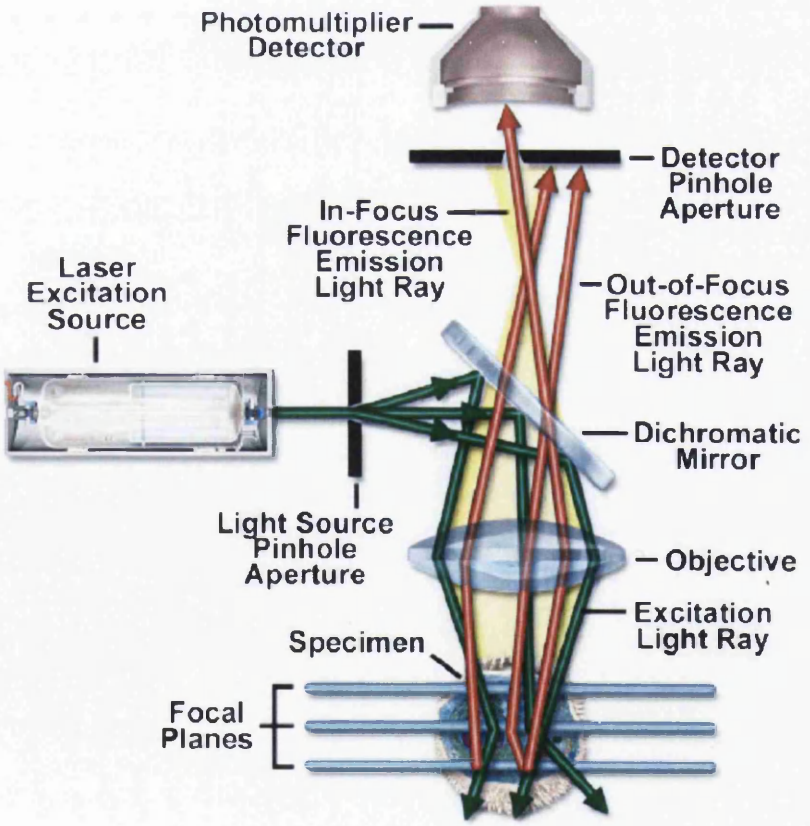

Figure 5.1. Schematic diagram of the optical pathway and principal components in a laser scanning confocal microscope.

The decisive design feature of a LCSM compared with a conventional microscope are these confocal pinhole apertures arranged in a plane conjugate to the intermediate image plane and, thus, to the object plane of the microscope. As seen in Figure 5.1, the detector aperture obstructs the so called out-of-focus (or out-of-plane) light, fluorescent light not originating from the focal plane of the objective lens. Light rays from below the focal plane come to a focus before reaching the detector pinhole, and then they expand out so that most of the rays are physically blocked from reaching the detector by the pinhole. In the same way, light from above the focal plane is focused behind the detector pinhole, so that most of this light also hits the edges of the pinhole and is not detected.. In this way, out-of-focus information from above and below the focal plane is greatly reduced, which results in sharper images with significantly reduced background haze that is typical of conventional microscopy techniques. Therefore, the confocal microscope is an inherently depth-discriminating optical system. By varying the pinhole diameter, the degree of confocality can be adapted to practical requirements. With the aperture fully open, the image is non-confocal.

The detected light originating from an illuminated volume element within the specimen represents one pixel in the resulting image. As the laser scans over the plane of interest a whole image is obtained pixel by pixel and line by line, while the brightness of a resulting image pixel corresponds to the relative intensity of detected fluorescent light. The beam is scanned across the sample in the horizontal plane using one or more (servo-controlled) oscillating mirrors. This scanning method usually has a low reaction latency and the scan speed can be varied as slower scans provide a better signal to noise ratio resulting in better contrast and higher resolution. Information can be collected from different focal planes by raising or lowering the microscope stage. It is therefore possible with a LSCM to exclusively image a thin optical slice out of a thick specimen (typically, up to 100 μm), a method known as optical sectioning. Under suitable conditions, the thickness (z dimension) of such a slice may be less than 500 nm.

5.2 Laser Scanning Confocal Microscope Configuration

Basic microscope optical system characteristics have remained primarily unchanged for many decades due to engineering restrictions on objective design, the static properties of most specimens, and the fact that resolution is governed by the wavelength of light (Pawley, 1995; Paddock, 1999; Diaspro, 2002; Matsumoto, 2002; Sheppard and Shotton, 1997; Müller, 2002; and Hibbs, 2004). Although, fluorescent probes that are employed to add contrast to biological specimens, and other technologies associated with optical microscopy techniques, have improved considerably. The growth and development of the confocal approach is a direct result of a renaissance in optical microscopy that has been largely fuelled by advances in modern optical and electronics technology.

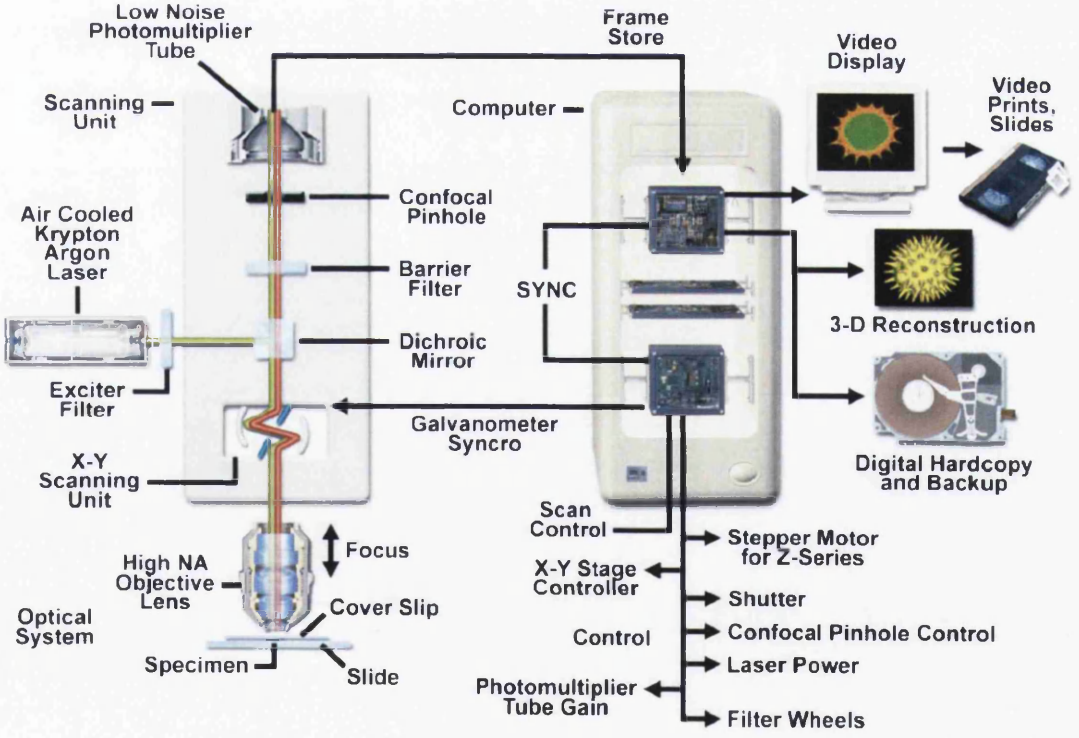

Figure 5.2. Laser scanning confocal microscope configuration and information flow schematic diagram.

These include stable multi-wavelength laser systems that provide better coverage of the ultraviolet, visible, and near infra-red spectral regions, improved interference filters, sensitive low noise wide band detectors, and, far more powerful computers. Computer systems are now available with relatively low cost memory arrays, image analysis software packages and high resolution video displays. The flow of information through a modern confocal microscope and standard system configuration is presented diagrammatically in Figure 5.2 (Paddock, 1999).

5.3 Confocal Scanning Implementations

Thus far, we have only touched upon how scanning the illumination and collection is achieved. In modern confocal microscopes, two fundamentally different techniques for beam scanning have been developed, single-beam scanning and multiple beam scanning.

5.3.1 Single-beam Scanning

Single-beam scanning, one of the more popular methods implemented in a majority of the commercial laser scanning microscopes, uses a pair of computer-controlled galvanometer mirrors to scan the specimen in a raster pattern at a rate of approximately one frame per second. Single-beam scanning can most conveniently be employed either by the lateral movement of the specimen in the focal plane relative to a stationary optical path (specimen scanning), or by the angular movement of the illuminating beam filling the back focal plane of a stationary objective (illumination scanning), which causes the focused light beam to move laterally in the focal plane relative to the stationary specimen.

Specimen scanning is more commonly used in industrial settings, whereas such a scheme for biological samples, especially living ones, will not tolerate the

shaking from fast scanning. The main advantage of specimen scanning is that it avoids off-axis aberrations and thus can be used with a variety of objective.

In illumination scanning, the scanning spot is typically moved in a raster scan fashion over the specimen. There are several different approaches for illumination scanning. In all implementations, however, if the lens suffers from off-axis aberrations (astigmatism, coma and field curvature), this will degrade the image. Specifically, coma spreads the excitation light away from the location of the aberration free scanning spot, thus decreasing the amount of fluorescence from this location that reaches the detector. Astigmatism and field curvature both move the scanning spot away from the nominal plane of focus, thus exciting light that would otherwise be out of focus.

The most common method for illumination scanning is based on using two oscillating mirrors to deflect the angle of the light beam going into the specimen (scanning) and deflecting the angle of emitted light in the return light path (descanning). One mirror scans the illumination and detection along the 'fast axis' (e.g. horizontal direction), and the other mirror scans the 'slow axis' (e.g. vertical direction). This process continues until an entire 2D image is collected, and it can be repeated at the same focus to generate a time series of images, or the focus can be vertically stepped up or down to generate a 3D image stack. The speed of this method is limited by the mechanical characteristics of the fast axis mirror. Faster scanning rates near to video speed can be achieved using acousto-optic devices or oscillating mirrors.

5.3.2 Multiple-beam Scanning

In contrast, multiple-beam scanning confocal microscopes are equipped with a spinning Nipkow disk containing an array of pinholes and micro lenses (Nakano, 2002). These instruments frequently use arc-discharge lamps for illumination instead of lasers to reduce specimen damage and enhance the detection of low fluorescence levels during real time image collection. An additional important feature of the multiple-beam microscopes is their ability to readily capture images with an array

detector, such as a charge-coupled device (CCD) camera system. A notable advantage of the spinning-disk is that, because many spots can be illuminated simultaneously and rapid rotation of the disc illuminates the same spot several times within a frame time (for example, within the 33 ms exposure required for video rate), the total dwell time can be much larger than for the LSCM with a single pinhole aperture. This increase in dwell time allows for much faster frame rates.

5.4 Advantages and Disadvantages of Confocal Microscopy

Laser scanning confocal microscopy has emerged as a significant new technique which exhibits several advantages over convential optical microscopy. The most important of these stem from the fact that out-of-focus blur is essentially absent from confocal images, giving the capability for direct non-invasive serial optical sectioning of intact and living specimens under a variety conditions with enhanced clarity. This leads to the possibility of generating three-dimensional images of thick transparent objects such as biological cells and tissues. Laser scanning confocal microscopy has the ability to serially produce thin optical sections through fluorescent specimens that have a thickness ranging up 100 μm. The image series is collected by coordinating incremental changes in the microscope fine focus mechanism with sequential image acquisition at each step. Image information is restricted to a well-defined plane, rather than being complicated by signals arising from remote locations in the specimen. The technique allows profiling of the surfaces and dimensions of three-dimensional objects and multi-layer structures by a non-contacting and non-destructive method. Furthermore, optical sectioning eliminates artifacts that occur during physical sectioning and fluorescent staining of tissue specimens for traditional forms of microscopy.

Many probes of cell and tissue structure are amenable to light microscopy, especially fluorescence microscopy, and commercially available confocal microscopes can be equipped with multiple light sources of differing wavelengths so that a variety of fluorophores can be excited. Commonly used sources of of excitation in laser-based confocal microscopes include argon (Ar; 488 nm and 514 nm), krypton (Kr; 568 nm), argon-krypton (Ar-Kr; 488 nm, 514 nm, and 568 nm),

and helium-neon (He-Ne; 633 nm) lasers. Hence, most systems can excite a set of fluorescent probes spanning nearly the full range of visible wavelengths.

The majority of software packages accompanying commercial confocal instruments are capable of generating composite and and multi-dimensional views of optical section data acquired from z-series image stacks. The software packages can be implemented to create either a single three-dimensional representation of the specimen (Figure 5.3) or a video movie sequence compiled from different views of the specimen volume.

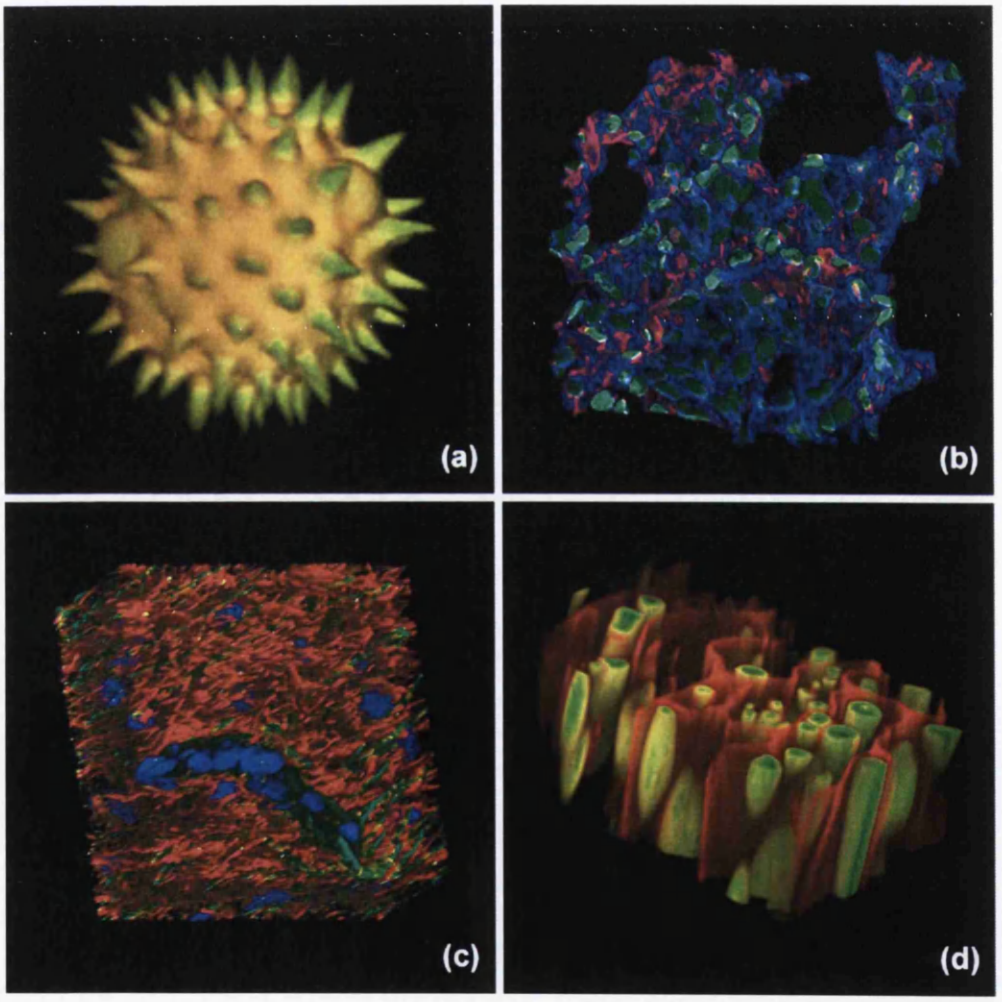

Figure 5.3. Three-dimensional volume renders from confocal microscopy optical sections. (a) Three-dimensional representation of a sunflower pollen grain. (b) Mouse lung tissue section. (c) Rat brain thick section. (d) Auto-fluorescence in a thin section of fern root.

These representations often mimic the effect of rotation or similar spatial transformation that enhances the appreciation of the specimen's three-dimensional character. Also, many software packages enable investigators to conduct measurements of length, volume, and depth, and specific parameters of the images, such as opacity can be interactively altered to reveal internal structures of interest at differing levels within the specimen.

Further advantages of scanning confocal microscopy include the feature termed, the zoom factor, which employs the ability to adjust magnification electronically by varying the area scanned by the laser without having to change objectives. The zoom factor is usually implemented to adjust the spatial resolution by altering the scanning laser sampling period (Pawley, 1995 and Paddock, 1999). Increasing the zoom factor reduces the specimen area scanned and simultanously reduces the scanning rate. This allows an increased number of samples along a comparable length, which increases both the image spatial resolution and display magnification. Confocal zoom is typically employed to match digital image resolution with the optical resolution of the microscope when low numerical aperture and magnification objectives are being used to collect data.

In most cases, the images generated by the confocal microscope are in digital form. Thus, a wide range of digital image processing capabilities can be applied to the data set. Features of cell and tissue structure can be quantified and analysed with the aid of software packages that either stand alone or are already integrated into the confocal system software.

5.5 Molecular Fluorescence

Max Planck in the early 20th Century published a revolutionary idea suggesting the energy of atoms or molecules is discontinuous and energy changes occur by means of moving through energy levels. This has become a well-known phenomenon aiding the creation of a general theory for atomic transitions. Similar to the well-known electronic states, molecules can exist in various other energy states due to their rotational and vibrational behaviour with electrons being able to move through these states by the association of a finite amount of energy.

An example of a molecular state is shown in Figure 5.4 where an electron from the ground state, S^0 is excited to the first excited state, $S^{1'}$ by a photon of energy supplied by an external source.

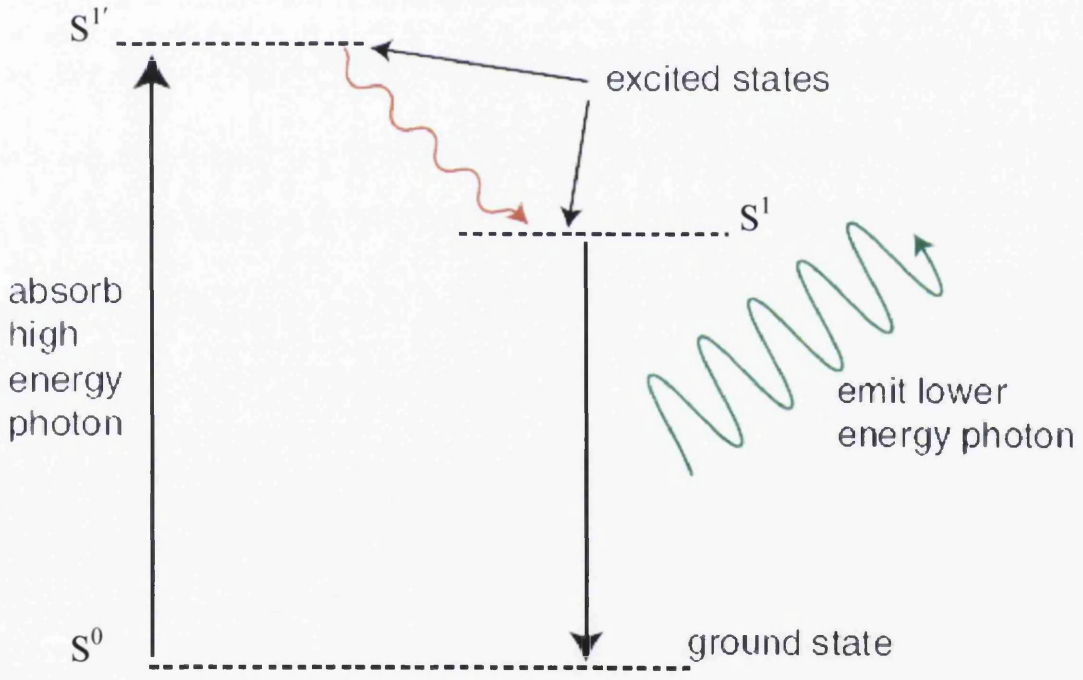

Figure 5.4. Mechanism of fluorescence. The horizontal lines indicate quantum energy levels of the molecule. A fluorescent dye molecule is raised to an excited energy state by a high-energy photon. It loses a little energy to other molecules and drops to a lower excited state. It loses the rest of the energy by emitting light of a lower energy.

Typically, the molecule quickly (within 10^{-8} sec) dissipates some of the absorbed energy through collisions with surrounding molecules causing the electron to drop to a lower energy level, S^1 (the second black line). If the surrounding molecules are not able to accept the larger energy difference needed to further lower the molecule to its ground state, it may undergo spontaneous emission, thereby losing the remaining energy, by emitting light of a longer wavelength.

5.5.1 Fluorophores for Confocal Microscopy

Biological laser scanning confocal microscopy relies profoundly on fluorescence as an imaging mode. This is primarily due to the high degree of sensitivity afforded by the technique coupled with the ability to specifically target structural components and dynamic processes in complex biomolecular assemblies, including living cells, with exquisite sensitivity and selectivity. Many fluorescent probes are constructed around synthetic aromatic organic chemicals designed to bind with a biological macromolecule, such as a protein or nucleic acid.

The history of synthetic fluorescent probes dates back over a century to the late 1800s when many of the cornerstone dyes for modern histology were developed. These include pararosaniline, methyl violet, malachite green, safranin O, methylene blue, and numerous azo (nitrogen) dyes, such as Bismarck brown. Even though these dyes were highly coloured and capable of absorbing selected bands of visible light, most were only weakly fluorescent and would not be useful for the fluorescence microscopes that would be developed several decades later. However, several synthetic dye classes synthesized during this period, based on the xanthene and acridine heterocyclic ring systems, proved to be highly fluorescent and provided a foundation for the development of modern synthetic fluorescent probes. Among the most notable of these early fluorescent dyes were the substituted xanthenes, fluorescein and rhodamine B, and the biaminated acridine derivative, acridine orange.

In the early twentieth century fluorochromes were introduced to fluorescence microscopy as vital stains for bacteria, protozoa, and trypanosomes, but did not see widespread use until the 1920s when fluorescence microscopy was first used to study dye binding in fixed tissues and living cells (Hibbs, 2004). During the past 60 years, advances in immunology and molecular biology have produced a wide spectrum of secondary antibodies and provided insight into the molecular design of fluorescent probes targeted at specific regions within macromolecular complexes.

Fluorescent probe technology and cell biology were dramatically altered by the discovery of the green fluorescent protein (GFP) from jellyfish and the development of mutant spectral variants, which have opened the door to non-invasive fluorescence multicolour investigations of sub cellular protein localization, intermolecular interactions, and trafficking using living cell cultures. (Lippincott-Schwartz and Patterson, 2003). Regardless of the numerous advances made in fluorescent dye synthesis during the past few decades, very little solid evidence exists about molecular design rules for developing new fluorochromes, particularly with regard to matching absorption spectra to available confocal laser excitation wavelengths. Consequently, the number of fluorophores that have found widespread use in confocal microscopy is a limited subset of the many thousands that have been discovered.

5.5.2 Significant Characteristics of Fluorophores

Fluorophores are catalogued and specified according to their absorption and fluorescence properties, including the spectral profiles, wavelengths of maximum absorbance and emission, and the fluorescence intensity of the emitted light. One of the most useful and recognised quantitative parameters for characterizing absorption spectra is the molar extinction coefficient, ε (see Figure 5.5), which is a direct measure of the ability of a molecule to absorb light. The quantum yield of a fluorophore represents a quantitative measure of fluorescence emission efficiency, and is expressed as the ratio of the number of photons emitted to the number of photons absorbed. In other words, the quantum yield represents the probability that a

given excited fluorophore will produce an emitted (fluorescence) photon. Quantum yields typically range between a value of 0 and 1, and fluorescent molecules commonly employed as probes in microscopy have quantum yields ranging from very low (0.05 or less) to almost unity. In general, a high quantum yield is desirable in most imaging applications. The quantum yield of a given fluorophore varies considerably with environmental factors, such as metallic ion concentration, pH, and solvent polarity.

Fluorophores selected for confocal applications must exhibit a brightness level and signal persistence sufficient for the instrument to obtain image data that does not suffer from excessive photo bleaching, artefacts and low signal-to-noise ratios. Excitation conditions in confocal microscopy are several orders of magnitude more severe than in wide field fluorescence, however, restrictions imposed by characteristics of the fluorophores and efficiency of the microscope optical system become the dominating factor in determining excitation rate and emission collection strategies (Pawley, 1995; Hibbs, 2004).

In LSCM, irradiation of the fluorophores with a focused laser beam at high power densities increases the emission intensity up to the point of dye saturation, a condition whose parameters are dictated by the excited state lifetime (Tsien and Waggoner, 1995). In the excited state, fluorophores are unable to absorb another incident photon until they emit a lower-energy photon through the fluorescence process. When the rate of fluorophore excitation exceeds the rate of emission decay, the molecules become saturated and the ground state population decreases. Consequently, a majority of the laser energy passes through the specimen undiminished and does not contribute to fluorophore excitation. Balancing fluorophore saturation with laser light intensity levels is, therefore, a critical condition for achieving the optimal signal-to-noise ratio in confocal experiments (Pawley, 1995; Hibbs, 2004; Tsien and Waggoner, 1995). The number of fluorescent probes currently available for confocal microscopy runs in the hundreds (Haugland, 2005; Kasten, 1999), with many dyes having absorption maxima closely associated with common laser spectral lines (Haugland, 2005). An exact match between a

particular laser line and the absorption maximum of a specific probe is not always possible, but the excitation efficiency of lines near the maximum is usually sufficient to produce a level of fluorescence emission that can be readily detected.

5.5.3 Traditional Fluorescent Dyes

The selection of fluorescent probes for confocal microscopy must address the specific capabilities of the instrument to excite and detect fluorescence emission in the wavelength regions made available by the laser systems and detectors. Although the current lasers used in confocal microscopy produce discrete lines in the ultraviolet, visible, and near-infrared portions of the spectrum, the location of these spectral lines does not always coincide with absorption maxima of popular fluorophores. In reality, it is not necessary for the laser spectral line to correspond exactly with the fluorophore wavelength of maximum absorption, but the intensity of fluorescence emission is regulated by the fluorophore extinction coefficient at the excitation wavelength (as discussed above). The most common lasers for confocal microscopy are air-cooled argon and krypton-argon ion lasers, the new blue diode lasers, and a variety of helium-neon systems (Hibbs, 2004; Murphy 2001). Collectively, these lasers are capable of providing excitation at ten to twelve specific wavelengths between 400 and 650 nanometres.

Most of the classical fluorescent probes that have been successfully utilised for many years in confocal microscopy (Kasten, 1999) are fluorescein isothiocyanate, Lissamine rhodamine, and Texas red. Fluorescein is one of the most popular fluorochromes ever designed, and has enjoyed extensive application in immunofluorescence labelling. This xanthene dye has an absorption maximum at 495 nanometres, which coincides quite well with the 488 nanometre (blue) spectral line produced by argon-ion and krypton argon lasers, as well as the 436 and 467 principal lines of the mercury and xenon arc-discharge lamps (respectively). Also, the quantum yield of fluorescein is very high and a significant amount of information has been gathered on the characteristics of this dye with respect to the physical and

chemical properties (Wessendorf and Brelje, 1992). On the negative side, the fluorescence emission intensity of fluorescein is heavily influenced by environmental factors (such as pH), and the relatively broad emission spectrum often overlaps with those of other fluorophores in dual and triple labelling experiments (Wessendorf and Brelje, 1992; Entwistle and Noble, 1992; Johnson, 1998).

Tetramethyl rhodamine (TMR) and the isothiocyanate derivative (TRITC) are frequently employed in multiple labelling investigations in wide-field microscopy due to their efficient excitation by the 546 nanometre spectral line from mercury arc-discharge lamps.

Several of the acridine dyes are useful as fluorescent probes in confocal microscopy (Kasten, 1999). The most widely utilised, acridine orange, consists of the basic acridine nucleus with dimethylamino substituents located at the 3 and 6 positions of the tri-nuclear ring system. In physiological pH ranges, the molecule is protonated at the heterocyclic nitrogen and exists predominantly as a cationic species in solution. Acridine orange binds strongly to DNA by intercalation of the acridine nucleus between successive base pairs, hence its suitability in this area of biological matter (Johnson, 1998; Kasten, 1999).

In this Thesis, the sought fluorescent dye Alexa Fluor was chosen for the imaging of the biological evolution of fibrinogen-thrombin systems, which is discussed further below.

5.5.4 Alexa Fluor Dyes

Dramatic advances in modern fluorophore technology are exemplified by the Alexa Fluor dyes (Haugland, 2005; Panchuk-Voloshina *et al.*, 1999; Berlier *et al.*, 2003) introduced by Molecular Probes (*Alexa Fluor* is a registered trademark of Molecular Probes). These sulfonated rhodamine derivatives exhibit higher quantum yields for more intense fluorescence emission than spectrally similar probes, and have several additional improved features, including enhanced photo-stability, absorption spectra matched to common laser lines, pH insensitivity, and a high degree of water solubility. In effect, the resistance to photo-bleaching of Alexa Fluor dyes is so dramatic (Berlier *et al.*, 2003) that even when subjected to irradiation by

high-intensity laser sources, fluorescence intensity remains stable for relatively long periods of time in the absence of antifade reagents. This characteristic enables the water soluble Alexa Fluor probes to be readily utilized for both live-cell and tissue section investigations, as well as in traditional fixed preparations.

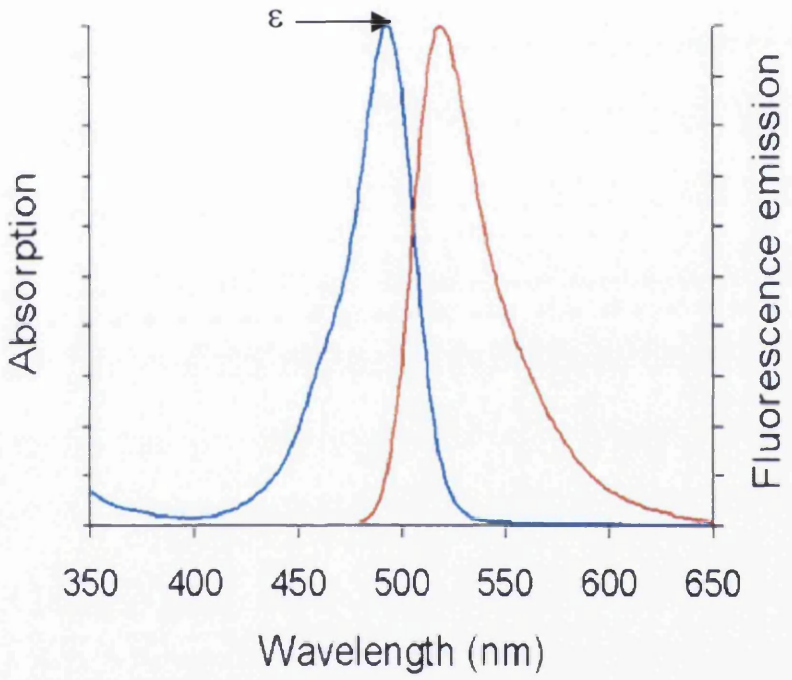

Figure 5.5. Absorption and fluorescence emission spectra for an Alexa Fluor 488 dye.

Alexa Fluor dyes are available in an extensive range of fluorescence excitation and emission wavelength maxima, ranging from the ultraviolet and deep blue to the near-infrared regions (Haugland, 2005). Alphanumeric names of the individual dyes are associated with the specific excitation laser or arc-discharge lamp spectral lines for which the probes are intended. For example, Alexa Fluor 488 is designed for excitation by the blue 488-nanometre line of the argon or krypton-argon

ion lasers. With spectra almost identical to those of fluorescein, but with far greater fluorescence in its conjugates and significantly better photo-stability, the Alexa Fluor 488 dye is indisputably the best green-fluorescent reactive dye available (Panchuk-Voloshina *et al.*, 1999; Turner *et al.*, 2000; Triantafilou *et al.*, 2000). It is probably the best dye available for single-molecule detection of bio-conjugates, for fluorescence correlation spectroscopy and for fluorescence polarization measurements.

This green-fluorescent dye exhibits several unique features,

- Fluorescence spectra almost identical to those of fluorescein, with excitation/emission maxima of 495/519 nm and a fluorescence lifetime of ~ 4.1 nanoseconds.
- Strong absorption, with an extinction coefficient greater than 65,000 $cm^{-1}M^{-1}$.
- Much greater photo-stability than fluorescein (Figure 5.6), allowing more time for observation and image capture.
- pH-insensitive fluorescence between pH 4 and 10.
- Superior fluorescence output per protein conjugate, surpassing that of any other spectrally similar fluorophore-labelled protein, including fluorescein conjugates (Figure 5.7) and Cy2 conjugates of antibodies.
- Water solubility, with no organic co-solvents required in labelling reactions.

After considering the above, the green-fluorescent Alexa Fluor 488 fibrinogen conjugate (Molecular Probes) was used to investigate the structural evolution of fibrinogen clot networks using fluorescence microscopy.

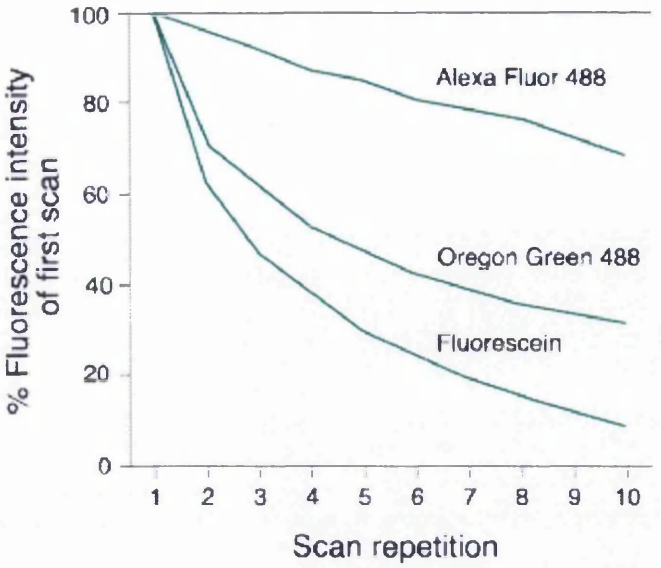

Figure 5.6. Photo-bleaching resistance of the green-fluorescent Alexa Fluor 488, Oregon Green 488 and fluorescein dyes, as determined by laser-scanning cytometry. Data are expressed as percentages derived from the mean fluorescence intensity (MFI) of each scan divided by the MFI of the first scan. Data contributed by Bill Telford, Experimental Transplantation and Immunology Branch, National Cancer Institute.

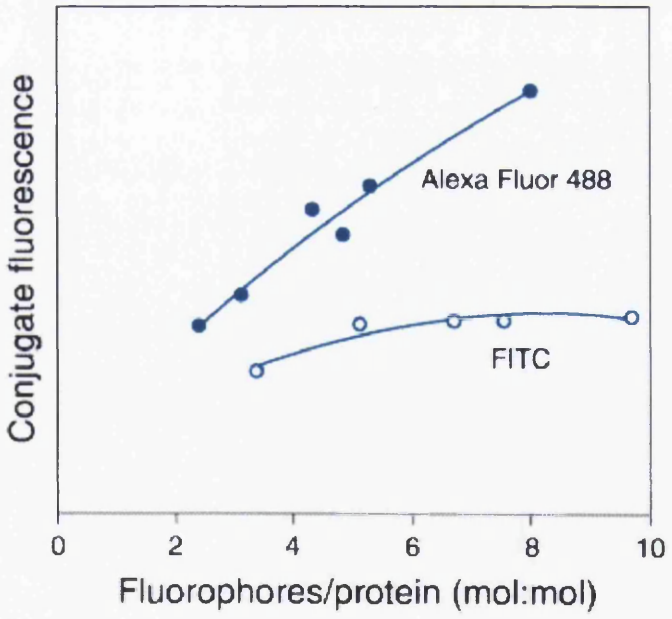

Figure 5.7. Comparison of the relative fluorescence of goat anti–mouse IgG antibody conjugates prepared from the Alexa Fluor 488 dye and from fluorescein isothiocyanate (FITC). [www.Invitrogen.com].

5.6 Quantifying Structural Complexity with Fractal Analysis

5.6.1 Materials

Human conjugated fibrinogen (Alexa Flour 488 conjugate, 5 mg/ml) was purchased from Invitrogen, and dissolved in 0.1 M sodium bicarbonate (pH 8.3) at room temperature. For long-term storage, the solution was aliquoted and stored at -20°C. Human thrombin was purchased from Enzyme Research Laboratories Inc and stored at 50 NIHU/mL at -70°C. Fibrin polymerisation was initiated at room temp by the addition of thrombin at 2 NIH to a constant fibrinogen conc. of 1.5 mg/ml along with 0.005 M calcium and 5 % albumin solution.

5.6.2 Laser Scanning Confocal Microscopy Observation

The fibrin networks were scanned with an LSM 510 confocal laser scanning microscope (Carl Zeiss, Inc) at 15 mins after initiation. An Ar-ion laser, with wavelength 488 nm, was used for excitation. The emission of 505–530 nm from the fluorescence conjugate was detected through a filter system.
A computer equipped with standard Carl Zeiss software was used for operating the system and for the processing of images that were collected in a format of 512 × 512 pixels. The observed areas of LSCM were randomly chosen and imaged with a Zeiss ×40 water immersion objective.

5.6.3 Derivation of Fractal Dimension

To quantify clot structure, fractal analysis was performed using the Benoit 1.3 Fractal Analysis System software (Trusoft Int'l Inc., FL). The software has several fractal analysis methods capable of estimating fractal dimensions for self-similar patterns. In the present work, fractal dimension was calculated using the box and information dimension estimation methods. The fractal dimension obtained by these

methods depends on the threshold level. Therefore, a proper adjustment of the threshold level for the binarization of fluorescence intensity is necessary.
The box dimension is defined as the exponent D_b in the relationship:

$$N(d) \approx \frac{1}{d^{Db}} \qquad (5.1)$$

Where N (d) is the number of boxes of linear size d necessary to cover a data set of points distributed in a two-dimensional plane.

The basis of this method is that, for objects that are Euclidean, equation 5.1 defines their dimension. The information dimension method is generally different from the box dimension. In the definition of box dimension, a box is counted as occupied and enters the calculation of N(d) regardless of whether it contains one point or a relatively large number of points. The information dimension effectively assign weights to the boxes in such a way that boxes containing a greater number of points count more than boxes with fewer points.

An extensive study of the Benoit 1.3 software was performed looking at each parameter involved in the derivation of the fractal dimension for the fibrin network structures. The parameters involved in the calculation of the fractal dimension using the box and information estimation methods are discussed below.

5.6.4 Grid Parameters

Side-length of largest box - This is the length of the side of the largest box that will be used to analyze the pattern in the units user has chosen. When the user chooses no units then the units are pixels. The default is one-fourth of the height or width, which ever is smaller.

Coefficient of box size decrease - This is factor by which the box sizes will be divided during the progression from the largest to the smallest box side-lengths. Note that the smallest box side-length will be approximately equal to the value of the coefficient. The progression is always geometric. (i.e. box side-length = 16, 8, 4, 2, 1 for a coefficient = 2)

Number of box sizes - The number of points in the progression from the largest box size to the smallest box size. This is the number of points that will be plotted. The program, using the following equation, automatically calculates this number:

$$\text{Number of box sizes} = \frac{\log(\text{side-length of largest box})}{\log(\text{coefficient of box size decrease})} \qquad (5.2)$$

Increment of grid rotation - This is the angle (in degrees) by which the box grid will be rotated. For each box size, Benoit calculates the minimum number of boxes occupied by the selected pattern.

Pattern size - This is the height and width of the smallest rectangle that circumscribes the selected pattern.

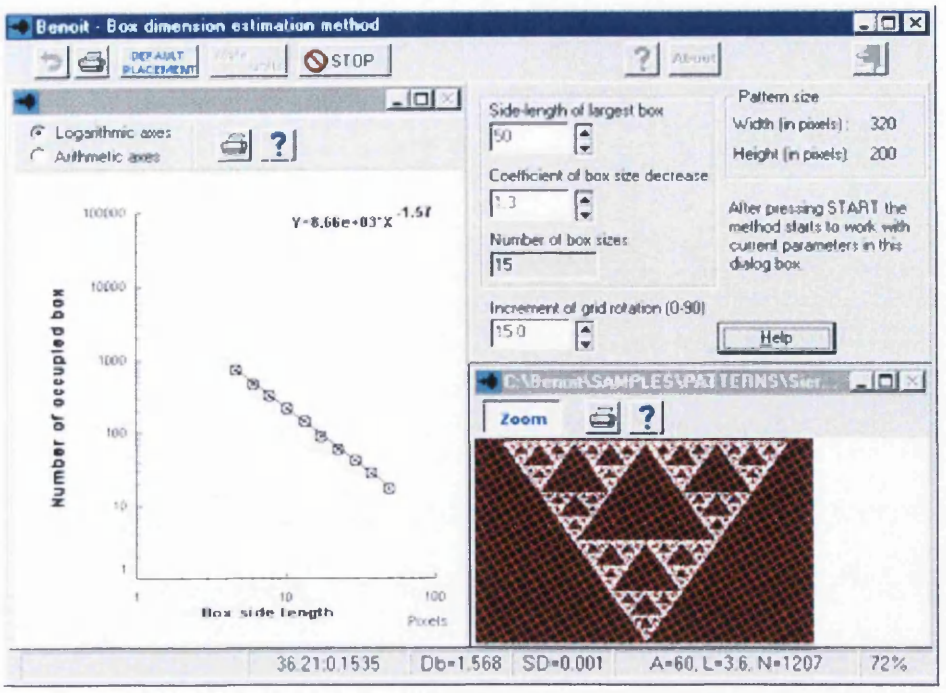

Figure 5.8. Program analysis used for derivation of fractal dimension.

The parameters shown in Figure 5.8 significantly alter the final calculation of the fractal dimension, d_f. Fractal analysis was performed on a processed image (Figure 5.9) investigating the characteristics of each grid parameter. The importance of image processing in image analysis and quantification is described below.

5.6.5 Image Processing

Various image processing operations may need to be performed on 2D and 3D images before they are displayed or analysed. Some operations attempt to correct for distortion introduced by microscope optics and tissue during image acquisition (e.g. deconvolution, spherical aberration correction, noise reduction), or spectral overlap of fluorophores (e.g. linear un-mixing), while ratiometric operators are used when studying ion concentration or pH, and various filters and intensity transformations may be used to improve the visibility of structures. The simpler image processing operations, such as intensity and colour transformations, are often performed interactively during volume rendering.

Image processing becomes imperative within this area of work because effectively quantitative descriptions of structural complexity within fibrin clot networks are being distinguished. Application of image-processing techniques to reduce artefacts and correct some of the non-linearity present in the images has been explored for quite some time now, with vast amounts of image processing tools and algorithms readily available.

Hence, a detailed study was required for the suitability of an image processing algorithm for the acquired fibrin network structure images. An appropriate image processing algorithm was disclosed from work done by Bateman *et al*, 2005, on fibrin clot structure imaged by multiphoton microscopy and quantified by fractal analysis.

The image processing algorithm applied for this work is a slight adaptation of the algorithm used by Bateman *et al*, although involves similar principles. The algorithm consists of background signal subtraction, median filter, image thresholding (Otsu's method [Otsu, 1979]) and binarization.

Median filtering is a non-linear signal enhancement technique for the smoothing of signals, the suppression of impulse noise, and preserving of edges. When performing median filtering (figure 5.9), each pixel is determined by the median value of all pixels in a selected neighborhood (mask, template, window).

Unfiltered values

6	2	0
3	97	4
19	3	10

In order: 0, 2, 3, 3, ***4***, 6, 10, 15, 97

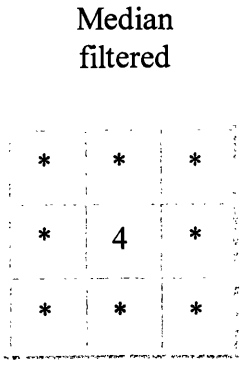

Centre value (previously 97) is replaced by the median of all nine values (4).

Figure 5.9. Description of median filtering.

Median filtering is a simple and very effective noise removal filtering process, that smoothes the data while maintaining the small and sharp details.

The Otsu method is a form of image thresholding that acts on the principle of segmentation. Segmentation involves separating an image into regions (or their contours) corresponding to objects. We usually try to segment regions by identifying common properties. Or, similarly, we identify contours by identifying *differences* between regions (edges). The simplest property that pixels in a region can share is intensity. So, a natural way to segment such regions is through *thresholding*, the separation of light and dark regions. Thresholding creates binary images from grey-level ones by turning all pixels below some threshold to zero and all pixels about that threshold to one.

The Otsu method (clustering) sets the threshold so as to try to make each cluster as tight as possible, thus minimising their overlap. Obviously, we can't change the distributions, but we can adjust where we separate them (the threshold). As we adjust the threshold one way, we increase the spread of one and decrease the spread of the other. The goal then is to select the threshold that minimizes the combined spread. This step effectively filters out random noise, as well as particles

that are not well focused. The overall image is rendered binary, where particles with sharp edges are identified and separated from the background. To extract the greatest amount of information, this step requires good quality images with the least distortion of the edge of the particles.

We can define the *within-class* variance as the weighted sum of the variances of each cluster,

$$\sigma^2_{Within}(T) = n_B(T)\sigma^2_B(T) + n_O(T)\sigma^2_O(T) \qquad (5.3)$$

Where

$$n_B(T) = \sum_{i=0}^{T-1} p(i) \qquad (5.4)$$

$$n_O(T) = \sum_{i=T}^{N-1} p(i) \qquad (5.5)$$

$\sigma^{2|}_B(T)$ = the variance of the pixels in the background (below the threshold) (5.6)

$\sigma^2_O(T)$ = the variance of the pixels in the foreground (Above the threshold) (5.7)

And [0, N – 1] is the range of intensity levels.

Computing this within-class variance for each of the two classes for each possible threshold involves a lot of computation, but there's an easier way.

If you subtract the within-class variance from the total variance of the combined distribution, you get something called the between-class variance,

$$\sigma^2_{Between}(T) = \sigma^2 - \sigma^2_{Within}(T)$$

$$= n_B(T)[\mu_B(T) - \mu]^2 + n_O(T)[\mu_O(T) - \mu]^2 \qquad (5.8)$$

Where σ^2 is the combined variance and μ is the combined mean. Notice that the between-class variance is simply the weighted variance of the cluster means themselves around the overall mean. Substituting $\mu = n_B(T)\mu_B(T) + n_O(T)\mu_O(T)$ and simplifying, we get

$$\sigma^2_{Between}(T) = n_B(T)n_O(T)[\mu_B(T) - \mu_O(T)]^2 \qquad (5.9)$$

So, for each potential threshold, T we,

1. Separate the pixels into two clusters according to the threshold.
2. Find the mean of each cluster.
3. Square the difference between the means.
4. Multiply by the number of pixels in one cluster times the number in the other.

This depends only on the difference between the means of the two clusters, thus avoiding having to calculate differences between individual intensities and the cluster means. The optimal threshold is the one that maximizes the between-class variance (or, conversely, minimizes the within-class variance).

We can update $n_B(T)$, $n_O(T)$, and the respective cluster means $\mu_B(T)$ and $\mu_O(T)$ as pixels move from one cluster to the other as T increases. Using simple recurrence relations we can update the between-class variance as we successively test each threshold:

$$n_B(T+1) = n_B(T) + n_T$$
$$n_O(T+1) = n_O(T) - n_T$$

$$\mu_B(T+1) = \frac{\mu_B(T)n_B(T) + n_T T}{n_B(T+1)}$$

$$\mu_O(T+1) = \frac{\mu_O(T)n_O(T) - n_T T}{n_O(T+1)} \qquad (5.10)$$

This method is the *Otsu* method, after its first publisher (Otsu, 1979).

5.7 Results and Discussion

Figure 5.10 shows a typical observation of the two-dimensional image of the fibrin gel network obtained from confocal microscopy.

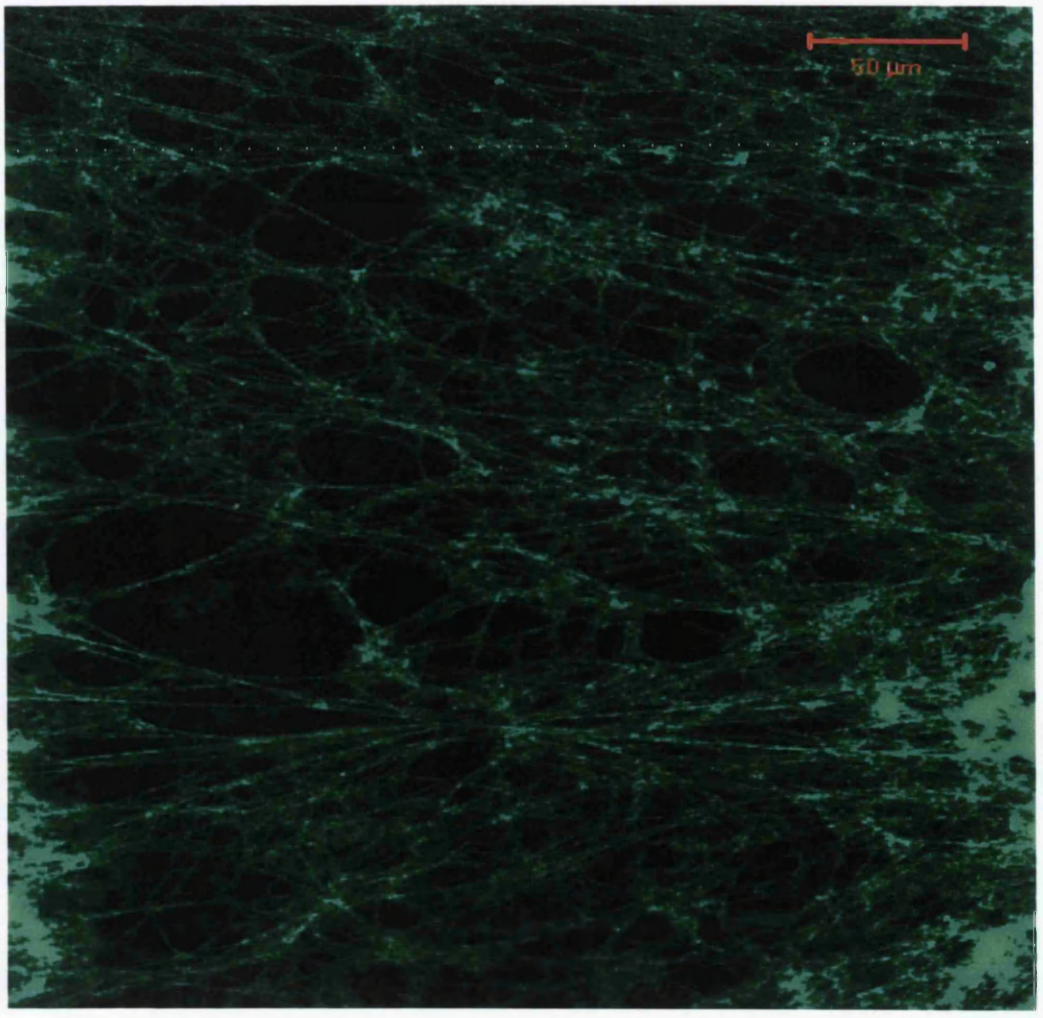

Figure 5.10. Confocal image of fibrin network structure. The bar indicates 50 µm.

5.7.1 Effect of side-length of largest box on Fractal Dimension, d_f

As described above, this is the length of the side of the largest box used to analyse the selected fractal, which can significantly change the fractal dimension as shown in figure 5.11. The results below also illustrate the considerable difference between both estimation methods. The fractal dimension, d_f fluctuates between 1.6 and 1.7 for the selected fibrin network, although greater variation is evident with the box counting estimation method. This result indicates that the network structure has a self-similar nature and a fractal one.

Benoit proceeds with a default setting for this parameter as one fourth the length or width of the selected frame image. For this setting, a value of 1.659 ± 0.095 was obtained for d_f using the box counting method, while a value of 1.657 ± 0.002 was obtained for the information dimension method. Here, $\pm$ denotes one standard deviation, and a distinct difference is apparent from the estimation methods.

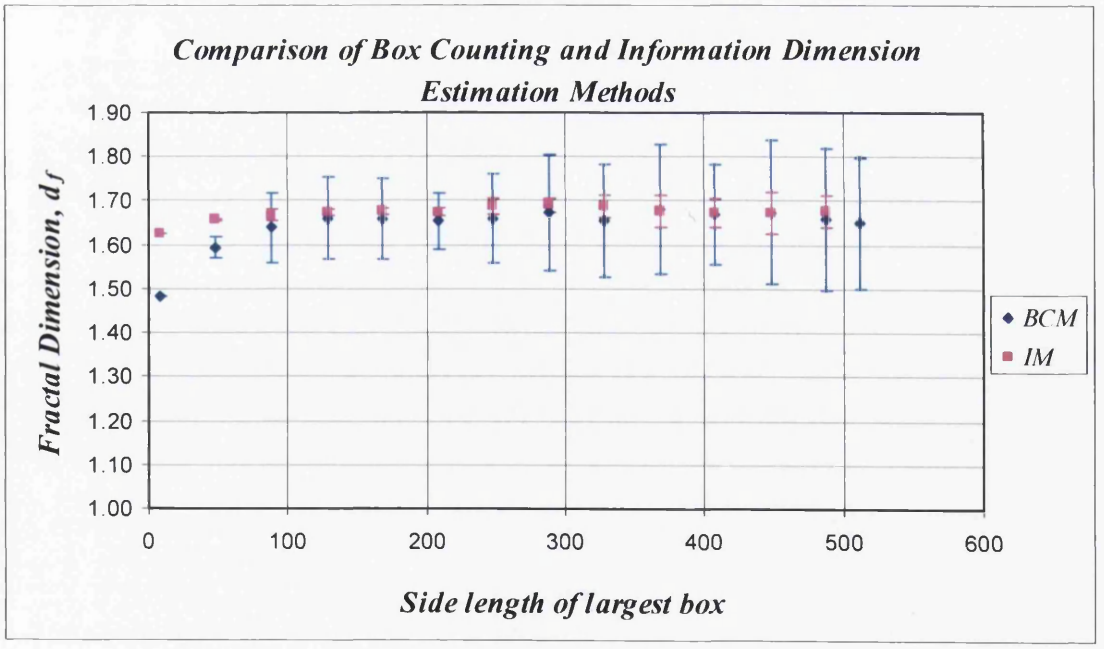

Figure 5.11. Comparison of fractal dimension, d_f, calculated from box counting (BCM) and information (IM) dimension estimation methods with varying side length of largest box.

5.7.2 Effect of Coefficient of Box size decrease on Fractal Dimension

The general trend illustrated (figure 5.12) here is the lower the coefficient of box size decrease, the greater number of boxes used in the program analysis as shown in Equation 5.2. Both fractal analysis methods produce significantly diverse results. Again, most clearly, the information dimension method exhibits exceedingly more reliable results. This method reveals a fractal dimension of 1.65 with a maximum deviation of ± 0.01.

On the other hand the box counting method reveals considerable variation in fractal dimension around 1.7 with increased deviation up to a value of ± 0.20. Considering the results, a reliable and acceptable range for coefficient box size decrease falls within a value of 1 and 2.

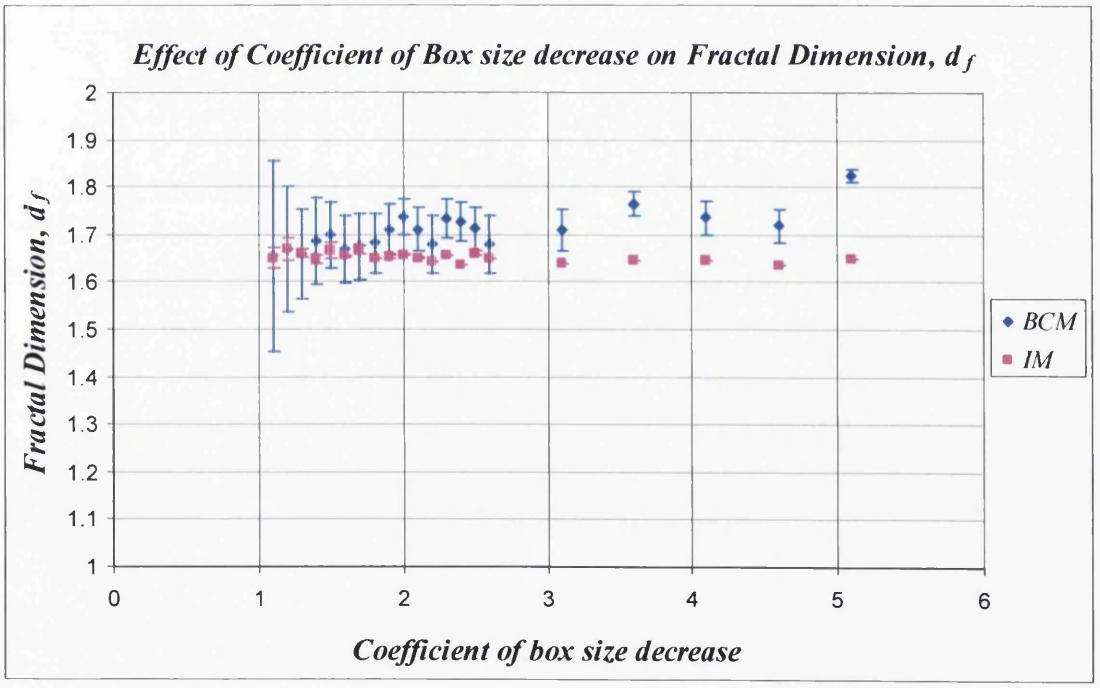

Figure 5.12. Effect of coefficient of box size decrease on fractal dimension for box counting (BCM) and information (IM) estimation methods.

5.7.3 Effect of increment of box rotation (°) on Fractal Dimension

The effect of increment of box rotation reveals the least amount of variation in fractal dimension for all the program analysis grid parameters (fig 5.13). The general trend once again is significant differences in error for the selected fractal analyses. Both fractal dimension methods reveal consistent dimensions, d_f in the region of 1.65, although the box counting method illustrates deviation up to ± 0.097, and the information dimension method illustrates deviation up to ± 0.008. These results demonstrate extensive reliability with the information dimension method. It is imperative to obtain reliable values of fractal dimension to determine quantification for structural complexity in fibrin clot networks.

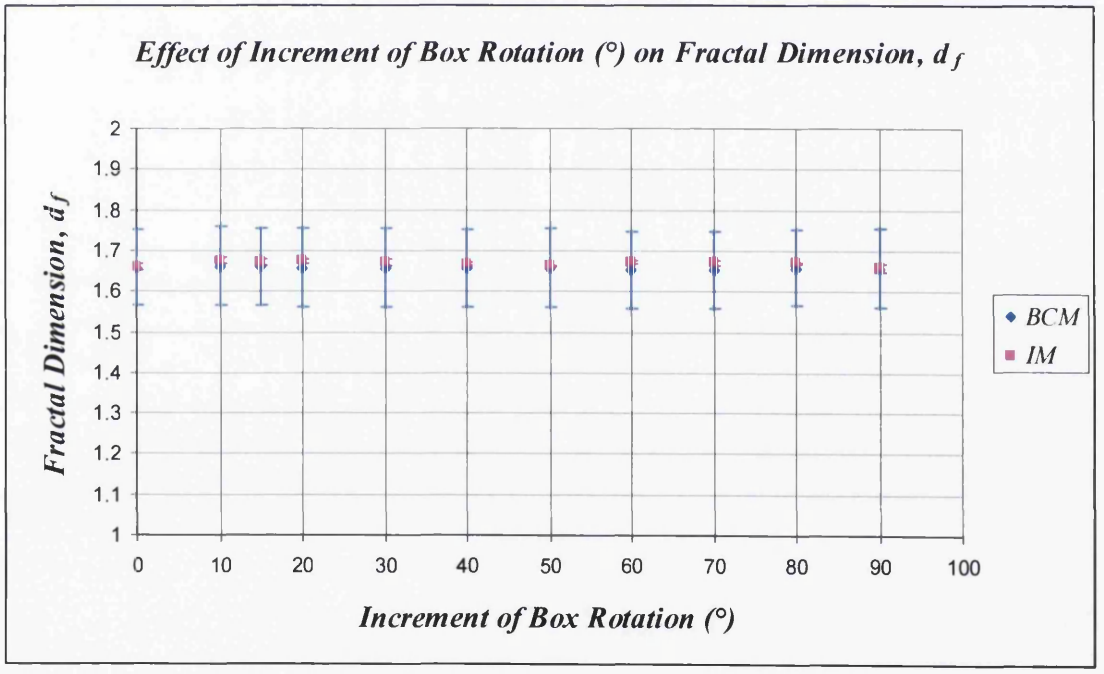

Figure 5.13. Effect of increment of box rotation (°) on fractal dimension for box counting (BCM) and information (IM) dimension methods.

5.8 Summary

The results illustrated here demonstrate how an optical based technique such as Laser Scanning Confocal Microscopy can be implemented to provide a foundation for performing fractal analysis as a quantitative basis for defining, where appropriate, morphological/micro-structural differentiation in clotting. The optical based technique allows us to report studies of the micro-structural characteristics of fibrin clot networks at physiologically relevant concentrations and temperatures. For characterisation of fibrin clot networks, the results reported here exhibit a clear advantage towards an information dimension method over a box counting method. The data reveal significant accuracy, consistency and reliability for the information estimation method. In design, the information estimation method effectively assigns weights to the boxes in such a way that boxes containing a greater number of points count more than boxes with fewer points. Whereas, in the definition of box dimension, a box is counted as occupied and enters the calculation of N(d) regardless of whether it contains one point or a relatively large number of points. Hence, one can assign the enhanced consistency and reliability for these evident reasons.

Following the comprehensive study of existing fractal analyses, the subsequent chapter looks at the structural evolution and significant structural characteristics of fibrinogen-thrombin systems. Fractal analysis provides the framework for structural complexity and allows us to develop relationships between the structural features of fibrin clots and their rheological properties. With the establishment of fractal dimensions from rheological methods, we consider the validity for quantifying fibrin clots using fractal analysis for Laser Scanning Confocal Microscopy techniques.

Chapter 6

Structural Characterisation of Maturing Clot Growth in Fibrin-Thrombin Gels

6.1 Introduction

Diseases associated with the development of thrombosis are a major cause of morbidity and mortality in the developed world. Atherothrombotic vascular disorders develop over many decades and involve the interaction of classic atherogenic risk factors such as diabetes, hyperlipidemia, and hypertension with abnormalities of the inflammatory and haemostatic systems. Arterial disease develops in a high-pressure, high-flow system, with lipid deposition and smooth muscle hyperplasia occurring to form an atherosclerotic plaque (Libby, 2001). Subsequently, the plaque becomes unstable and ruptures exposing a prothrombotic lipid core activating the clotting cascade and leading to the development of a platelet-rich fibrin blood clot and arterial thrombotic occlusion. The extent of this process determines clinical outcome, ranging from no clinically noticeable event to acute coronary artery syndromes including myocardial infarction (MI), cerebrovascular and peripheral vascular disease, or sudden death. New evidence indicates important roles for the proteins that generate fibrin (fibrinogen, factor XIII) in the pathogenesis of coronary heart disease and myocardial infarction. There is additionally emerging evidence that the structure of the fibrin clot may determine risk of thrombotic vascular disease, and that genetic variants of fibrinogen and factor XIII may impart alterations in fibrin structure.

6.2 Fibrin Structure and Disease

Possibly the best documented evidence that alterations in fibrin structure directly contribute to disease derive from studies of hereditary dysfibrinogenaemias. Approximately, 55% of dysfibrinogenaemias are asymptomatic and 25% are associated with bleeding tendencies. In the remaining 20%, thrombotic events with or without haemorrhage can be found. The mechanism by which the risk for pathological events is increased is still unknown and is likely to be specific for each individual defect.

However, in thrombophilic dysfibrinogenaemias, common features emerge, many mutations lie within the αC domains or within the thrombin cleavage sites of

the Bβ chain, leading to impaired polymerisation and structural alterations. In depth studies of the ultra structure of some of the thrombophilic fibrinogens have consistently found the formation of networks characterised by thin fibres and small pores, heightened resistance to fibrinolysis and increased clot stiffness (Collet *et al.*, 1996; Sugo *et al.*, 1998; Lefebvre *et al.*, 2004).

These structural features were also found in clots formed of plasma taken from men who had suffered myocardial infarction at a young age (Fatah *et al.*, 1992; Fatah *et al.*, 1996). Rheological studies from Chapter 3 have shown that the storage modulus (G′), which is inversely proportional to the deformability of the clot, increases as the concentration of fibrinogen from which the gel is formed increases. As elevated fibrinogen levels are a risk factor for ischemic heart disease (Meade *et al.*, 1986), this correlation may explain a relationship between increased plasma fibrinogen levels, fibrin clot structure and myocardial infarction. It has been suggested that less deformable clots formed from plasma with high levels of fibrinogen are more likely to lead to block coronary arterioles and cause subsequent myocardial infarction (Scrutton *et al.*, 1994).

Diabetic patients have a two to fourfold increased risk to of developing cardiovascular disease. The underlying mechanisms, which determine the proatherogenic tendencies in diabetics, have not been fully determined, but it is possible that alterations in fibrin clot properties may contribute. These could be caused by an observed increase in circulating fibrinogen levels (Dunn and Ariens, 2004) and/or by direct molecular interaction between glucose and fibrinogen, leading to alterations in the structure and function of fibrinogen, possibly by glycation of lysine residues (Henschen-Edman, 2001). Considering the involvement of lysine residues in both cross-linking and plasmin-induced lysis of fibrin, it is feasible that glycation could alter the polymerisation and lysis properties of clots as well as FXIII cross-linking and could therefore provide a direct mechanism by which fibrin structure could contribute to the increased cardiovascular risk in diabetics. A study of polymerisation and cross linking of fibrin in plasma of diabetic and control subjects by Lütjens *et al* found that fibrinogen isolated from the diabetic patients was 35% more glycated compared to controls. The same study, however, found that α-chain cross-linking was impaired in the diabetic subjects, which resulted in increased

susceptibility to clot lysis. The authors also observed no difference in the rate and extent of polymerisation between the groups. Structural analysis of fibrin clots formed from plasma of diabetic subjects revealed clots with decreased porosity compared to healthy controls (Jorneskog *et al.*, 1996). More recent work found that ambient glucose levels independently affect fibrin clot structure and that increasing glycosylated haemoglobin (HbA1c) is independently associated with the formation of clots characterised by a tight fibre network consisting of thin fibres (Collet *et al.*, 2000). Formation of denser clots in subjects with diabetes may therefore increase their atherothrombotic risk.

Fibrinogen is an established risk marker for CVD in the general population (Ernst and Resch, 1993), and current evidence suggests that it is likely to be an important cardiovascular risk factor in diabetic subjects. The mechanism via which it becomes elevated is as yet unclear, but at least in type 2 diabetes, it is likely to be related to the presence of underlying insulin resistance. Fibrinogen may exert its influence over atherosclerotic risk, at least in part via associated changes in fibrin structure and function, which may result from alterations to the fibrinogen molecule itself (e.g., from glycation/oxidation, etc.). Further research is needed to clarify the mechanisms via which levels become elevated, and via which fibrin clot structure is altered, as this may lead in time to the development of treatments/preventative measures to reduce future atherothrombotic risk in patients.

6.3 Factors Altering Fibrin Structure

Fibrin gel structure is determined to a significant extent by kinetic factors. As discussed in previous chapters, the self-assembly of fibrin fibers is influenced by the concentration of fibrinogen, calcium and thrombin as well as other proteins (Weisel and Nagaswami, 1992). While ionic strength and hydrogen ion concentration are important, clotting time is a dominant parameter in the determination of structure (Blomback and Okada, 1982; Blomback and Bark, 2004). Rheological studies performed in chapter 3 demonstrated increases in thrombin concentration are associated with faster gelation times, and significant differentiation in viscoelastic properties. Additionally the study allowed us to identify the Gel Point of fibrin clot formation in terms of the Chambon–Winter Gel Point criterion and to use it as the basis for the rheometrical detection of the establishment of the incipient clot and as the basis of characterising its fractal microstructure.

In the study presented here, we examined how changes in thrombin concentration at the time of gelation influence the morphology of 3-D network structure of fibrin gels with LSCM, and in turn how matrix morphology affect the macroscopic material properties of these fibrin scaffolds. The results are also analysed using a fractal concept, where appropriate, to quantify morphological/micro structural differentiation in the clotting process.

Following this work we hope to determine what features of gel preparation and matrix morphology are desirable in producing robust fibrin scaffolds and develop an appropriate quantitative basis for defining what is meant by clot 'quality'/'structure' (good, bad, dense, tight, and loose). With rheological studies from chapter 3, the validity for characterising fibrin gel networks using LSCM and fractal analysis methods can be assessed, and appropriate correlations between the structural features of fibrin clots and their rheology distinguished.

6.3.1 Role of thrombin concentration in fibrin clot formation and structure

6.3.1.1 Materials

Human conjugated fibrinogen (Alexa Flour 488 conjugate) was dissolved in 0.1 M sodium bicarbonate (pH 8.3) at room temperature. For long-term storage, the solution was aliquoted and stored at -20°C. Human thrombin was purchased from Enzyme Research Laboratories Inc and stored at 50 NIHU/ml at -70°C. To understand the role of thrombin in fibrin clot formation and structure, fibrin polymerisation was initiated at room temp by the addition of varying thrombin concentrations. Thrombin was added at 0.01, 0.05 and 0.1 NIHU/ml to a constant fibrinogen conc. of 2.2 mg/ml along with 0.005 M calcium and 5 % albumin solution.

6.3.1.2 Laser Scanning Confocal Microscopy Observation

Optical sections were collected at intervals of 0.5 microns in the z-axis (z stack) at 10, 20, 30 and 60 mins after initiation with an LSM 510 confocal laser-scanning microscope (Carl Zeiss, Inc). An Ar-ion laser, with wavelength 488 nm, was used for excitation. The emission of 505–530 nm from the fluorescence conjugate was detected through a filter system.

A computer equipped with standard Carl Zeiss software was used for operating the system and for the processing of images that were collected in a format of 1024 × 1024 pixels. The observed areas of LSCM were randomly chosen and imaged with a Zeiss ×40 water immersion objective.

6.3.1.3 Derivation of Fractal Dimension

To quantify clot structure, fractal analysis was performed using the Benoit 1.3 Fractal Analysis System software as discussed in chapter 5. The fractal dimension obtained by the box-counting method depends on the threshold level; therefore, appropriate adjustment of the threshold level for the binarization of fluorescence intensity is necessary.

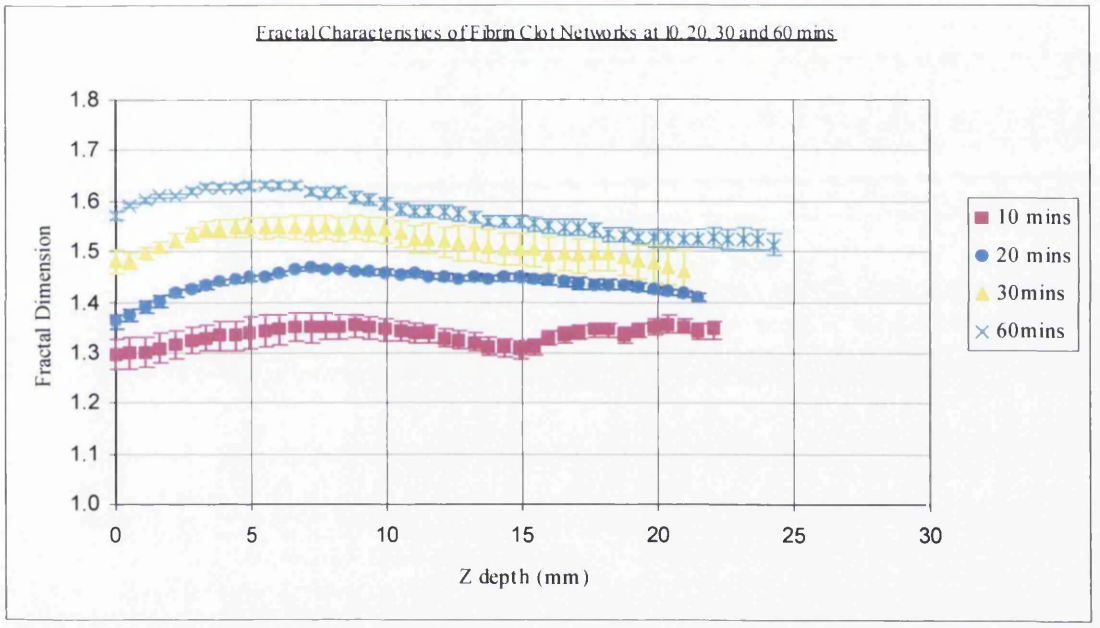

Figure 6.1. Fractal characteristics of fibrin clot network. (Fibrinogen concentration 2.2 mg/ml, thrombin concentration 0.05 NIH units/ml.

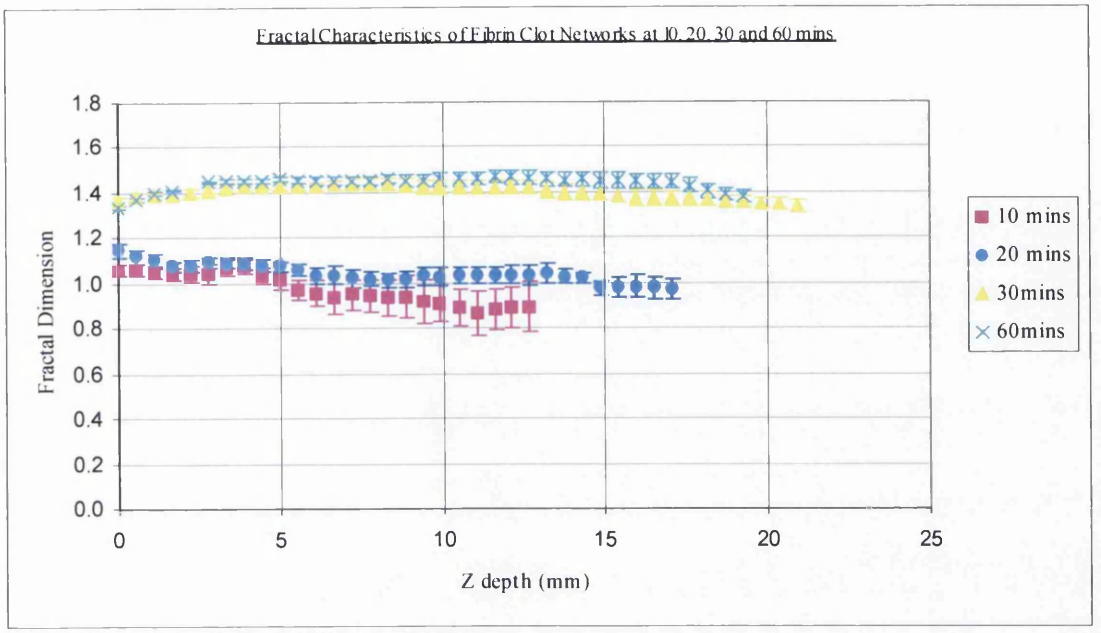

Figure 6.2. Fractal characteristics of fibrin clot network. (Fibrinogen concentration 2.2 mg/ml, thrombin concentration 0.01 NIH units/ml.

6.3.1.4 Results and Discussion

Laser Scanning confocal micrographs of clots formed at concentrations of 0.1 NIH units/ml, results in tight networks with fibre bundles that are thinner, whereas decreasing thrombin concentrations to a level of 0.01 NIH units/ml lead to thicker fibres, with intermediate fibre sizes at intermediate thrombin concentrations, and the gel becomes more porous. This observation has been put into a physiological context by a recent study by Wolberg *et al.*, (2003) who found that an increase of prothrombin levels in vivo could lead to alterations of fibrin structure that essentially corresponded to the in vitro structures generated from higher thrombin concentrations.

Figures 6.1 and 6.2 illustrate as thrombin concentration increases, the clot fractal dimension, d_f increases, indicating fibrin clot structure is dependent on thrombin concentration. The results reveal that the fibrin network structure has a self-

similar nature with enhanced complexity at higher thrombin concentrations. The fractal dimension, d_f, was obtained using the Benoit 1.3 Fractal Analysis System software. These values are in agreement with those obtained by Kubota *et al.*, 2003, and Ferri *et al.*, 2003.

During fibrinolysis, fibrin performs dual roles, functioning as both a cofactor and substrate for the fibrinolytic enzyme plasmin. The significance of this role arguably justifies the observation that clots with altered fibrin structure exhibit altered susceptibility to fibrinolysis (Collet *et al.*, 1993; 1996 and 2000). First, thinner fibrin fibres support a slower rate of tissue plasminogen activator (tPA)-mediated plasmin generation than thick fibres, reducing the overall fibrinolytic activity of the system (Gabriel *et al.*, 1992). Second, clots with thinner fibrin fibres are more resistant to fibrinolysis than clots with thick fibres. Previous studies have exposed an interesting paradox to explain this relationship between fibrin fibre thickness and susceptibility to fibrinolysis. Collet *et al.*, (2000) proposed on the level of individual strands, thick fibres are lysed more quickly than thin fibres. However, because clots that are produced by low thrombin concentrations are composed of thick fibrin fibres that are loosely woven, hence there are fewer individual fibres for a given amount of fibrinogen. Consequently, these clots are more susceptible to fibrinolysis than clots produced by high thrombin concentrations that are composed of tightly packed thin fibrin fibres with more individual fibres per fibrinogen content (Gabriel *et al.*, 1992; Collet *et al.*, 1993; 1996 and 2000; Carr and Alving, 1995). These data suggest that while plasmin generation occurs on individual fibres, movement through the three-dimensional fibrin network is rate limiting for plasmin's activity (Wolberg, 2007).

In contrast to studies in which a specific amount of thrombin is added to fibrinogen to initiate clotting, thrombin generation in vivo is a dynamic process, where the thrombin concentration actively changes during the reaction path in accord with the local conditions.

Wolberg *et al* proposes differences in the nature and origin of the TF-bearing surface, platelet function, and levels of plasma factors can alter the relative influence of extrinsic and intrinsic activities during a procoagulant response (Wolberg *et al.*, 2003, 2005; Allen *et al.*, 2004). Furthermore, fibrin clots themselves can change

platelet procoagulant activity and fibrin formation via release of fibrin-bound thrombin during fibrinolysis (Kumar *et al.*, 1995). Therefore, resulting variations in the thrombin generation pattern and thus, concentration or location of thrombin present at the onset of clotting or while the fibrin network is being constructed, can cause different clot formation rates and final network structures. The general consensus is that extrinsic and intrinsic activities have specific roles during different stages of fibrin clot formation. In most cases, low thrombin concentrations (less than 1 nM) trigger the onset of fibrin clot formation (Wolberg *et al.*, 2005). These low thrombin levels are likely produced via extrinsic activities on the TF-bearing cell surface and depend on the nature and properties of the TF-bearing cells. The different TF-bearing cells (human aortic endothelial cells, smooth muscle cells, macrophages and lung fibroblasts) differ in their ability to initiate coagulation and support thrombin generation (Zwaginga *et al.*, 1990). These unique properties of various cell types result in differences in the initiation of fibrin clot formation (*Ovanesov et al.*, 2005).

Hence, there is strong evidence to suggest, intrinsic activities during the propagation phase must dictate propagation of the fibrin clot through space and the ultimate structure of the fibrin clot. Earlier work proposed low thrombin levels form an initial porous fibrin scaffold, while, subsequently higher levels of thrombin catalyse the formation of a secondary, less porous network superimposed on the primary scaffold (Torbet, 1986; Blomback *et al.*, 1994). More recently, Weisel (2005, 2007) suggested that following development of an initial fibrin scaffold; the network continues to evolve over time with the addition of new fibres and the elongation and branching of other fibrin fibres. In either case, it is likely that fibrin formation in the presence of increasing thrombin concentrations results in a diverse array of fibre thicknesses, and hence morphological/micro structural differentiation in the clotting process. The results presented here permit us to quantify micro structural complexity in fibrin clot formation.

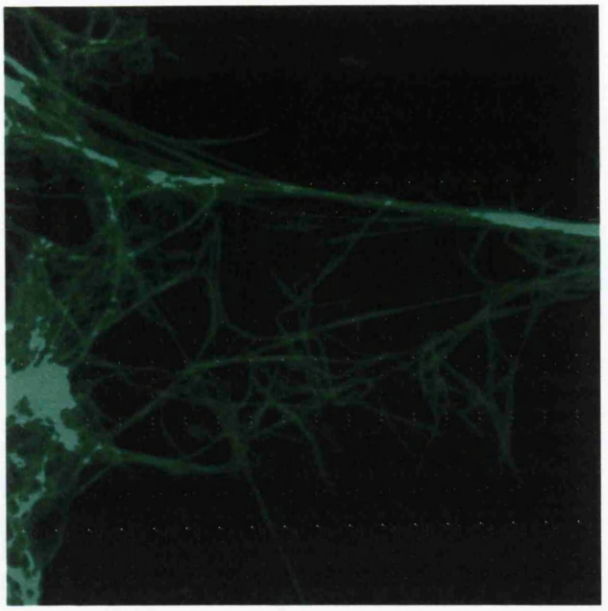

Figure 6.3. Structural characteristics of fibrin gel network (long, coarse fibrin fibres at low thrombin concentrations).

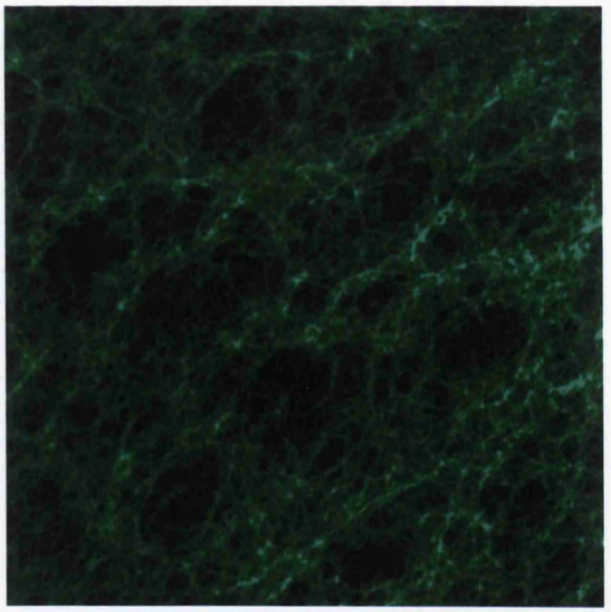

Figure 6.4. Tight fibrin gel network at high thrombin concentration (1.2 NIH Units/ml).

6.3.2 *Influence of Factor XIII on Fibrin Clot Structure*

As touched upon in previous chapters, the fibrin structure network is further stabilised in the presence of factor XIIIa through the formation of N^{ε}- (γ-glutamyl)lysine isopeptide bonds (cross-links or ligations)(Lorand *et al.*, 1968; Matacic and Loewy, 1968; Pisano *et al.*, 1968). Hence, the presence of factor XIII has evident implications on the final structure. An important conclusion of previous microscopy studies is that qualitative differences between the morphology of ligated and un-ligated clot networks are difficult to detect visually, and that no change is apparent in the general appearance of microscopy images of fibrin networks which are stabilised by FXIIIa. The introduction of fractal analysis allows us to disclose these subtle changes in the structural network.

6.3.2.1 *Experimental Method*

Fibrin polymerisation was initiated at room temp by the addition of thrombin to a constant fibrinogen conc. of 2.2 mg/ml along with calcium and albumin solution, as described in section 6.3.1. Experiments were performed with and without Factor XIII at a concentration of 4.5 NIH units/ml(Enzyme Research Laboratories Inc) with a constant thrombin concentration of 0.05 NIH units/ml to investigate its effect on the structural network of the fibrin gel. The fibrin networks were imaged through the incorporation of fluorescently labelled fibrinogen (Invitrogen Alexa Fluor 488 Fibrinogen Conjugate) 20 mins after initiation (as described in section 6.3.1.2).

6.3.2.2 *Results*

Visualisation of the fibrin network structures in the absence and presence of factor XIII using confocal microscopy are shown in Figure 6.5. In the presence of factor XIII, the fibrin gel can be visualised to a z depth of 40 μm, in comparison to 20 μm in the absence of factor XIII signifying extensive variation in the gels structural framework. For comparative visual descriptions of each fibrin gel, the images displayed in figure 6.5 are obtained at a z depth of 20.40 μm.

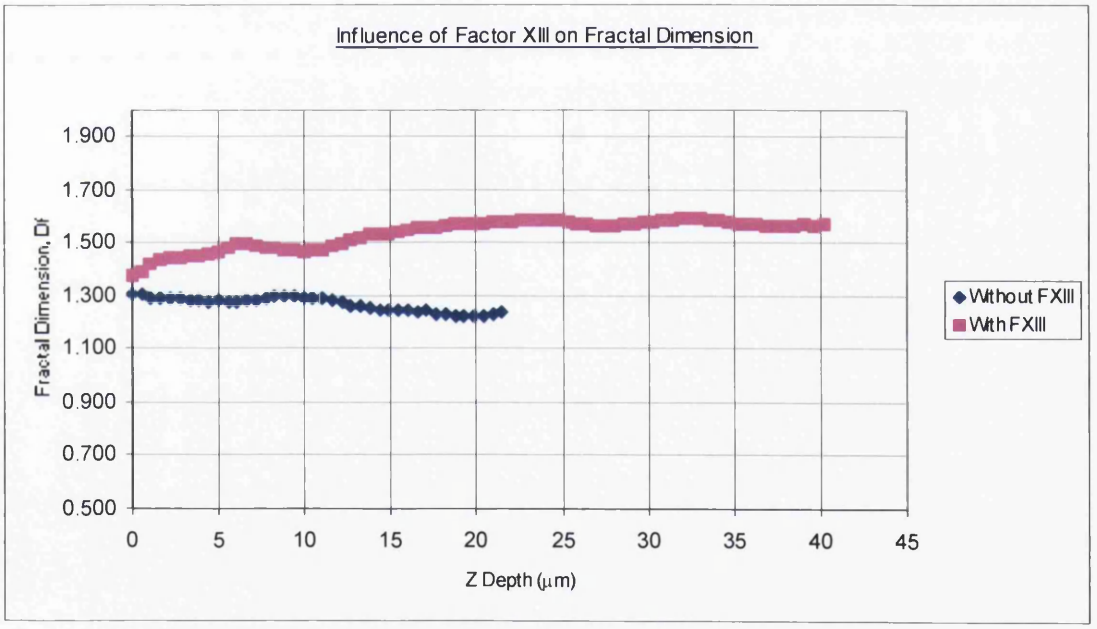

Figure 6.5. Influence of Factor XIII on fractal characteristics of fibrin gel networks.

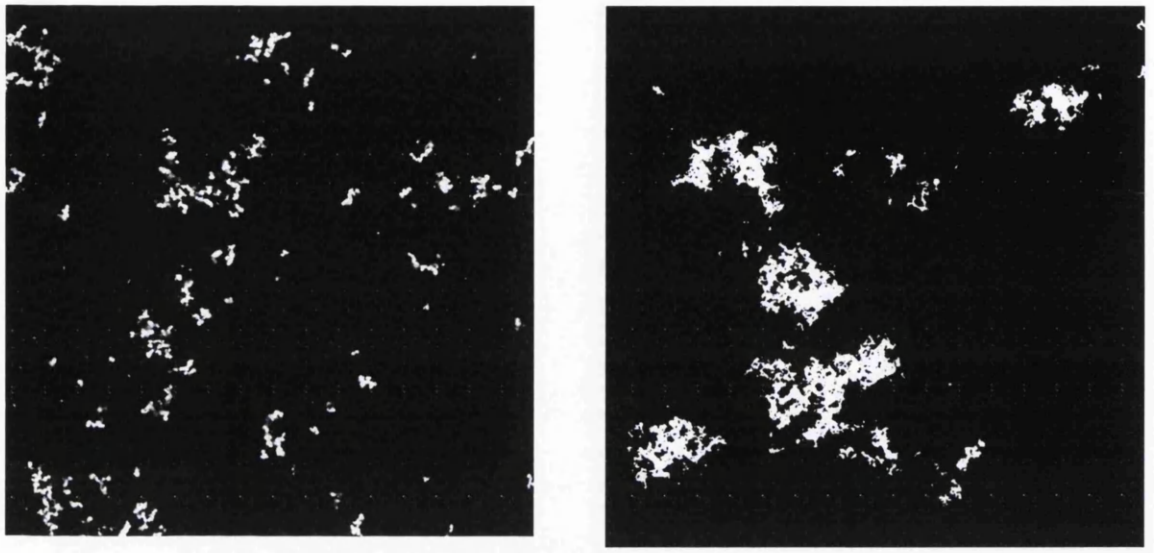

A **B**

Figure 6.6. LSCM image of fibrin in the absence and presence of factor XIII. (A = fibrinogen concentration 2.2 mg/ml, 0.05 NIH thrombin, 0.005 M calcium; B = fibrinogen concentration 2.2 mg/ml, 0.05 NIH thrombin, 0.005 M calcium, 4.5 NIH factor XIII).

As shown in Figure 6.5, in the absence of factor XIII, fractal dimensions remain consistent throughout the whole sample at around 1.3. On the other hand, in the presence of factor XIII, fractal dimensions vary from 1.35 to 1.6 representing extensive micro structural differentiation.

6.3.2.3 Discussion

Prior to delving into the clinical and biochemical details that characterise this fascinating clotting factor, it is worth taking note; factor XIII (FXIII) is not just another plasma protein in the clotting cascade. Like so many other discoveries, FXIII is defined by the function through which we first became aware of its existence, namely as a fibrin stabilizing factor in the earliest papers (Robbins, 1944; Laki and Lorand, 1948). However, it is now apparent that FXIII is capable of cross-linking an ever-growing list of proteins, not only within plasma, but also proteins within the vascular matrix, platelets, endothelial cells and monocytes. Clearly intracellular FXIII plays an important role in the platelet and vascular bed in achieving haemostasis, thrombosis and healing.

The changes in fibre structure generated by ligating are small, relative to the entire range of structural changes observed in this investigation; qualitative differences between the morphology of the unligated and ligated networks are difficult to detect visually without the aid of direct measurements.

Activated FXIII introduces a number of cross-links in the fibrin clot, of which the first are formed between γ-chains of 2 neighboring fibrin molecules in the longitudinal orientation of the (proto) fibril. (Spraggon *et al.*, 1997; Weisel *et al.*, 1993). Cross-linking occurs within 5 to 10 minutes between Gln398 or 399 on the γ-chain of one fibrin molecule and Lys406 on the γ-chain of another, (Spraggon *et al.*, 1997) resulting in the formation of 2 anti-parallel isopeptide bonds that connect the D-regions of 2 fibrinogen molecules longitudinally.

There has been some controversy regarding the spatial orientation of γ-chain cross-links. Some studies suggested that the isopeptide bond was formed between 2 fibrin molecules aligned end to end in the same strand of the protofibril (Fowler *et al.*, 1981; Weisel *et al.*, 1993) while others suggested that the γ-γ cross-link was oriented between 2 fibrin molecules aligned across the fibrin protofibril in a *trans*orientation (Selmayr *et al.*, 1988; Siebenlist *et al.*, 1995). Recent crystallography data of the cross-linked D-fragment indicate that the predominant orientation is the *cis*configuration (Spraggon *et al.*, 1997).

6.4 Structural Characteristics by Fractal Dimension

Martin *et al.*, (1991) first reported fractal dimensions of gels deduced from the correlation function g^2 (t) of dynamic light scattering. They revealed that the $g^{(2)}(t)$ showed power law behaviour and the fractal dimension of a gel network was determined based on Muthukumar's theory. On the other hand, more recently, Takahashi *et al.*, (2003) accomplished a real space observation of the three-dimension network structure of the fibrin gel in a hydrated state by means of confocal laser scanning microscopy. A three-dimensional box-counting analysis of the network structure gave the mass fractal dimensions as 1.42 ± 0.01 and 1.51 ± 0.01 for thrombin concentrations of 0.02 and 0.00125 NIH units/ml respectively.

Ferri *et al.*, (1998, 2001) reported that the mass fractal dimension for a fibrinogen-thrombin system was 1.2 and further analysis gave 1.3 by the angular dependence of scattered light intensity in the small q region. The present results obtained are in good agreement with these studies. Although the meaning of a similar value of static fractal dimension and the dynamic fractal dimension d_f (box counting) is not yet definite, the resultant values suggest that the structural image of a fibrin gel is largely inhomogeneous by means of axial growth of fibrin fibres.

Percolation theory predicts $d_f = 5/2$ for the percolating cluster and $d_f = 2$ for the solution in the reaction bath, which is substantially larger than the present values. Winter *et al.*, (1986, 1988) reported rheological measurements as a function of frequency and observed the power law behavior of elastic moduli for a polyurethane system. Antonietti *et al.*, (1989) accounted that the exponent depends on the chain length between the cross linkages. These facts indicate that the fractal dimension of the gelling system is not universal in agreement with other works but depends on the stoichiometry, the excluded volume effect, network structure, chain rigidity, and so on. As a conclusion in this section, we tentatively analysed the structural characteristics of the fibrin gel in terms of the fractal dimension deduced from confocal microscopy. The present results will provide useful clues to the study of blood coagulation, fibrinolysis, and antithrombogenesis. However, it needs to be considered further in order to clarify structural differentiation in terms of fractal dimension.

6.5 *Structural Evolution of Fibrin Gels*

In previous work, structural differentiation is investigated using fractal dimensions in a two-dimensional plane. To progress this work, it is important to consider morphological differentiation in a three-dimensional plane. The results will also permit us to develop relationships between the structural features of fibrin clots and their rheological properties in terms of fractal dimension.

Fractal geometry is well established in many areas of biomedical research as fractal patterns are intimately connected to natural optimisation principles in both dynamical processes and structure formation. It provides a framework for the quantification of structural complexity. The measurements will allow us to monitor the evolution of structure and mechanical properties over time following the attainment of the Gel Point.

Fractal clusters occupy an increasing fraction of the sol as they become larger, and may eventually fill the space (Martin *et al.*, 1990). Once they have done so, a continuous network of solid can be formed by developing links between the clusters. The formation of links between the relatively immobile impinging clusters is a process of percolation (Zallen, 1983). At the moment a network forms that extends throughout the volume (i.e. when clusters percolate), the sol is transformed into an elastic solid called a gel (Brinker and Scherer, 1990).

Images were taken to examine fibrin clot geometry and cluster size distributions at different times during each experiment. The images were analysed to track changes in gel morphology for a given experiment, as well as differences between experiments resulting from varying fibrinogen and thrombin concentrations.

6.5.1 Experimental Method

A confocal laser-scanning microscope (LSM 510, Carl Zeiss, Inc) was used to obtain sliced images at intervals of 0.5 microns in the z-axis (z stack) at 5, 10, 20, 30 and 60 minutes after initiation. Imaging procedures and fibrin gel make up are as described in section 6.3. Differentiation in gel morphology with time (gel network cluster distribution) was studied at thrombin concentrations of 0.01, 0.05 and 0.1 NIH Units/ml.

6.5.2 Image Processing and Analysis

Three-dimensional reconstructions of each z stack were rendered to visualise structural differentiation in fibrin gel evolution (see figure 6.7). Image processing involved the development of a numerical code that converts each TIFF z stack, that is a temporal snapshot of the clot structure, into a binary representation. This procedure replaces all pixels in the input image with luminance greater than *threshold* with the value 1 (white) and replaces all other pixels with the value 0 (black). The magnitude of the variable *threshold* is found by first computing a global threshold, from all of the TIFF stacks, that can be used to convert an intensity image to a binary image, this is a normalized intensity value that lies in the range [0, 1]. The code uses Otsu's method (Otsu, 1979), which chooses the threshold to minimise the intraclass variance of the black and white pixels.

A three-dimensional version of an algorithm proposed by Mart'ın-Herrero was developed to derive the fractal characteristics of the fibrin-thrombin networks. This is a hybrid method for the labelling of clusters in three-dimensional lattices, which combines the recursive approach with iterative scanning to reduce the stack size required by the pure recursive technique, while keeping its benefits: single pass and straightforward cluster characterisation and percolation detection parallel to the labelling. The algorithm finds the largest 200 clusters from the binary stack and computes the fractal dimension of the 200 clusters using the box-counting technique.

6.5.3 Results and Discussion

Figure 6.7 illustrates the rendered three-dimensional reconstructions of fibrin clot evolution. It demonstrates the evolving sample-spanning network of fibrin-thrombin gels. The fractal clusters occupy an increasing volume of the sol as they become larger, and may eventually fill the space. The clusters hence develop links with each other to form a continuous network of solid. The formation of links between the relatively immobile impinging clusters is a process of percolation, and at the moment a network forms that extends throughout the volume (i.e. when clusters percolate), the sol is transformed into an elastic solid called a gel. At this point of percolation (incipient clot), the fractal dimension is derived at varying concentrations of thrombin and the results are displayed in figure 6.8.

Studying the results reveals an interesting 'step' change in the early stages of maturing clot growth. At thrombin concentration of 0.01 NIH Units/ml at 5 mins (Fig 6.8), we observe a collection of clusters with a d_f range of 1.4 to 1.6, then a step up to 2.2 and a second step change up to 2.5. As the fibrin-thrombin microstructure evolves to maturity we see this step effect move left and as it does so becomes less significant at 10 and 20 minutes. After 30 minutes this feature is gone and we see a sort of relaxation of the clusters of lower fractal dimension.

At higher concentrations of thrombin (0.1 NIH Units/ml – Fig 6.10) this relaxation process at 30 minutes is also evident, although the step effect is not evident. An explanation for this could be as there is a ten-fold increase in thrombin concentration, which creates on average clusters with a more complex geometry due to the increased number of interactions going on, significant micro-structural changes are not as apparent.

The results reveal there is a dominant cluster (the 200^{th} for all cases), which as time evolves 'mops-up' the other larger clusters (here larger refers to larger d_f's and vice-versa), and subsequently the position of the remaining clusters shifts to the right. On the left, the programme finds smaller clusters that are included at later times.

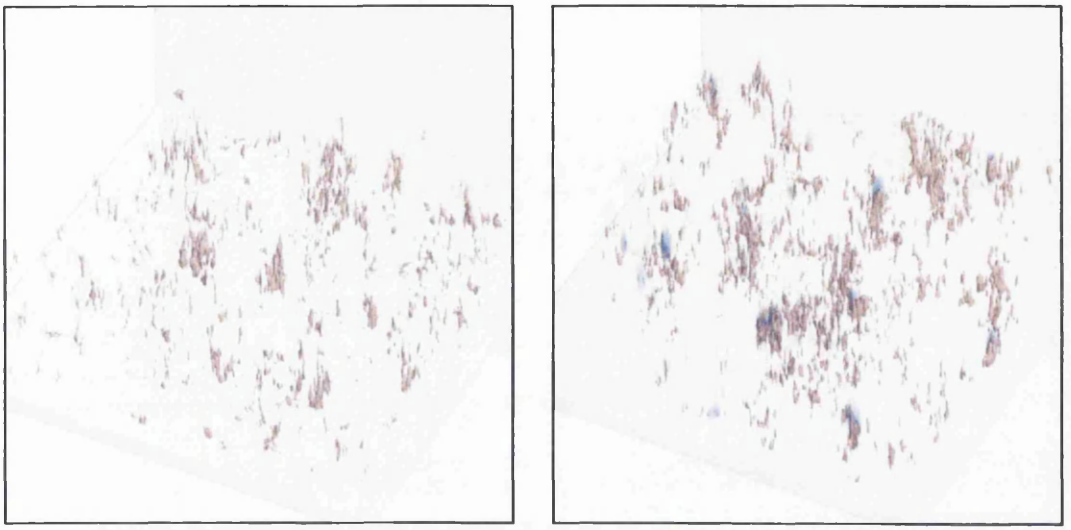

A

B

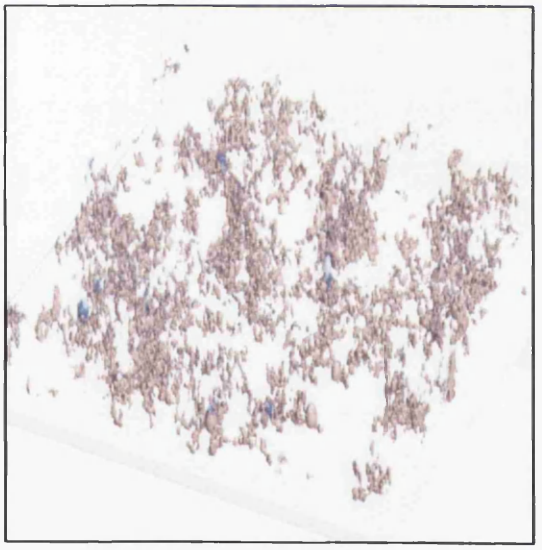

C

Figure 6.7. Three-dimensional confocal reconstruction of fibrin clot evolution. (A = 5 mins after initiation, B = 10 mins and C = 20 mins).

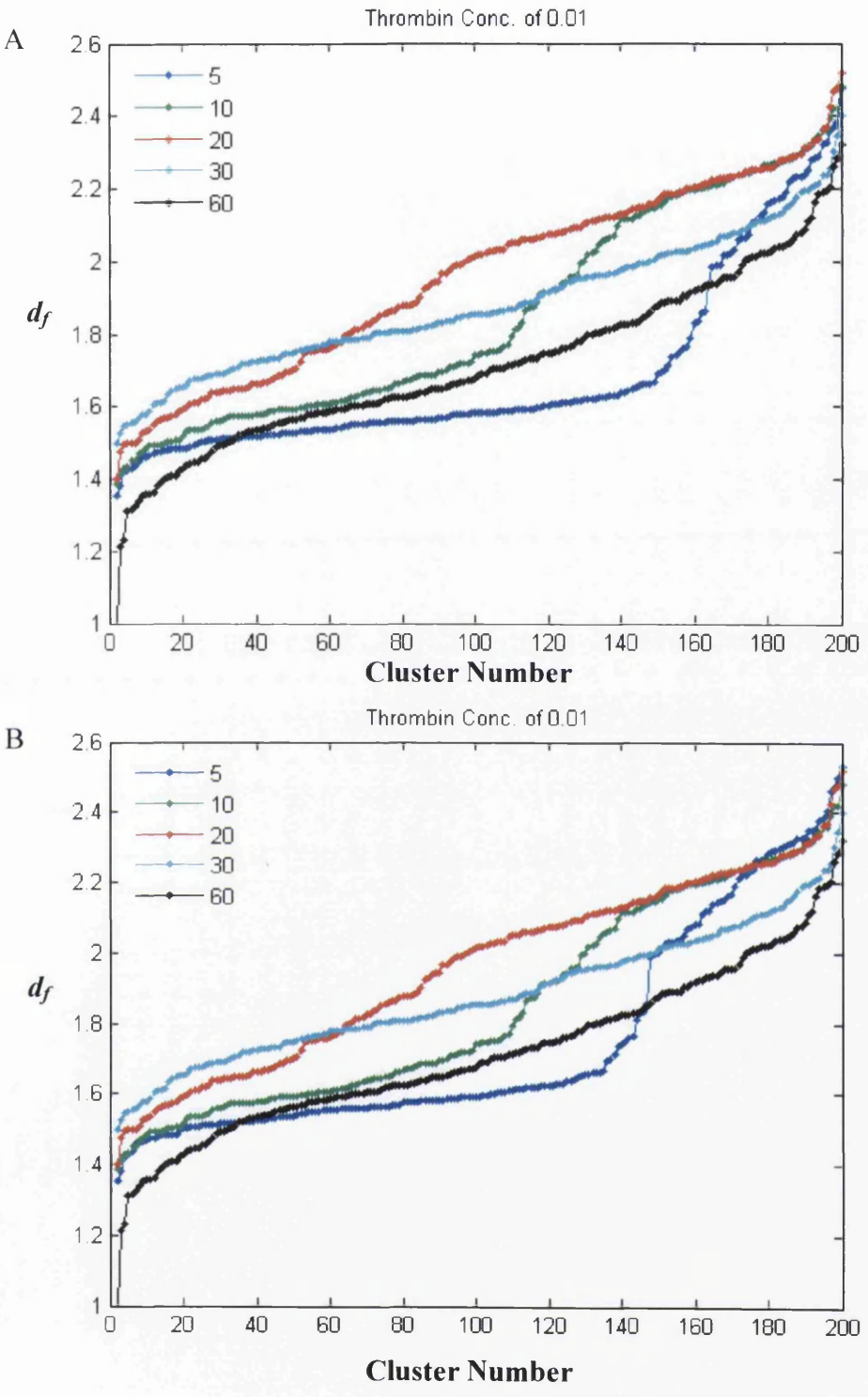

Figure 6.8. Computation of fractal dimension for fibrin-thrombin gel at 0.01 NIH Units/ml thrombin at 5, 10, 20, 30 and 60 mins (A=first data set, B=second data set).

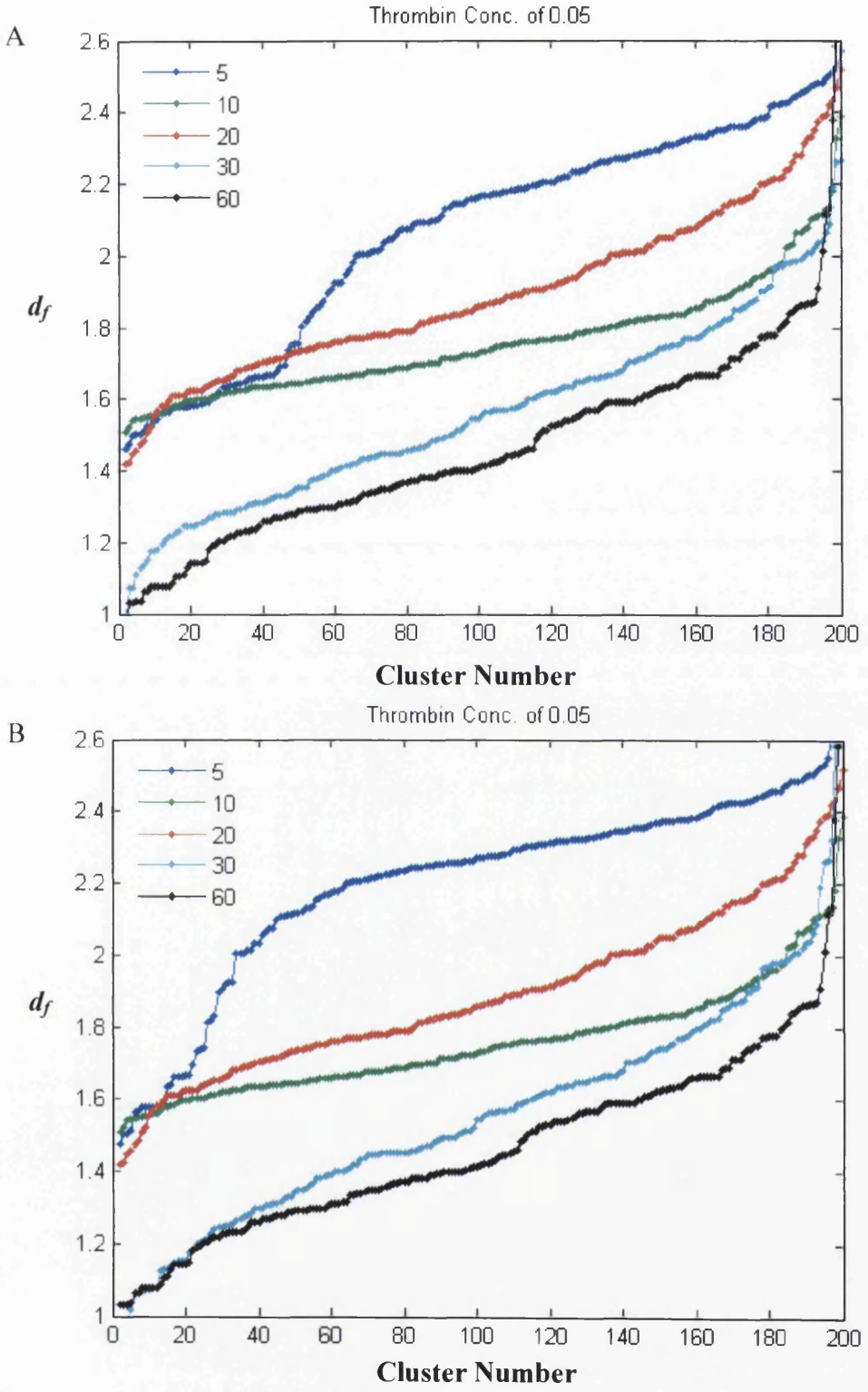

Figure 6.9. Computation of fractal dimension for fibrin-thrombin gel at 0.05 NIH Units/ml thrombin at 5, 10, 20, 30 and 60 mins (A=first data set, B=second data set).

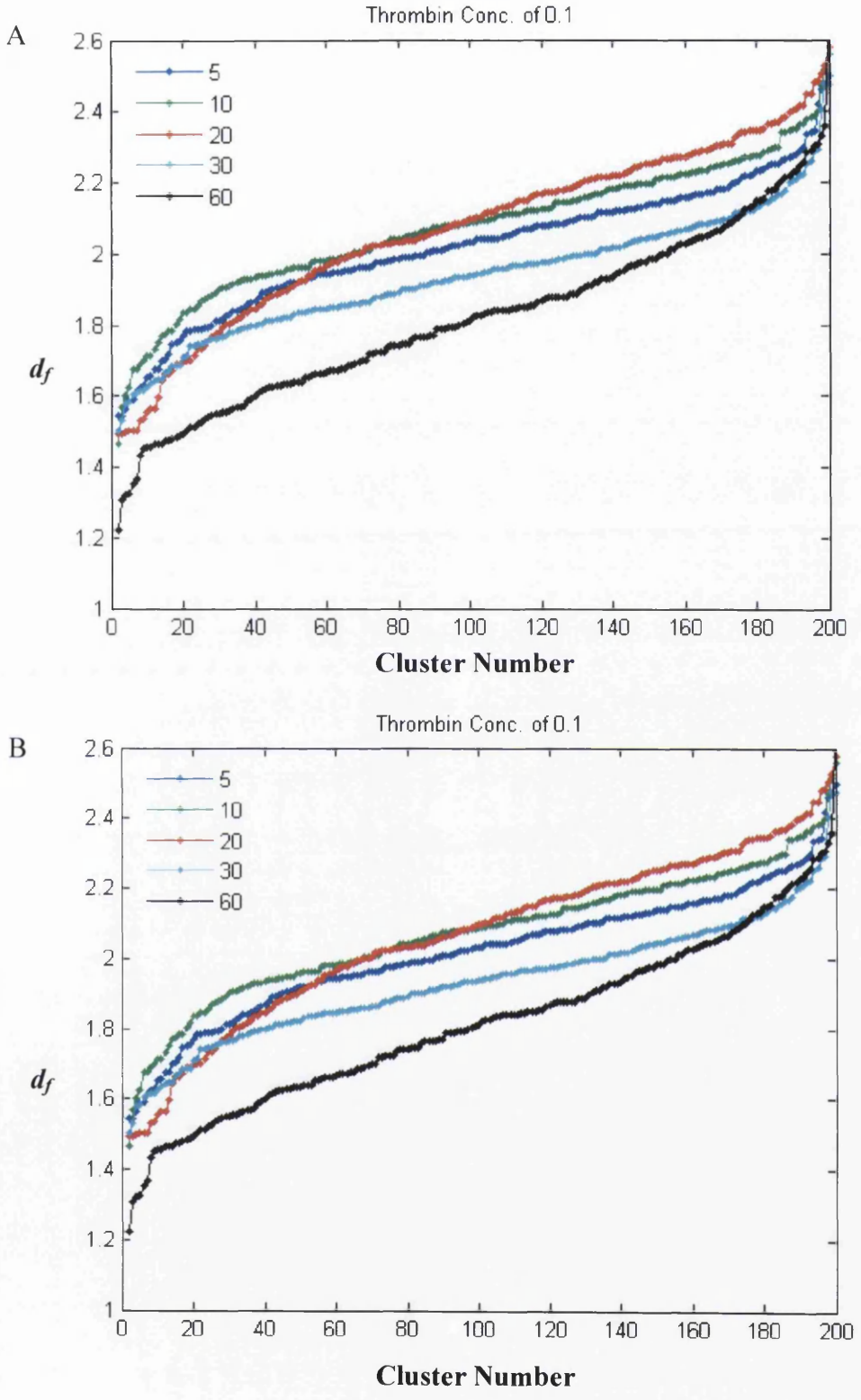

Figure 6.10. Computation of fractal dimension for fibrin-thrombin gel at 0.1 NIH Units/ml thrombin at 5, 10, 20, 30 and 60 mins (A=first data set, B=second data set).

The fractal dimension of mature blood clots has been measured using NMR and the values obtained are in range 2.1 to 2.5 (Williams *et al.*, 2006). The results obtained here are in good agreement to those obtained in the study by Williams *et al.* Interestingly, the upper limit ($d_f = 2.5$) coincides with limiting diffusion-limited and cluster-cluster aggregation models in a 3-dimensional embedding space (Meakin, 1983, and 1988). Clearly, the structure of the mature clot is a measure of the bloods ability to coagulate but also the process by which mass is added to the incipient clot is believed to be directly linked to the health of the blood sample. The altered fibrinolytic pathways in disease states, such as atherosclerotic vascular disease, reportedly result in abnormal coagulation and altered clot microstructures (Isogai *et al.*, 1973). At present it is not experimentally possible to discriminate between mature clots with the same fractal dimension that originate from patients with vastly different backgrounds. The results described here have shown a degree of discrimination can be induced by interrogating the fractal nature of fibrin-thrombin clot structures.

6.5.4 Conclusions

In this study we set out to use fractal geometry to characterise the structural properties of fibrin-thrombin systems. Using microscopy techniques, representations of extensive fibrin-thrombin networks were characterised as set point-masses spatially arranged, in a 3-dimensional volume, exhibiting diverse fractal dimensions. This set may be referred to as a random fractal aggregate that demonstrates a self-similar nature over a range of length scales. A three-dimensional version of an algorithm proposed by Mart'ın-Herrero was developed to derive the fractal characteristics of the fibrin-thrombin networks. Interrogation, of varying fibrin-thrombin structures, reveals that values of the fractal dimension differ considerably depending on the growth parameters. The results support the findings of a recent confocal microscopy study (Bateman *et al.*, 2005) insofar as the value of d_f increases with increasing levels of thrombin.

As a final thought, from these results, we conclude that the structural characteristics of fibrin-thrombin clot networks differ considerably depending on the growth parameters between incipiency and maturity allowing the utilisation as a discriminatory parameter when analysing mature clusters through fractal geometry. Direct visualisation and quantification of the microstructure provides new data for comparison with simulation and testing of theoretical models. The measurements also identify new structural features helpful for future theoretical development.

Chapter 7

Conclusions and Recommendations

7.0 Conclusions and Recommendations

Although it is one of the most abundant and well characterised polymers in nature, fibrin continues to reveal fascinating features of self-assembly and soft elasticity, and presents many potential uses both as a haemostatic agent in clinical applications and as a scaffold for tissue engineering. Distinct to nearly all-native cellular matrices and even many synthetic scaffolds, fibrin is designed to assemble rapidly under physiological conditions by the activation of the soluble fibrinogen monomer by the proteolytic enzyme thrombin.

The work presented here utilises rheology and microscopy based techniques to study extensively the microstructure and mechanical properties of fibrin gels in association with blood clotting, and exploiting fractal analysis where appropriate, to quantify morphological/micro structural differentiation in clotting. We have demonstrated herein, for the first time, that for physiologically relevant concentrations of fibrinogen, the formation of the incipient clot in fibrin-thrombin gels formed by polymerisation of fibrinogen in the presence of thrombin (over a wide range of thrombin concentration) is characterised by frequency independence of δ in oscillatory shear. This work supports the hypothesis that the self-similar (fractal) stress relaxation behaviour recorded at the gel point of samples of coagulating blood (Evans *et al.*, 2008c) is associated with the micro-structural characteristics of the incipient blood clot's fibrin network. Detection of the incipient blood clot defined as the Chambon-Winter Gel Point (Chambon and Winter, 1987) provides a basis for detecting the onset of clot formation far earlier (several minutes) and more accurately than that of global coagulation monitoring techniques such as thromboelastography. Following our assessment of the suitability of sequential frequency sweeps for the detection of the gel point, we conclude that the gel time must be at least an order of magnitude greater than the time taken to perform each frequency sweep in order to obtain an accurate measure of the stress relaxation exponent α, and hence a reliable estimate of the incipient clot's fractal dimension d_f.

In the present work the values of d_f obtained for fibrin-thrombin gels formed with high and low levels of thrombin are bounded by those associated with widely

reported gel formation mechanisms, namely reaction limited cluster-cluster aggregation (RLCCA, $d_f = 2.05$) and diffusion limited cluster-cluster aggregation (DLCCA, $d_f = 1.8$), respectively. The results support the findings of the confocal microscopy study in Chapter 6 and also a study (Bateman *et al.*, 2005) insofar as the value of d_f increases with increasing levels of thrombin. However, it is important to note that all other studies in this area to date refer to the inferred fractal characteristics of a fully formed, mature gel. The present study is the first to report modification of the fractal characteristics of incipient clots. Given that the incipient clot is widely assumed to provide the micro-structural 'template' for ensuing clot development, this is a significant finding. There is evidence that fibrin polymers formed *after* the GP are incorporated into the general architecture of the existing network i.e. they do not form *de novo* networks within fluid spaces of the original (i.e. incipient) network (Weisel 2004). The finding that the highest value of d_f is associated with shortest gel time in fibrin-thrombin gels supports the observation of rapidly formed "tight" clot structures which have been associated with prothrombotic conditions in several physiological states (Scott *et al.*, 2004). The provision of a new technique, based on the rheometrical work reported herein, capable of detecting the formation of altered clot microstructure at the incipient clot state could have significant clinical diagnostic potential e.g. in thromboembolic disease screening applications.

Laser scanning confocal microscopy proves a useful tool for visualising the dynamic and extensive process of conversion of fibrinogen to fibrin and of the formation of fibrin gel networks induced by thrombin. The evolution of respective fibrin gel clusters during the transformation was clearly detected and provides useful clues to the study of blood coagulation and fibrinolysis. Developed microscopy techniques allowed representations of extensive fibrin-thrombin networks to be characterised, in a 3-dimensional volume, which may be referred to as a random fractal aggregate that demonstrates a self-similar nature over a range of length scales. A three-dimensional version of an algorithm proposed by Mart'ın-Herrero was developed to derive the fractal characteristics of the fibrin-thrombin networks. Interrogation, of varying fibrin-thrombin structures, reveals that values of the fractal dimension differ considerably depending on the growth parameters, which is in good agreement with the results attained from rheology-based techniques.

Atherothrombotic vascular disease has reached epidemic proportions in the developed world and represents the major cause of morbidity and mortality in westernised populations. The final phenotypes of acute coronary syndromes, including MI, cerebrovascular disease, and acute limb ischemia are most commonly related to the development of a platelet-rich fibrin mesh on a damaged vessel wall, leading to occlusive thrombus formation. The fibrin clot plays a pivotal role in the pathophysiology of vascular disease, and it is becoming clear that the structure/function of the fibrin clot is complex with genetic and environmental determinants. However, the information known about this is relatively limited and further research is required to fully understand the factors that modify fibrin structure/function and the clinical implications of these modifications. Additional work also needs to be directed at the relationship of fibrin clot structure to its stability and how this relates to atherogenesis.

Continued study of the combined effects of fibrin network mechanics and the biochemical features of fibrin is likely to lead to many new applications of this venerable biomaterial. Already, applications in areas such as wound healing and tissue engineering (Jamney *et al.*, 2009) are being explored.

REFERENCES

Allen G. A., Wolberg A. S., Oliver J.A., Hoffman M., Roberts H. R., Monroe D. M. (2004).
Impact of procoagulant concentration on rate, peak and total thrombin generation in a model system.
J Thromb Haemost 2, 402–13.

Amos W. B., White J. G. (2003). How the Confocal Laser Scanning Microscope entered Biological Research. Biology of the Cell 95, 335-342.

Amrani D. L., Plant P. W., Pindyck J., Mosesson M. W., and Grieninger G. (1983). Structural analysis of fibrinogen synthesised by cultured chicken hepatocytes in the presence or absence of dexamethasone.
Biochim. Biophys. Acta 743, 394-400.

Aral B. K. and Kalyon D. M. (1994). Effects of temperature and surface roughness on time-dependent development of wall slip in steady torsional flow of concentrated suspensions.
J. Rheol 38, 957.

Ariens R. A., Philippou H., Nagaswami C., Weisel J. W., Lane D. A., and Grant P. J. (2000). The factor XIII V34L polymorphism accelerates thrombin activation of factor XIII and affects cross-linked fibrin structure.
Blood 96, 988–995.

Bailey, K., Bettelheim F. R., Lorand, L. and Middlebrook, W. R. (1951). Action of thrombin in the clotting of fibrinogen.
Nature 167, 233-234.

Bailey, K and Bettelheim F.R. The clotting of fibrinogen. (1955). I. The liberation of peptide material.
Biochem Biophys Acta 18, 495-503.

Barnes H. A (1995). A review of the slip (wall depletion) of polymer solutions, emulsions and particle suspensions in viscometers: its cause, character, and cure.
J Non-Newtonian Fluid Mech 56, 221–251.

Barnes H. A. (2000). "A Handbook of Elementary Rheology".
Institute of Non-Newtonian Fluid Mechanics, University of Wales 2000.

Bassingthwaighte J. B., Liebovitch L. S., West B. J (1994). Fractal Physiology, Oxford, Oxford University Press, 1994.

Bateman R. M., Leong H., Podor T., Hodgson K. C., Kareco T., Walley K. R. (2005). The effect of thrombin concentration on fibrin clot structure imaged by multiphoton microscopy and quantified by fractal analysis.
Microsc. Microanal. 11, 1018-1019.

Berlier J. E., Rothe A., Buller G., Bradford J., Gray D. R., Filanowski B. J., Telford W. G., Yie S., Liu J., Cheung C. Y., Chang W., Hirsch J. D., Beechem J. M., Haugland R. P. and Haugland R. P. (2003). Quantitative Comparison of Long-Wavelength Alexa Fluor Dyes to Cy Dyes: Fluorescence of the Dyes and their Conjugates
J. Histochem. Cytochem 51, 1699-1712.

Bernocco S., Ferri F., Profumo A., Cuniberti C., and Rocco M. (2000).
Biophys. J. 79, 561.

Bingham E. C. and Green H. (1919). Paint, a plastic material and not a viscous liquid.
Proc. Amer. Assoc. Testin Materials II 19, 640-676.

Bingham (1929). American Society of Rheology, Lafayette College, PA.

Blomback B., and Vestermark A. (1958). Isolation of fibrinopeptides by chromatography.
Arkiv Kemi. 12, 173-182.

Blomback B., Blomback M., Laurent T. C., and Pertoft H. (1966). Effect of EDTA on fibrinogen.
Biochim. Biophys. Acta. 127, 560-562.

Blombäck B., Hessel B., Hogg D., Therkildsen L. (1978). A two-step fibrinogen-fibrin transition in blood coagulation.
Nature 275, 501-505.

Blomback B., Carlsson K., Hessel B., Liljeborg A., Procyk R., and Aslund N. (1989). Native fibrin gel networks observed by 3D microscopy, permeation and turbidity.
Biochem Biophys Acta 997, 96-110.

Blomback B., Banerjee D., Carlsson K, Hamsten A, Hessel B, Procyk R, Silveira A, Zacharski L. (1990). Native fibrin gel networks and factors influencing their formation in health and disease.
Adv Exp Med Biol. 281, 1-23.

Blomback B., Carlsson K., Fatah K., Hessel B., and Procyk R. (1994). Fibrin in human plasma: gel architectures governed by rate and nature of fibrinogen activation.
Thromb Res 75, 521-538.

Blomback B. (1996). *Thromb. Res.* 83, 1.

Blomback B., and Bark N. (2004). Fibrinopeptides and fibrin gel structure.
Biophys. Chem. 112, 147-151.

Bode W., and Stubbs M. T. (1993). Spacial structure of thrombin as a guide to its multiple sites of interaction.
Semin. Thromb. Hemost. 19, 321-333.

Boger D. V. and Ramamurthy A. V. (1969). Normal stress measurement and evaporation effects on the Weissenberg rheogoniometer.
Trans. Soc. Rheol. 13, 405-408.

Brennan S. O., Fellowes A. P., and George P. M. (2001). Molecular mechanisms of hypo- and afibrinogenemia.
Ann. NY. Acad. Sci. 936, 91-100.

Brinker C. J., and Scherer G.W. (1990). Sol-Gel Science.
Academic Press, NewYork, Ch. 5.

Broadbent, S. R. and Hammersley, J. M. (1957).
Proc. Camb. Phil. Soc. 53, 629.

Brown, J. H, Volkmann N., Jun G., Henschen-Edman A. H., and Cohen C. (2000). The crystal structure of modified bovine fibrinogen.
Proc. Natl. Acad. Sci. USA. 97, 85-90.

Bunde A. and Havlin S. (1994). *Fractals in Science* Springer-Verlag, Berlin

Carnali I. O. (1992). Gelation in physically associating biopolymer systems.
Rheologica Acta. 31, 399-412.

Carr M. E. Jr. (1987). Turbidimetric evaluation of the impact of albumin on the structure of thrombin-mediated fibrin gelation.
Haemostasis. 17(4),189-194.

Carr M. E., and Hermans J.(1978). Size and density of fibrin fibres from turbidity.
Macromolecules 11, 46-50.

Carr M. E., Jr., Alving B. M. (1995). Effect of fibrin structure on plasmin-mediated dissolution of plasma clots.
Blood Coagul Fibrinolysis 6, 567–573.

Cates M. E. (1985). Brownian dynamics of self-similar macromolecules.
Journal de Physique 42, 1059-1077.

Chambon F., Winter H. H. and Morganelli P. (1987). *Macromolecules.*

Chambon F. and Winter H. H. (1987). Linear viscoelasticity at the Gel Point of a crosslinking PDMS with imbalanced stoichiometry.
J. Rheology 31(8), 683-697.

Chmiel H., Anadere L., and Waltiza E. (1990). The determination of blood viscoelasticity in clinical hemorheology.
Biorheology. 27, 883-94.

Chung D. W., Rixon M. W., Que B. G., and Davie E. W. (1983). Cloning of fibrinogen genes and their cDNA.
Ann. NY Acad. Sci. 408, 499-456.

Chung D. W., Harris J. E., and Davie E. W. (1990). Nucleotide sequences of three genes coding for human fibrinogen.
Adv. Exp. Med. Biol. 281, 39-43.

Collet J. P., Soria J., Mirshahi M., Hirsch M., Dagonnet F. B., Caen J., Soria C. (1993). Dusart syndrome: a new concept of the relationship between fibrin clot architecture and fibrin clot degradability: hypofibrinolysis related to an abnormal clot structure.
Blood. 82, 2462–2469.

Collet J. P., Woodhead J. L., Soria J. et al (1996). Fibrinogen Dusart: electon microscopy of molecules, fibers and clots, and viscoelastic properties of clots.
Biophys. J. 70, 500-510.

Collet J. P., Park D., Lesty C., Soria J., Soria C., Montalescot G., Weisel J. W. (2000). Influence of fibrin network conformation and fibrin fiber diameter on fibrinolysis speed: dynamic and structural approaches by confocal microscopy. *Arterioscler Thromb Vasc Biol.* 20, 1354–1361.

Collet J. P., Lesty C., Montalescot G., Weisel J. W. (2003). Dynamic changes of fibrin architecture during fibrin formation and intrinsic fibrinolysis of fibrin-rich clots.
J Biol Chem 278, 21331–5.

Conrad H., Li Y. and Chen Y. (1995). The temperature dependence of the electrorheology and related electrical properties of corn starch/corn oil suspensions. *J. Rheology* 39(5), 1041-1057.

Crabtree G. R. (1987). The molecular biology of fibrinogen. *In* "The Molecular Basis of Blood Diseases" (G. Stamatoyannopoulos, A.W. Nienhuis, P. Leder, and P.W. Majerus, Eds), pp. 631. W.B. Saunders, Philadelphia.

Cuvelier G. and Launay B. (1990). Frequency dependence of viscoelastic properties of some physical gels near the gel point.
Macromol Chem, Macromol. Symp. 40, 23-31.

Davidovits P., and Egger M. D. (1973). Photomicrography of Corneal Endothelial Cells in vivo.
Nature 244, 366-367.

Davie E. W. (1995). Biochemical and molecular aspects of the coagulation cascade. *Thromb Haemost* 74, 1–6.

Davies J. M., and Jones T. E. R. (1994). Complex viscosity predictions for the S1 fluid using harmonic analysis on applied non-sinusoidal stress waveforms. *Journal of Non-Newtonian Fluid Mechanics.* 52, 177–182.

de Gennes, P. G. (1976). *J. Phys. Lett. 37*, L1.

de Gennes P.G. (1979). Scaling concepts in polymer physics, Cornell University Press, Ithaca, NY, USA.

Diaspro A. (2002 ed.). Confocal and Two-Photon Microscopy: Foundations, Applications, and Advances, New York: Wiley-Liss.

Doolittle R. F. (1973). Structural aspects of the fibrinogen to fibrin conversion *Adv Protein Chem.* 27, 1-109.

Doolittle R. F. (1984). *Annu. Rev. Biochem.* 53, 195.

Doolittle R. F. (1984). Fibrinogen and Fibrin.
Annu. Rev. Biochem. 53, 195-229.

Doolittle, R. F. (2003). Structural basis of the fibrinogen-fibrin transformation: contributions from x-ray crystallography.
Blood Rev. 17, 33-41.

Dunn E. J., Ariens R. A. (2004). Fibrinogen and fibrin clot structure in diabetes.
Herz 29, 470–479.

Edwards S. F., and Muthukumar M. (1984). Brownian dynamics of polymer solutions.
Macromolecules 17, 586-596.

Egger M. D., and Petran M. (1967). New Reflected-Light Microscope for Viewing Unstained Brain and Ganglion Cells.
Science 157, 305-307.

Entwistle A. and Noble M. (1992). The use of Lucifer Yellow, BODIPY, FITC, TRITC, RITC and Texas Red for Dual Immunofluorescence Visualized with a Confocal Scanning Laser Microscope.

Journal of Microscopy 168, 219-238.

Ernst E., Resch K. L. (1993). Fibrinogen as a cardiovascular risk factor: a meta-analysis and review of the literature.
Ann Intern Med. 118, 956–963.

Evans P. A. , Hawkins K., Williams P. R., Williams R. L. (2008). Rheometrical detection of incipient blood clot formation by Fourier transform mechanical spectroscopy.
*J. Non-Newton. Fluid Mech.*148, 122-127.

Evans P. A., Hawkins K., Lawrence M., Williams P. R., Williams R. L. (2008). Studies of whole blood coagulation by oscillatory Shear, thromboelastography and free oscillation rheometry.
Clin. Hemorheol. Microcirc. 38, 267-277.

Evans P. A, Hawkins K., Lawrence M., Williams R. L., Barrow M. S., Thirumalai N., Williams P.R. (2008). Rheometry and associated techniques for Blood Coagulation Studies.
Med. Eng. Phys. 30, 671-679.

Falconer K. Fractal Geometry: Mathematical Foundations and Applications (Wiley, Chichester, 1990).

Fatah K, Hamsten A, Blomback B, Blomback M. (1992). Fibrin gel network characteristics and coronary heart disease: relations to plasma fibrinogen concentration, acute phase protein, serum lipoproteins and coronary atherosclerosis.
Thromb Haemost 68, 130–135.

Fatah K., Silveira A., Tornvall P., Karpe F., Blomback M., and Hamsten A. (1996). Proneness to formation of tight and rigid fibrin gel structures in men with myocardial infarction at a young age.
Thromb. Haemost. 76, 535-540.

Fernandez M., Munoz M. E., Santamaria A., Azaldegui R., Diez R., and Pelaez M. (1998). Rheological analysis of highly pigmented inks: Flocculation at high temperatures.
J. Rheology 42 (2), 239-253.

Ferri F., Greco M., Arcovito G., De Spirito M., and Rocco M. (2002).
Phys Rev. E. 66, 11913/13.

Ferry J. D., and Morrison P. R. (1947). Preparation and properties of serum and plasma proteins: VIII. The conversion of human fibrinogen to fibrin under various conditions.
J. Am. Chem. Soc. 69, 388-400.

Ferry, J. D., Miller M., and Shulman S. (1951). The conversion of fibrinogen to fibrin. VII. Rigidity and stress relaxation of fibrin clots; effects of calcium.
Arch. Biochem. Biophys. 34, 424-436.

Ferry J. D., Shulman S., Gutfreund K., and Katz S. (1952). The conversion of fibrinogen to fibrin: XI. Light scattering studies on clotting systems inhibited by hexamethylene glycol.
J. Am. Chem. Soc. 74, 5709-5715.

Ferry J. D. (1974). Rheology of fibrin clots. I. Dynamic viscoelastic properties and fluid permeation.
Biophys. Chem. 1, 152-160.

Ferry, J. D. (1980). "Viscoelastic Properties of Polymers," 3rd. ed., Wiley, New York (1980).

Ferry J. D. (1988). Structure and rheology of fibrin networks. In Biological and Synthetic Polymer Networks.
O. Kramer, editor. Elsevier, Amsterdam. 41-55.

Flory P. J. (1941). *J. Am. Chem. Soc.* 63, 3083.

Flory P. J. (1942). *J. Phys. Chem.* 46, 132.

Flory P.J. (1953). Principles of polymer chemistry.
Ithaca, NY: Cornell University Press, 1953.

Fowler W. E., Erickson H. P., Hantgan R. R., McDonagh J., Hermans J. (1981).
Cross-linked fibrinogen dimmers demonstrate a feature of the molecular packing in fibrin fibers.
Science. 211, 287-289.

Fractals in Science, edited by A. Bunde and S. Havlin (Springer, Berlin, 1994).

Freundlich H. (1935). *Thixotropy,* Paris.

Gabriel D. A., Muga K., Boothroyd E. M. (1992). The effect of fibrin structure on fibrinolysis.
J Biol Chem 267, 24259–24263.

Gailani D., and Broze G. J. Jr. (1991). Factor XI activation in a revised model of blood coagulation.
Science 253, 909–12.

Galanakis D. K., Lane B. P., Simon S. R. (1987). Albumin modulates lateral assembly of fibrin polymers: unique synergism with fibrinogen.
Biochemistry. 26, 2389-2400.

Gerth C., Roberts W. W. and Ferry J. D. (1974). Rheology of fibrin clots. II. Linear viscoelastic behaviour in shear creep.
Biophys. Chem. 2, 208-217.

Glover C. J., McIntire L. V., Brown C. H., and Natelson E. A. (1977).
Mechanical trauma effect on clot structure formation.
Thromb. Res. 10, 11–25.

Godal H. C. (1960). The effect of EDTA on human fibrinogen and its significance for the coagulation of fibrinogen with thrombin.
Scand. J. Clin. Lab. Invest. 12. Suppl. 53, 1-20.

Gorkun O. V., Veklich Y. I., Medved L. V., Henschen A. H., and Weisel J. W. (1994). Role of the αC domains in fibrin formation.
Biochem. 33, 6986-6997.

Goldenfeld N., Goldbart P. (1992). Dynamic scaling and spontaneous symmetry breaking at the gel point.
Phys. Rev. E. 45, 5343-5346.

Greilich P., Carr M. E., Zekert S. L., and Dent R. M. (1994). Quantitative assessment of platelet function and clot structure in patients with severe coronary artery disease.
Am. J. Med. Sci. 307, 15-20.

Guenet J. M. (1992). Thermoreversible gelation of polymers and biopolymers; Academic Press, London.

Guerrero A., Partal P. and Gallegos C. (1998). Linear viscoelastic properties of sucrose ester-stabilized oil-in-water emulsions.
J. Rheology 6, 1375-1388.

Guthold M., Liu W., Stephens B., Lord S. T., Hantgan R. R., Erie D. A., Taylor Jr.R. M., and Superfine R. (2004). Visualization and Mechanical Manipulations of Individual Fibrin Fibres suggest that fiber cross section has fractal dimension 1.3.
J. Biophys. 87, 4226-4236.

Haidaris P. J., Francis C. W., Sporn L. A., Arvan D. S., Collichio F. A., and Marder V. J. (1989). Megakaryocyte and hepatocyte origins of human fibrinogen synthesis exhibit hepatocyte-specific expression of gamma chain-variant polypeptides.
Blood. 74, 743-750.

Hall, C. E., and Slayter H. S. (1959). The fibrinogen molecule: its size, shape and mode of polymerisation.
J. Biophys. Biochem. Cytol. 5, 11-15.

Hantgan R. R., Simpson-Haidaris P. J., Francis C. W., and Marder V. J. (2000). Fibrinogen structure and physiology. *In* "Haemostasis and Thrombosis: Basic Principles and Clinical Practice" (R. W. Colman, J. Hirsh, V. J. Marder, A. W. Clowes and J. N. George, Eds.), pp. 203-232. Lippincott, Williams & Wilkins, Philadelphia.

Harrison P., Wilbourn B., Debili N., Vainchenker W., Breton-Gorius J., Lawrie A. S., Masse J. M., Savidge G. F., and Cramer E. M. (1989). Uptake of plasma fibrinogen into the alpha granules of human megakaryocytes and platelets.
J. Clin. Invest. 73, 1123-1129.

Hatzikiriakos S. G. and Dealy J. M. (1991). Wall slip of molten high density polyethylene. I. Sliding plate rheometer studies.
J. Rheol. 35, 497.

Haugland R. P. (2005). *The Handbook: A Guide to Fluorescent Probes and Labeling Technologies*, Chicago: Invitrogen Molecular Probes, 2005.

Haverkate F. and Timan G. (1977). Protective effect of calcium in the plasmin degradation of fibrinogen and fibrin fragments D.
Thromb. Res. 10, 803-812.

Henschen, A. & McDonagh, J. (1986). In *Fibrinogen, Fibrin and Factor XIII in Blood Coagulation*, pp. 171–241. Edited by R. F. A. Zwaal & H. C. Hemker. Amsterdam: Elsevier Science Publishers.

Henschen-Edman A. H. (2001). Fibrinogen non-inherited heterogeneity and its relationship to function in health and disease.
Ann N Y Acad Sci 936, 580–93.

Hermans P. H. In Colloid science II; Kruyt, H.R., Ed; Elsevier, Amsterdam, 1949, p483.

Hess W., Vilgis T. A., and Winter H. H. (1988). Dynamical critical behaviour during chemical gelation and Vulcanization.
Macromolecules 21, 2536-2542.

Hibbs A. R. (2004). *Confocal Microscopy for Biologists*, New York: Kluwer Academic.

Hodgson D. F. and Amis E. J. (1990). Dynamic Viscoelastic Characterization of Sol Gel reactions.
Macromolecules 23, 2512-2519.

Hoffman M. (2003). Remodeling the blood coagulation cascade.
J Thromb Thrombolysis 16, 17–20.

Holly E. E., Venkataraman S. K., Chambon F. and Winter H. H. (1988). Fourier Transform Mechanical Spectroscopy of viscoelastic materials with transient structure.
J. Non-Newtonian Fluid Mechanics 27, 17-26.

Ikeda S., Foegeding E. A., and Hagiwara T. (1999). Rheological study on the fractal nature of the protein gel structure.
Langmuir 15, 8584-8589.

Isogai Y., Iida A., Chikatsu L., Mochizuki K., and Abe M. (1973). Dynamic viscoelasticity of blood during clotting in health and disease.
Biorheology 10, 411–424.

Janmey P. A., Amis E. J., and Ferry J. D. (1983). Rheology of fibrin clots.VI. Stress relaxation, creep, and differential dynamic modulus of fine clots in large shearing deformations.
J. Rheol. 27, 135–153.

Jamney P. A., Euteneur U., Traub P., and Schliwa M. (1991). Viscoelastic properties of vimentin compared with filamentous biopolymer networks.
J. Cell. Biol. 113, 155-160.

Janmey P. A., Winer J. P., Weisel J. W. (2009). Fibrin gels and their clinical and bioengineering applications.
J. R. Soc. Interface 6, 1-10.

Jana S. C., Kapoor B., and Acrivos A. (1995). Apparent wall slip velocity coefficients in concentrated suspensions of noncolloidal particles.
J. Rheol. 39, 1123.

Jandrot-Perrus M., Mosesson M. W., and Menache D. (1979). Studies of platelet fibrinogen from a subject with a congenital plasma fibrinogen abnormality (fibrinogen Paris I).
Blood. 54, 1109-1116.

Johnson I. (1998). Fluorescent Probes for Living Cells.
Histochem. J. 30, 123-140.

Jones T. E. R., Davies J. M. and Barnes H. A. (1984). Dynamic flow properties of materials in a constant stress rheometer in *Advances in Rheology*, Mena B., Garcia-Rejon A. and Rangel-Nafaile C. (Eds) 4, 45-52.

Jordon Lloyd D. (1926). In *Colloid Chemistry, Vol 1*; *Alexander, J., Ed; Chemical Catalogue Company, New York,* pp 767.

Jorneskog G., Egberg N., Fagrell B., et al. (1996). Altered properties of the fibrin gel structure in patients with IDDM.
Diabetologia 39, 1519–23.

Kaibara, M., and E. Fukada. (1971). The influence of the concentration of thrombin and the dynamic viscoelasticity of clotting blood and fibrinogen- thrombin systems.
Biorheology. 8, 139 –147.

Kaibara, M. (1973). Dynamic viscoelastic study of the formation of fibrin networks in fibrinogen-thrombin systems and plasma.
Biorheology. 10, 61–73.

Kalika D. S. and Denn M. M. (1987). Wall slip and extrudate distortion in linear low-density polyethylene.
J. Rheol. 31, 815.

Kasten F. H. (1999). Introduction to Fluorescent Probes: Properties, History, and Applications, in W. T. Mason (ed.), *Fluorescent and Luminescent Probes for Biological Activity*, New York: Academic Press, 17-39.

Kaye B. H. "A Random Walk Through Fractal Dimensions". VCH Publishers (UK) Ltd, (1989).

Koenig W. (2003). Fibrin(ogen) in cardiovascular disease: an update.
Thromb Haemost. 89, 601–609.

Kraft R.: Fractals and Dimensions. HTTP-Protocol at:
http://www.edv.agrar.tu-muenchen.de/dvs/idolon/dimensions/dimensions.html

Kumar R., Beguin S., Hemker H. C. (1995). The effect of fibrin clots and clot-bound thrombin on the development of platelet procoagulant activity.
Thromb Haemost 74, 962–968.

Laki K., Lorand L. (1948). On the solubility of fibrin clots.
Science 108, 280.

Lange J., Johansson M., Kelly C. T., and Halley P. J. (1999). Gelation behaviour during chainwise crosslinking polymerisation of methacrylate resins.
Polymer 40, 5699-5707.

Langer B. G., Weisel J. W., Dinauer, P. A., Nagaswami C., and Bell W. R. (1988). Deglycosylation of fibrinogen accelerates polymerization and increases lateral aggregation of fibrin fibers.
J. Biol. Chem. 263, 15056-15063.

Lefebvre P., Velasco P. T., Dear A. et al (2004). Severe hypodysfibrinogenemia in compound heterozygotes of the fibrinogen AalphaIVS4 + 1G > T mutation and an AalphaGln328 truncation (fibrinogen Keokuk).
Blood. 103, 2571-2576.

Libby P. (2001). Current concepts of the pathogenesis of the acute coronary syndromes.
Circulation 104, 365–372.

Lippincott-Schwartz J., and Patterson G (2003). Development and Use of Fluorescent Protein Markers in Living Cells.
Science. 300, 87-91.

Lipshitz S. D and Macosko C. W (1976). Rheological changes during a urethane network polymerization.
Polymer Engineering and Science. 16(12), 803-810.

Liu X.Y. and Sawant P. D. (2001). Formation Kinetics of Fractal Nanofiber Networks in Supramolecular Materials.
Appl. Phys. Lett. 79, 3518-3520.

Lorand L., Rule N. G., Ong H. H., Furlanetto R., Jacobsen A., Downey J., Oner N., and Bruner-Lorand J. (1968).
Amine specificity in transpeptidation. Inhibition of fibrin cross-linking.
Biochemistry. 7, 1214-1223.

Lorand L. (2000). A possible goal: inhibiting clot stabilisation to promote thrombolytic therapy.
Arterioscler. Thromb. Vasc. Biol. 20, 2-9.

Lorand L. (2001). Factor XIII: Structure, activation, and interactions with fibrinogen and fibrin.
Ann. NY. Acad. Sci. 936, 291-311.

Losa G. A., Merlini D., Nonnenmacher T. F., Weibel E. (2002). Fractals in biology and medicine.
Volume 3, Birkhauser Verlag, Basel.

Louache F., Debili N., Cramer E. M., Breton-Gorius J., and Vainchenker W. (1991). Fibrinogen is not synthesised by human megakaryocytes.
Blood. 77, 311-316.

Lütjens A., Jonkhoff-Slok T. W., Sandkuijl C., Van der Veen E. A., and Van der Meer J. (1988). Polymerisation and crosslinking of fibrin monomers in diabetes mellitus.
Diabetologia. 31, 825-830.

Macosko C. W. (1994). Rheology. Principles, Measurements and Applications VCH Publishers Inc., NY.

Malkin A. Ya., Begishev V. P. and Mansurov V. A. (1984). Method of non-harmonic oscillations for determining dynamic properties of dynamic liquids.
Vysokomol Soedin 26A, 869.

Mandelbrot B. B. *The Fractal Geometry of Nature* (Freeman, San Francisco, 1982).

Mann K. G., and Lorand L. (1993). Introduction: blood coagulation.
Methods Enzymol 222, 1–10.

Mann K. G., van't Veer C., Cawthern K., Butenas S. (1998). The role of the tissue factor pathway in initiation of coagulation.
Blood Coagul Fibrinolysis. 9, S3–7.

Mannucci P. M., Duga S., and Peyvandi F. (2004). Recessively inherited coagulation disorders.
Blood 104, 1243–52.

Marchi R., Lundberg U., Grimbergen J. et al (2000). Fibrinogen Caracas V, an abnormal fibrinogen with an Aalpha 532 Ser → Cys substation associated with thrombosis.
Thromb. Haemost. 84, 263-270.

Martin J. E., Adolf D., and Wilcoxon J. P. (1988). Viscoelasticity of near-critical gels.
Phys. Rev. Lett. 61, 2620 – 2623.

Martin J. E., Adolf D., and Wilcoxon J. P. (1989). Viscoelasticity near the sol-gel transition.
Phys. Rev. A 39, 1325 – 1332.

Martin J. E., Adolf D., and Odinek J. (1990). Relaxation phenomena near the sol-gel Transition.
Makromol Chem, Macromol Symp. 40, 1–21.

Martin J. E. and Adolf D. (1991). The Sol-Gel Transition in Chemical Gels.
Annu. Rev. Phys. Chem. 42, 311-339.

Martín-Herrero J. (2004). Hybrid Cluster Identification.
J. Phys. A: Math. Gen. 37, 9377–9386.

Marx, G. (1988). Elasticity of fibrin and protofibrin gels is differentially modulated by calcium and zinc.
Thromb. Haemostasis. 59, 500 –503.

Mataic S. and A. G. Loewy. (1968). The identification of isopeptide cross-links in insoluble fibrin.
Biochem. Biophys. Res. Commun. 30, 356-362.

Matsumoto B. (2002 ed.). Cell Biological Applications of Confocal Microscopy, in Methods in Cell Biology, Volume 70, New York: Academic Press, 2002.

Meade T. W., Mellows S., Brozovic M., et al. (1986). Haemostatic function and ischaemic heart disease: principal results of the Northwick Park Heart Study.
Lancet 2, 533–537.

Meakin P. (1983). Formation of fractal clusters and networks by irreversible diffusion-limited aggregation.
Physical Review Letters 51(13),1119-1122.

Meakin P. (1983b). Diffusion-controlled cluster formation in 2-6 dimensional space.
Physical Review A 27(3), 1495-1507.

Meakin P. (1988). Fractal Aggregates.
Advances in Colloid and Interface Science 28, 249-331.

Meakin P. (1988b). Models for colloidal aggregation.
Annual Review of Physical Chemistry 39, 237-267.

Medved L., Ugarova T. P.,Veklich Y., Lukinova N., and Weisel J. W. (1990).
Electron microscope investigation of the early stages of fibrin assembly.Twisted protofibrils and fibers.
J. Mol. Biol. 216, 503-509.

Meh D. A., Siebenlist K. R., Bergstrom G., and Mosesson M. M. (1995). Sequence of release of fibrinopeptide A from fibrinogen molecules by thrombin or Atroxin.
J. Lab. Clin. Med. 125, 384-391.

Mihalyi E. (1988). Clotting of bovine fibrinogen. Calcium binding to fibrin during clotting and its dependence of release of fibrinopeptide B.
Biochemistry. 27, 967-976.

Minsky M. (1988). Memoir on Inventing the Confocal Scanning Microscopy
Scanning, 10, 128-138.

Mockros L. F., Roberts W. W., Lorand L. (1974). Viscoelastic properties of ligation-inhibited fibrin clots.
Biophys. Chemist. 2, 164-169.

Mosesson M. W., DiOrio J. P., Muller M. F., Shainoff J. R., Siebenlist K. R., Amrani D. L., Homandberg G. A., Soria J., Soria C., and Samama M. (1987). Studies on the ultrastructure of fibrin lacking fibrinopeptide B.
Blood. 69, 1073-1081.

Mours M. and Winter H. H. (1996). Relaxation patterns of nearly critical gels.
Macromolecules 29(22), 7221-7229.

Müller M. (2002). Introduction to Confocal Fluorescence Microscopy, Maastricht, Netherlands: Shaker, 2002.

Murphy D. B. (2001). *Fundamentals of Light Microscopy and Electronic Imaging*, New York: Wiley-Liss, 2001

Muthukumar M. and Winter H. H (1986). Fractal dimension of a cross-linking polymer at the gel point.
Macromolecules 19, 1284-1285.

Muthukumar M. (1989). Screening effect on viscoelasticity near the gel point.
Macromolecules. Vol. 22. No. 22.

Nakano A. (2002). Spinning-Disk Confocal Microscopy – A Cutting-Edge Tool for Imaging of Membrane Traffic.
Cell Struct. Funct., 2, 349- 355.

Nelb G. W., Gerth C., Ferry J. D., and Lorand L. (1976). Rheology of fibrin clots. III. Shear creep and creep recovery of fine ligated and coarse unligated clots.
Biophys. Chem. 5, 377–387.

Nelb G. W., Kamykowski G. W., and Ferry J. D. (1981). Rheology of fibrin clots. V. Shear modulus, creep, and creep recovery of fine unligated clots.
Biophys. Chem. 13, 15–23.

Nesheim M., Wang W., Boffa M., Nagashima M., Morser J., Bajzar L. (1997). Thrombin, thrombomodulin and TAFI in the molecular link between coagulation and fibrinolysis.
Thromb Haemost 78, 386–91.

Nossel H. (1976). Radioimmunoassay of fibrinopeptides in relation to intravascular coagulation and thrombosis.
N. Engl. J. Med. 295, 428-432.

Odrljin T. M., Rybarczyk B. J., Francis C. W., Lawrence S. O., Hamaguchi M., and Simpson-Haidaris P. J. (1996). Calcium modulates plasmin cleavage of the fibrinogen D fragment gamma N-terminus: Mapping of monoclonal antibody J88B to a plasmin sensitive domain of the gamma chain.
Biochim. Biophys. Acta. 1298, 69-77.

Olexa S. A, Budzynski A. Z. (1980). Evidence for four different polymerisation sites involved in human fibrin formation.
Proc Natl Acad Sci USA 77, 1374-1378.

Ostwald W. O. (1925). Ueber die geschwindigkeitsfunktion der viscosität disperser systeme.
Kolloid-Z 36, 99-117.

Otsu N. (1979). IEEE 9(1), 62.

Ovanesov M. V., Ananyeva N. M., Panteleev M. A., Ataullakhanov E. L., Saenko E. L. (2005). Initiation and propagation of coagulation from tissue factor-bearing cell monolayers to plasma: initiator cells do not regulate spatial growth rate.
J Thromb Haemost 3, 321–31.

Paddock S. W. (1999 ed.). Confocal Microscopy: Methods and Protocols, Totowa, New Jersey: Humana Press, 1999.

Pal R. (1997). Dynamics of flocculated emulsions.
Chemical Engineering Science 52, 1177-1187.

Panchuk-Voloshina N., Haugland R. P., Bishop-Stewart J., Bhalgat M. K., Millard P. J., Mao F., and Leung W. Y. (1999). Alexa Dyes, A Series of New Fluorescent Dyes that Yield Exceptionally bright, Photostable Conjugates.
J. Histochem. Cytochem. 47, 1179-1188.

Pawley J. B. (1995 ed.). *Handbook of Biological Confocal Microscopy*, New York: Plenum Press, 1995

Pisano, J. J., Finlayson J. S., and Peyton M. P. (1968). Cross-link in fibrin polymerized by factor XIII: ε(γ-glutamyl)lysine.
Science (Wash. DC.). 160, 892-893.

Reiner M. and Schoenfeld-Reiner R. (1933). Viscometrische untersuchungen an Lösungen hochmolecularer naturstoffe. I. Mitteilung kautschuk in Toluol.
Kolloid-Z. 65, 44-62.

Robbins K. C. (1944). A study on the conversion of fibrinogen to fibrin.
Am J Physiol. 142, 581–8.

Roberts H. R., Stinchcombe T. E., and Gabriel D. A. (2001). The dysfibrinogenemias.
British J. Haematol. 114, 249-257.

Roberts W. W., Lorand L., and Mockros L. F. (1973). Viscoelastic properties of fibrin clots.
Biorheology 10, 29-42.

Rodd A. B., Cooper-White J., Dunstan D. E. and Boger D. V. (2001). Gel point studies for chemically modified biopolymer networks using small amplitude oscillatory Rheometry.
Polymer 42, 185-198.

Rouse P. E. (1953). *J. Chem. Phys.* 21 (1953) 1272

Rueb C. J. and Zukoski C. F. (1997). Viscoelastic properties of colloidal gels.
J. Rheology 41(2), 197-217.

Ryan E. A., Mockros L. F., Weisel J. W., and Lorand L. (1999). Structural origins of fibrin clot rheology.
J. Biophys. 77, 2813-2826.

Sadler J. E. (1998). Biochemistry and genetics of von Willebrand factor.
Annu Rev Biochem. 67, 395–424.

Scanlan J. C and Winter H. H (1991). Composition dependence of the viscoelasticity of end-linked poly(dimethylsiloxane) at the gel point.
Macromolecules. 24, 47-54.

Scheissel H and Blumen A (1995). Mesoscopic pictures of the sol-gel transition: Ladder models and fractal networks.
Macromolecules. 28, 4013-4019.

Scherer G. W. (1999). Structure and properties of gels.
Cement and Concrete Research 29, 1149-1157.

Schrag J. L. (1977). Deviation of velocity gradient profiles from the "gap loading" and "surface loading" limits in dynamic simple shear experiments.
Transactions of the society of rheology 21(3), 399-413.

Scott E. M., Ariëns R. A. S. , Grant P. J. (2004). Genetic and environmental determinants of fibrin structure and function: relevance to clinical disease.
Arterioscler. Thromb. Vasc. Biol. 24, 1558-1566.

Selmayr E., Deffner M., Bachmann L., Muller-Berghaus G. (1988).
Chromatography and electron microscopy of cross-linked fibrin polymers: a new model describing the cross-linking at the DD-trans contact of the fibrin molecules.
Biopolymers. 27, 1733-1748.

Sheppard C. J. R., and Shotton D. M. (1997). Confocal Laser Scanning Microscopy, Oxford, United Kingdom: BIOS Scientific Publishers.

Shulman S., Ferry J. D., and Tinoco Jr.I. (1953). The conversion of fibrinogen to fibrin: XII. Influence of pH, ionic strength and hexamethylene glycol concentration on polymerization of fibrinogen.
Arch. Biochem. Biophys. 42, 245– 256.

Siebenlist K. R., Meh D. A., Wall J. S., Hainfeld J. F., Mosesson M. W. (1995).
Orientation of the carboxy-terminal regions of fibrin gamma chain dimers determined from the crosslinked products formed in mixtures of fibrin, fragment D, and factor XIIIa.
Thromb Haemost. 74, 1113-1119.

Siebenlist K. R., Meh D. A., Mosesson M. W. (2001). Protranglutaminase (factor XIII) mediated cross linking of fibrinogen and fibrin.
Thromb. Haemost. 86, 1221–1228.

Scrutton M. C., Ross-Murphy S. B., Bennett G. M., Stirling Y., and Meade T. W. (1994). Changes in clot deformability-a possible explanation for the epidemiological association between plasma fibrinogen concentration and myocardial infarction. *Blood Coagul. Fibrinolysis.* 5, 719-723.

Shen L. L., and Lorand L. (1983). Contribution of fibrin stabilization to clot strength. Supplementation of factor XIII-deficient plasma with the purified zymogen. *J. Clin. Invest.* 71, 1336 –1341.

Smith Jr. T. G., Marks W. B., Lange G. D., Sheriff Jr. W. H., and Neale E. A. (1989). A fractal analysis of cell images. *J. Neurosci. Meth.* 27, 173-180.

Spraggon G., Everse S. J., and Doolittle R. F. (1997). Crystal structures of fragment D from human fibrinogen and its crosslinked counterpart from fibrin. *Nature*. 389, 455-462.

Standeven K. F., Ariens R. A., and Grant P. J. (2005). The molecular physiology and pathology of fibrin structure/function. *Blood Reviews* 19, 275–288.

Stauffer, D. J. (1976). *Chem. Soc. Farad. Trans.* II 72, 1354.

Stauffer D. (1985). Introduction to Percolation theory, Taylor and Francis, London, England (1985).

Stockmayer W. H. (1944). *J. Chem. Phys.* 12, 125.

Stockmayer W. H. (1952). *J. Polym. Sci.* 9, 69.

Stubbs M. T. and Bode W. (1993.) A player of many parts: the spotlight falls on thrombin's structure. *Thrombosis Research.* 69, 1-58.

Sugo T., Nakamikawa C., Takebe M., et al. (1998). Factor XIIIa crosslinking of the Marburg fibrin: formation of alpham.gam-man-heteromultimers and the alpha-chain-linked albumin. Gamma complex, and disturbed protofibril assembly resulting in acquisition of plasmin resistance relevant to thrombophila.
Blood 91, 3282–8.

Takahashi A., Kita R., Shinozaki T., Kubota K. (2003). Real space observation of 3D network structure of hydrated fibrin gel.
Colloid Polym. Sci. 28, 832–838.

Takayasu, *Fractals in the Physical Sciences* (J. Wiley & Sons, Chichester, 1990).

Takeda Y. (1966). Studies of the metabolism and distribution of fibrinogen in healthy men with autologous 125-I-labelled fibrinogen.
J. Clin. Invest. 45, 103-111.

The Fractal Approach to Heterogeneous Chemistry: Surfaces, Colloids, Polymers, edited by D. Avnir (John Wiley & Sons Ltd., Chichester, 1992).

Thurston G. B., and Henderson N. M. (1992). Theoretical and applied rheology. In Proceedings of the XIth international congr.
Rheology. Elsevier. P.741.

Torbet J. (1986). Fibrin assembly in human plasma and fibrinogen/albumin mixtures.
Biochemistry. 25, 5309-5314.

Triantafilou K., Triantafilou M., and Fernandez N. (2000). Lipopolysaccharide (LPS) labeled with Alexa 488 hydrazide as a novel probe for LPS binding studies.
Cytometry 41(4), 316-320.

Tshoegl N. W. (1989). The Phenomenological Theory of Linear Viscoelastic Behavior. *Springer Verlag.*

Tsien R. Y. and Waggoner A. (1995). Fluorophores for Confocal Microscopy, in J. B. Pawley (ed.), *Handbook of Biological Confocal Microscopy*, New York: Plenum Press, 267-280.

Turner L., Ryu W. S., Berg H. C. (2000). Real-time imaging of fluorescent flagellar filaments.
J Bacteriol 182(10), 2793-2801.

Van Wazer J. R., Lyons J. W., Kim K. Y. and Colwell R. E. (1963.) *Viscosity and Flow Measurement - A Laboratory Handbook of Rheology* Interscience / Wiley.

Walters K. (1975). *Rheometry* Chapman and Hall, London.

Wangh L. J., Holland L. J., Spolski R. J., Aprison B. S., and Weisel J. W. (1983). Xenopus fibrinogen. Characterisation of subunits and hormonal regulation of biosynthesis.
J. Biol. Chem. 258, 4599-4605.

Weisel, J. W., Stauffacher C. V., Bullitt E, and Cohen C. (1985). A model for fibrinogen: domains and sequence.
Science (Wash. DC). 230, 1388-1391.

Weisel J. W. (1986a). The electron microscope band pattern of human fibrin: Various stains, lateral order, and carbohydrate localisation.
J. Ultrastruct. Mol. Struct. Res. 96, 176-188.

Weisel J. W. (1986b). Fibrin assembly. Lateral aggregation and the role of the two pairs of fibrinopeptides.
Biophys. J. 50, 1079-1093.

Weisel J.W., Nagaswami C., Makowski L. (1987). Twisting of fibrin fibers limits their radial growth.
Proc. *Natl. Acad. Sci. U. S. A.* 84, 8991– 8995.

Weisel, J. W. and Nagaswami C. (1992). Computer modelling of fibrin polymerisation kinetics correlated with electron microscope and turbidity observations: clot structure and assembly are kinetically controlled.
J Biophys. 63, 111-128.

Weisel J. W., Francis C. W., Nagaswami C., Marder V. J. (1993). Determination of the topology of factor XIIIa induced fibrin gamma-chain cross-links by electron microscopy of ligated fragments.
J Biol Chem. 268, 26618-26624.

Weisel J. W., and Medved L. (2001). The structure and function of the αC domains of fibrinogen.
Ann. NY Acad. Sci. 936, 312-327.

Weisel J. W. (2004). The mechanical properties of fibrin for basic scientists and clinicians.
Biophys. Chem. 112, 267-276.

Weisel, J. W. (2005). Fibrinogen and fibrin.
*Adv. Protein Chem.*70, 247–299.

Weisel, J. W. (2007a). Structure of fibrin: impact on clot stability.
J. Thromb. Haemost. 5(Suppl. 1), 116–124.

Wessendorf M. W. and Brelje T. C. (1992). Which Fluorophore is Brightest? A Comparison of the Staining Obtained Using Fluorescein, Tetramethylrhodamine, Lissamine Rhodamine, Texas Red and Cyanine 3.18
Histochemistry. 98, 81-85.

Whorlow R. W. (1992.) *Rheological Techniques* 2nd Ed., Ellis Horwood.

Williams P. R., Williams R. L., Hawkins K., Lawrence M., Evans A., and Wright C. (2006). Fractal characteristics of incipient and mature blood clot microstructures: viscoelastic measurements and PFG NMR studies.

Micro Mechanobiology of Cells. Tissues and Systems, 2006. European Soc. Clin. Hemorheol.(Avangard, Sofia (Eds. Antonova M. et al)): p. 50 - 52.

Williams, R. C. (1981). Morphology of bovine fibrinogen monomers and fibrin oligomers.
J. Mol. Biol. 150, 399-408.

Winter H. H. and Chambon F. (1986). Analysis of linear viscoelasticity of a crosslinking polymer at the gel point.
J. Rheology. 30(2), 367-382.

Winter H. H. (1987). Can the gel point of a crosslinking polymer be detected by the G′ - G″ crossover?
Polymer Eng and Sci. 27(22), 1698-1702.

Witten Jr T. A., and Sander L. M. (1981). Diffusion Limited Aggregation, a kinetic critical phenomenon.
Phys. Rev. Lett. 47, 1400-1403.

Wolberg A. S., Monroe D. M., Roberts H. R., Hoffman M. (2003). Elevated pro-thrombin results in clots with an altered fibre structure: a possible mechanism of the increased thrombotic risk.
Blood. 101, 3008-3013.

Wolberg A. S., Allen G. A., Monroe D. M., Hedner U., Roberts H. R., Hoffman M. (2005).
High dose factor VIIa enhances clot stability in a model of hemophilia B.
Brit J Haematol. 131, 645–55.

Wolberg A. S. (2007). Thrombin generation and fibrin clot structure.
Blood Reviews 21, 131–142.

Xu W., Chung D.W., and Davie E. W. (1996). The assembly of human fibrinogen. The role of the amino-terminal and coiled-coil regions of the three chains in the formation of the alpha gamma and beta gamma heterodimers and alphabetagamma half molecules.
J. Biol. Chem. 271, 27948-27953.

Yang, Z., Kollman J. M., Pandi L., and Doolittle R. F. (2001). Crystal structure of native chicken fibrinogen at 2.7 angstrom resolution.
Biochemistry. 40, 12515-12523.

Yee V. C., Pedersen L. C., Le Trong I., Bishop P. D., Stenkamp R. E., and Teller D. C. (1994). Three-dimensional structure of a transglutaminase; Human blood coagulation factor XIII.
Proc. Natl. Acad. Sci. USA. 91, 7296-7300.

Yee V. C., Pratt K. P., Cote H. C., Trong I. L., Chung D. W., Davie E. W., Stenkamp R. E., and Teller D. C. (1997). Crystal structure of a 30 kDa C-terminal fragment from the gamma chain of human fibrinogen.
Structure. 5, 125-138.

Yoshimura A. and Prud'homme R. K. (1988a). Wall slip correction for couette and parallel disk viscometers.
J. Rheology 32(1), 53-67.

Yoshimura A. and Prud'homme R.K. (1988b). Wall slip effects on dynamic oscillatory measurements.
J. Rheology 32(6), 575-584.

Zallen R. (1983). The Physics of Amorphous Solids, Wiley, New York, 1983, Ch. 4.

Zhang J. Z., and Redman C. M. (1996). Fibrinogen assembly and secretion. Role of intrachain disulphide loops.
J. Biol. Chem. 95, 30083-30088.

Zwaginga J. J., de Boer H. C., MJ IJ, et al. (1990). Thrombogenicity of vascular cells. Comparison between endothelial cells isolated from different sources and smooth muscle cells and fibroblasts.
Arteriosclerosis. 10, 437–48.